The Thesis Committee for Isaac Nathan Kravitz
Certifies that this is the approved version of the following Thesis:

DETERMINATION OF NEUTRON ABSORPTION SELF-SHIELDING FACTORS FOR LANTHANIDE ELEMENTS DURING NEUTRON ACTIVATION ANALYSIS

APPROVED BY
SUPERVISING COMMITTEE:

Sheldon Landsberger, Supervisor

William Charlton

Determination of Neutron Absorption Self-Shielding Factors for Lanthanide Elements during Neutron Activation Analysis

by

Isaac Nathan Kravitz

Thesis

Presented to the Faculty of the Graduate School of

The University of Texas at Austin

in Partial Fulfillment

of the Requirements

for the Degree of

Master of Science in Engineering

The University of Texas at Austin

December, 2019

Acknowledgements

I would like to convey my genuine thanks to my advisor and supervisor of this Thesis, Dr. Sheldon Landsberger. His support and trust in me have helped me culminate my tenure as a student with this research. He has been a faithful ally in my studies and has always pushed me towards excellence.

I would like to thank Dr. William Charlton, who provided much needed advice and direction with writing the decks of MCNP code. I would also like to express my gratitude to the rest of the reactor staff and nuclear and radiation engineering graduate students for their advice, assistance, and efforts while helping me conduct my experiments.

A special thanks to Dr. Cornelia Chilian who graciously offered the use of her computer code for use to verify the validity of results that were acquired experimentally. Her work was the foundation for this project and was invaluable to its success.

My heartfelt thanks to all the support I received from friends and family over the past two years. Special thanks to Alison Gibson, Elizabeth Kravitz, Vasko Lalkov, and Alison Flint, whose unyielding support has been instrumental in the successful completion of this thesis.

Funding for the first year of this research was provided by the Graduate School Mentoring Fellowship. I would like to thank Los Alamos National Laboratories, Dr. Sheldon Landsberger, and The University of Texas at Austin for providing additional financial support during the final semester of my research.

Abstract

Determination of Neutron Absorption Self-Shielding Factors for Lanthanide Elements during Neutron Activation Analysis

Isaac Nathan Kravitz, M.S.E.

The University of Texas at Austin, 2019

Supervisor: Sheldon Landsberger

Neutron Activation Analysis (NAA) is a non-destructive method of analyzing the elemental composition of a sample with fine detection limits that can reach parts per billion for some isotopes. When conducting NAA, materials with high absorption cross-sections reduce the overall neutron flux within the sample by absorbing incident neutrons. This effect is known as neutron self-shielding. The implementation of correction factors that can account for these effects are important in increasing the precision of NAA.

The objective of this research was to determine a wide variety of neutron self-shielding factors for each lanthanide element, with the exception of promethium, for a range of isotopic concentrations. This was done by experimentally irradiating solutions of these elements and using NAA to determine the activity of each sample. The results were then normalized to a standard to determine the self-shielding effects at varying concentrations.

The experimentally measured self-shielding factors were then compared to values generated from two computer models to verify the accuracy of the data. With the exception of elements with very

large absorption cross-sections, the results of these computer models were shown to be in excellent agreement with the data collected experimentally.

Table of Contents

List of Tables

List of Figures

I. Introduction

Neutron activation analysis (NAA) is a non-destructive analysis technique that is used to determine concentrations of elements within a sample. The foundations of NAA began when Hevesy and Levi utilized a radium beryllium neutron source to activate samples (Hevesy and Levi, 1936).

Aside from its accuracy and precision, NAA has several advantages that make it a good option for analyzing samples: (1) it is non-destructive, meaning that samples can be analyzed without chemical dissolution as often required by other methods; (2) the samples can be of any phase: solid, liquid or gas; (3) it has very good analytical sensitivity for many elements; (4) samples undergoing NAA can be analyzed for more than one element simultaneously; and (5) samples can be as small as a few micrograms (Kirstein, 1997). Its utility has made it a critical component for sample analysis in many different fields such as archaeology, geology, forensics, and semiconductor production.

As semiconductors are susceptible to low-level impurities, silicon semiconductors are ideally suited to be inspected using neutron activation analysis. Impurities can lead to structural damage or affect their electrical or optical properties. As the silicon matrix is not easily activated during irradiation and it allows for low background measurements of the samples (Newman, 1982; Smith, 1996). This allows for precise and accurate analysis of impurities within silicon semiconductors, whether they are intentionally or unintentionally present. ‘Doping’ refers to an intentional process of adding impurities to a semiconductor in order to change its properties to a more desired state. Elements such as boron, arsenic, phosphorus, and gallium are often used to dope silicon semiconductors and are referred to as dopants. The detection limits of some dopants can often be as low as parts per trillion (ppt).

Neutron activation has also become increasingly useful for industrial applications, allowing for bulk elemental inspection of materials in vessels, pipes, and on conveyor belts (Lim, 2004). The analysis of these materials can allow for internal degradation due to operation or corrosion, which cannot be seen via visual inspection. In comparison to neutron activation conducted within a nuclear reactor, this type of NAA utilizes portable neutron sources and detectors that can be deployed at a desired location.

Recently, more experiments have been conducted on human tissues and bodily fluids using NAA (Witkowska, 2005). Analysis of bone samples allows for the determination of bone strength based upon calcium and phosphorus content. Using NAA, new methods of diagnosing bone disorders were developed (Tzaphlidou, 2002). Analysis of hair via NAA has been used to determine exposure of workers to different materials. These results were used to attempt to correlate the health of these workers with the respective exposure to different elements like chromium and molybdenum. Chemical impurities in medicines have also been investigated to determine if there are potential health effects due to trace contaminants (Leal, 2006)

Just as NAA can be used to determine ailments and problems in the body, it can be used to find problems within the environment. Determination of trace elements as possible pollutants in sediments and other environmental samples are imperative to environmental studies. NAA has been used to assess air and water pollutants. Analysis of plant life has allowed for the study of how plants take in different elements and has shown that metal deposition in plants can be used as a biomonitor for pollution (Frontasyeva, 2004).

The idea of using NAA to analyze archeological samples and to determine their provenance was first proposed by Oppenheimer in 1954 (Sayre, 1957). Ceramics, obsidian, flint, basalt, and metals are some types of archaeological and historical materials that commonly undergo NAA. Scrapings

from archeological samples can be analyzed to determine its constituents and perhaps how an artifact was made. Using trace elements found within a sample, it is possible to track an artifact's point of origin and its past journey to its discovered location. It is believed that between 1957 and 2007 analyses of over 150,000 archaeological samples were conducted using NAA (Speakman, 2007)

While NAA is an industrious tool that can be applied to a wide range of fields, it is not without its drawbacks. Conducting NAA with a source that does not have a large enough neutron flux can often be time-consuming and laborious. Certain elements, such as lead, are unable to be identified due to very low neutron cross sections or radionuclide half-lives that are too short to count. There is also the health physics risk of exposure to gamma and beta radiation.

While these problems define the unambiguous drawbacks of NAA, there are several problems that pose significant challenges when conducting NAA. For instance, when analyzing samples, it is important to consider the possible elements that could be present in the sample, as well as the type of sample that is being analyzed and the neutron source that is being used.

One significant problem when conducting NAA is the disagreement of some databases concerning the isotopic abundances of some isotopes. Variations in isotopic abundances can be as high as 3-4% (De Soete, 1972). This can result in larger errors when trying to determine the composition of samples with these elements.

When looking for trace elements, the activation of other elements in the sample can cause significant background radiation so that the gamma-ray that is being inspected may be un-resolvable by Compton scattering interferences. Similarly, the gamma-ray energy that is being examined may be close to that of another characteristic gamma-ray of a separate radionuclide in

the sample. When analyzing samples that contain uranium, or other fissile elements, the products of fission may be the radionuclides that are being inspected by NAA. The spectral interferences that are present as a result of fission can result in deviations from the correct values up over 0.2 parts per million for each part per million of uranium (Landsberger, 1989).

There are many methods for attempting to compensate for or reduce these interferences. The simplest method to address these challenges is to use interference factors to amend the raw counting data. Other methods to reduce these types of interferences can be the utilization of different types of neutron fluxes. The probability of a reaction occurring within a sample is dependent upon the energy of incident radiation. By exposing a sample to a more thermal or epithermal flux an experimenter can alter the fractions of elements that are become radioactive in the sample. Using an epithermal neutron flux can reduce the amount of uranium fission interferences in a sample, while using thermal fluxes can increase the overall activity of a sample—as most nuclides typically have higher thermal cross-sections than epithermal cross-sections or resonance integrals.

Cross-sections represent the probability of a nuclear reaction occurring. There are several types of nuclear reactions that are key to NAA. These reactions are radiative capture, elastic and inelastic scattering, and fission. There are two other types of reactions—charged particle reactions, spallation, and multiplication reactions—but they are not typically useful for NAA.

Elastic scattering occurs when a neutron collides with a nucleus and recoils in another direction, and the conservation of linear momentum, and the kinetic energy of the system is conserved. This type of reaction slows the incoming neutron and imparts some of its kinetic energy into the target nucleus. This reaction leaves the target nucleus in the same state as the original atom: ground state to ground state. This type of reaction is abbreviated to (n,n).

Inelastic scattering is like elastic scattering where an incoming neutron collides with a nucleus and then recoils in another direction. The primary difference is that in an inelastic reaction the target nucleus briefly absorbs the neutron before it is ejected. However, in this instance, kinetic energy is not conserved as after the neutron's ejection, the nucleus is left in an excited state. This reaction is abbreviated to (n,n').

Fission reactions occur when a neutron collides with a fissionable nucleus. The collision splits the nucleus into several parts called fission products. These fission products usually are not equal in weight and tend to be radioactive. The fission of a nucleus also results in the release of several neutrons. This reaction is abbreviated to (n,f).

The most crucial reaction type, radiative capture or also called absorption, is when a nucleus absorbs a neutron. The new compound nucleus is left in an excited state; to return to its ground state, the atom releases a gamma-ray of some energy, characteristic to the compound nucleus. The time at which the gamma-ray is released from the compound nucleus is dependent on the nuclide. For radiative capture reactions, the gamma-ray is immediately released. These gamma-rays are known as prompt gamma-rays. Others are released during the decay of the nucleus into another more stable nuclide or during the de-excitation of the compound nucleus (Lamarsh, 1983). The simplest of these reactions is abbreviated to (n,γ).

Equation (1-1) shows the radiative capture reaction that is used during NAA.

$$n + {}^{A}Z \rightarrow {}^{A+1}Z^{*} \rightarrow {}^{A+1}Z + \gamma \qquad (1\text{-}1)$$

During NAA it is often assumed that the neutron flux inside a sample is equal throughout. This results in uniform activation of all material throughout the entire sample. While this is normally a reasonable assumption to make, the neutron flux in the center of a sample can experience a flux

depression when a sample contains stable isotopes with large absorption cross-section. This flux depression results in the overall activity of a sample being less than expected (Chilian, 2006).

The difference in neutron flux within a sample due to neutron absorption by the sample is known as neutron self-shielding or self-attenuation. As all nuclides absorb neutrons, all materials experience some sort of neutron self-shielding. However, in many instances, absorption cross-sections are relatively small, and thus do not alter the flux shape significantly; the assumption that the neutron flux is uniform throughout the sample is valid. When high absorption cross-section nuclides are present in a sample, the averaged neutron flux, ϕ_{avg}, can be much lower than the assumed neutron flux, ϕ_{∞}, within the sample:

$$\phi_{avg} \neq \phi_{\infty} \tag{1-2}$$

There have been several attempts to create correction factors and universal equations to allow for more accurate measurements of high cross-section materials. Previous work has shown that when measuring samples containing chlorine, iodine, and bromine, deviation from the true amount can be as large as 33% (Chilian, 2006).

The self-shielding factor can be defined as the quotient of the average flux divided by the assumed uniform flux:

$$f = \frac{\phi_{avg}}{\phi_{\infty}} \tag{1-3}$$

Another method of dealing with the self-shielding of samples is by diluting the sample. By decreasing a sample's concentration within another material with lower absorption cross-sections, such as water, it is possible to reduce the self-shielding effect. The problem with this method is that the sample needs to be homogenized within the solution in order to reduce the chances of a

deviation of the average neutron flux within the sample due to a slightly higher concentration of the investigated element. This requires that the sample be in liquid form or to be converted into a liquid. A noticeable drawback of this is that it requires large amounts of preparation work with potential for cross contamination.

There has been significant work into the development of neutron self-shielding factors for the purposes of increasing the precision of NAA. While the methods for calculating self-shielding factors have grown increasing complex and strenuous, a universal equation has yet to be fully developed. Because of this, the utilization of individual self-shielding factors still has its usefulness for individual sample calculations.

II Background Theory
II.I Neutron Self-Shielding

As mentioned in the previous section, neutron activation analysis is dependent upon a neutron being captured by a target atom. The resulting compound nucleus increases in mass number, or the total sum of neutrons and protons, by one, and the nucleus usually releases a gamma ray. A radiative capture reaction involving ^{152}Eu can be seen in Eq. (2-1):

$$^{151}Eu + {}^{1}n \rightarrow {}^{152}Eu + \gamma \qquad (2\text{-}1)$$

In Eq. (2-1), a neutron collides with a stable ^{151}Eu atom and is absorbed by the nucleus to create ^{152}Eu. The reaction also results in a prompt gamma ray emission from the compound nucleus. During these reactions, both the products and reactants of the reactions are governed by four fundamental laws: conservation of charge, momentum, nucleons, and energy. The mass of these particles is not conserved because as nucleons form together, some of their mass is converted into binding energy to hold them together.

Because of this, some reactions are only possible when the energy of an incoming neutron is high enough to overcome the binding energy required to become a part of the nucleus. Using the conservation of energy it is possible to determine this energy. Equation (2-2) is a simplified version of Eq. (2-1):

$$a + b \rightarrow c + d \qquad (2\text{-}2)$$

The conservation of energy states that the total energy of the reactants—*a* and *b*—is equal to the total energy of the products—*c* and *d*—in any reaction. In radiative capture reactions there are two contributing sources of energy in both the reactants and products: the total rest-mass energy of the particles and the total kinetic energy of each particle. The conservation equation is as follows:

$$KE_a + KE_b + m_a c^2 + m_b c^2 = KE_a + KE_d + m_c c^2 + m_d c^2 \quad (2\text{-}3)$$

where KE_a, KE_b, KE_c, and KE_d are the kinetic energies of each particle, and m_a, m_b, m_c, and m_d are the rest-masses of each particle. When this equation is applied to Eq. (2-1) the rest-mass of the gamma-ray is assumed to be zero. In Eq. (2-3) the rest-mass energy is calculated by multiplying the rest-mass energy by the square of the speed of light: c^2.

Upon rearranging Eq. (2-3), the Q-value of a reaction can be calculated, or the difference in energy between the products and reactants.

$$Q = [(m_a + m_b) - (m_c + m_d)]c^2 \quad (2\text{-}4)$$

When the Q-value is positive it means that the reaction will leave the products in an excited state. Conversely, if the Q-value is negative it means the reaction results in a net-decrease in the kinetic energy of the particles.

The radiative capture reaction of ^{152}Eu—shown in Eq. (2-1)—will be used as an example for solving Eq. (2-4). ^{152}Eu and the neutron have rest-masses of 150.9198578 *amu* and 1.0086654 *amu*, respectively. This results in a total of 151.9285232 *amu* for the reactants. The products, ^{152}Eu and the gamma-ray, have rest-masses of 151.9217521 *amu* and 0 *amu*. The difference between the rest-masses of the products and reactants is 0.0067711 *amu*. The Q-value of reactions are most commonly reported in terms of MeV; to convert from *amu* to MeV, the Q-value is multiplied by 931.5 MeV/*amu*. This yields a result of 6.3073 MeV. Since the Q-value is positive, the reaction results in less kinetic energy among the products than in the reactants. This excess energy becomes excitation energy within the ^{152}Eu nucleus. This energy will inevitably be released from the nucleus in the form of a gamma-ray with particle emission—usually β^+ or β^-.

Sometime the compound nucleus is left in an excited state after a radiative capture takes place. The gamma ray that is released after the reaction has an energy which is equal to the difference between the unexcited Q-value state and this excitation energy. However, each radioactive isotope has set excitation energy levels, meaning that each isotope has distinct and discrete excitation energies. For instance, the first two excitation energies of ^{152}Eu are 45.5998 keV and 65.2969 keV. Heavier elements, like europium, can have greater values of excitation energies, but the lower excitation states are more frequently occurring.

Excited nuclei can have different half-lives from their ground-state counterparts. A ^{152}Eu atom that is at a 45.5998 keV excited state has a half-life of 9.31 hours, while its ground state has a half-life of 13.54 years. Excited states for high Z elements can have differing decay modes than their ground states. For instance, ^{152}Eu has different probabilities of decaying by β^+ or β^- decay in its excited states than in its ground state.

After a radiative capture reaction takes place, the compound nucleus can either be stable or unstable. In Eq. (2-1) the compound nucleus, ^{152}Eu, is unstable and will thus decay after some period. While it is impossible to determine the exact length of time it will take for a nucleus to decay, the half-life of an isotope can be used to calculate the decay speed of an activated sample.

A nuclide that has been activated by the absorption of a neutron can decay by multiple paths: β^+ or β^-, gamma rays, x-rays, alpha, electron emission, or fission. Using our example, ^{152}Eu, there are two possible decay modes for its ground state: β^+ and β^- decay. In either case, ^{152}Eu decays into a stable element: ^{152}Sm or ^{152}Gd, respectively. When releasing energy in the form of gamma-rays, a nucleus may not shed all its energy at once, but instead the nucleus may release several, different energy gamma rays before reaching the ground state. ^{60}Cobalt is known to have primarily two decay gamma rays that it emits when it decays into ^{60}Ni: 1.1732 MeV and 1.3325 MeV. Groups of

gamma-rays that appear as a meta-stable isotope decays to its ground state are called coincident gamma-rays. The sum of the energies of these coincident gamma-rays is equivalent to the excitation energy. There can be hundreds of different gamma-ray energy emissions paths that can be made by a de-exciting nucleus, but some paths are more likely to occur than others, as seen in Figure 2-1. The frequency with which one of these gamma-ray occurs is known as its intensity. The measurement of these coincidence is a powerful and important tool in characterizing the composition of a sample.

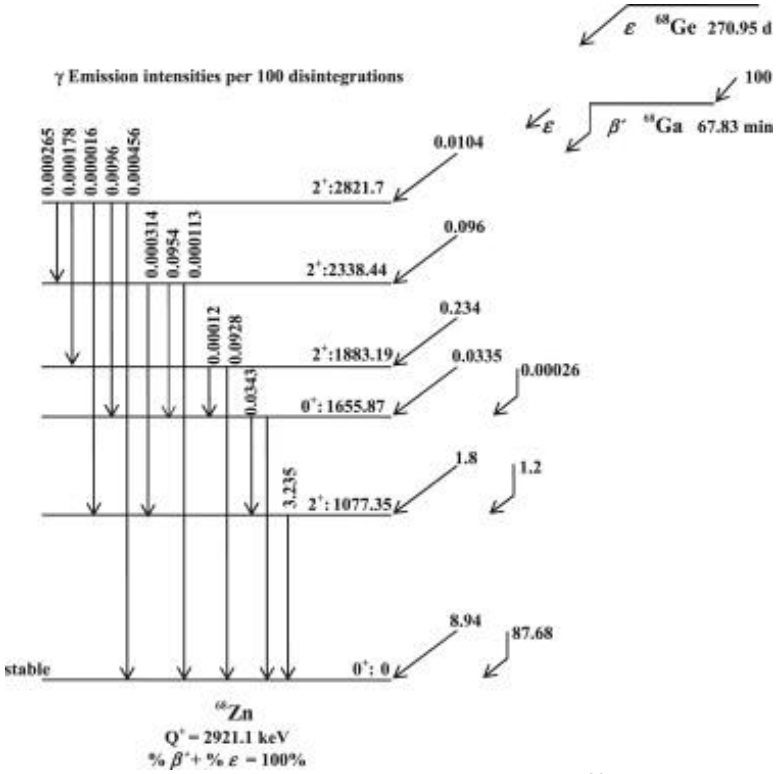

Figure 2-1: Gamma-ray emission probabilities for ^{68}Ga (Koskinas, 2014)

To effectively carry out neutron activation analysis there must be a sufficient number of activated atoms within a sample in order to attain ample measurements. The activation of samples is dependent upon several factors: (1) the neutron cross-sections of the isotopes present within the

sample; (2) the strength of the neutron flux incident on the sample during irradiation; and (3) the time with which the sample undergoes irradiation.

A microscopic cross-section, σ, is a numerical quantity that denotes the probability of a reaction taking place when a particle is incident on an atom. As seen in Figure 2-2, which shows a cross section spectrum for ^{113}Cd, cross-sections are dependent upon the energy of a neutron. Each stable isotope has a distinct cross-section spectrum, but there are several trends that are present among high Z and rare earth elements. For these elements the absorption cross-sections follow a *1/v* relationship for thermal energy neutrons. Above this energy region is the resonance energy region, where there are sharp increases in cross-section due to neutrons of these energies being more conducive for absorption due to specific quantum state criteria of the nuclide. At high energies, neutrons are less likely to be absorbed and thus the cross-section decreases. Thus, cross-sections can be divided into groups by two means: (1) by thermal, epithermal, and fast energy groups; and (2) by the type of reaction that is produced.

Microscopic cross-sections can describe a myriad of interactions with each one having its own characteristic cross-section: neutron scattering, radiative capture reactions, fission, etc. The total cross-section, σ_t, describes the total probability of any reaction taking place:

$$\sigma_t = \sigma_s + \sigma_i + \sigma_\gamma + \sigma_f + \sigma_{n,2n} + \cdots \quad (2\text{-}5)$$

The total microscopic cross-section can be simplified by grouping all cross-sections into two groups. The first group, the neutron scattering cross-section, σ_s, denotes the probability that a neutron will undergo an elastic or inelastic reaction. The second group, the total absorption cross section, σ_a, is the sum of all neutron absorbing reaction.

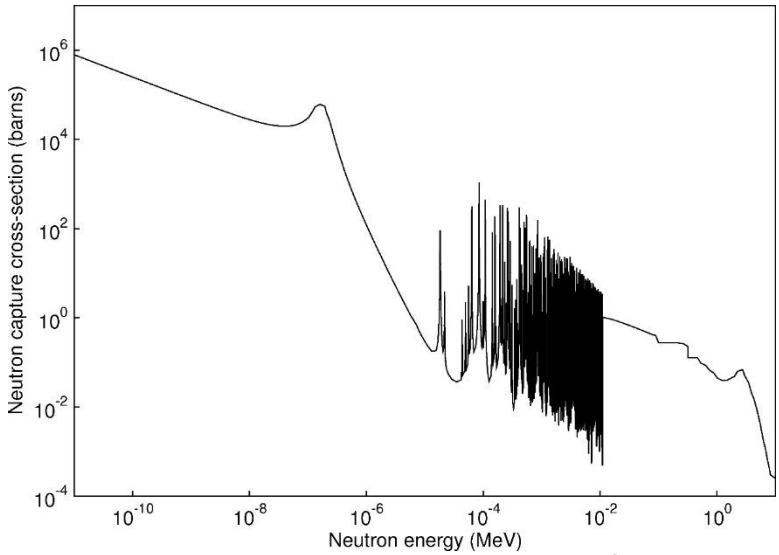

Figure 2-2: Neutron absorption cross-section for ^{113}Cd (NNDC, 2009)

A macroscopic cross-section, Σ, is a measure of the probability of an interaction occurring per unit path length through a sample of incident particles. The equation for the macroscopic cross-section is shown in Eq. (2-6), where *N* is the atom density of the target material in atoms per cubic centimeter, and microscopic cross-section is measured in units of barns, *b*, or 1×10^{-24}cm^2.

$$\Sigma = N\sigma \tag{2-6}$$

Both the macroscopic and microscopic cross-sections can be used to characterize the reaction rate that occurs within a sample during its irradiation. The rate of a specific reaction, R_n, can be calculated using the atom density of the sample, the microscopic cross-section of the sample, and the incident neutron flux, ϕ. The neutron flux is a measure of the total number of neutrons per square centimeter per second. The equation for the reaction rate for a reaction *n* is written as:

$$R_n = N\phi\sigma_n \tag{2-7}$$

By substituting the number density and microscopic cross-section for the macroscopic cross-section, Eq. (2-7) can be simplified to:

$$R_n = \phi \Sigma_n \quad (2\text{-}8)$$

Both Eqs. (2-7) and (2-8) assume a mono-energetic, homogenous neutron flux. However, neutron fluxes from nuclear reactors have their own neutron energy spectrum and are rarely mono-energetic. As both the neutron flux and the cross-section of the sample are energy dependent, Eq. (2-7) can be amended to account for all spectral neutron energies by integrating over all energies.

$$R_n = N \int_0^\infty \phi(E)\sigma_n(E)dE \quad (2\text{-}9)$$

This equation can be broken down into three components corresponding to the three different neutron energy groups. Simplified, the total reaction rate for a specific interaction is equal to the reaction rate due to thermal neutrons, the reaction rate due to epithermal neutrons, and the reaction rate due to fast neutrons.

$$R_n = R_{th} + R_{epi} + R_{fast} \quad (2\text{-}10)$$

In the irradiation of most samples fast neutrons are rarely present in neutron activation experiment facilities due to moderation and are seldom absorbed by nuclei and can therefore be ignored for most calculations. Additionally, by substituting Eq. (2-9) into the energy group reaction rates in Eq. (2-10) the reaction rate for a multi-energy group neutron flux can be created:

$$R_n = N \left[\int_{Th} \phi_{th}(E)\sigma_{th}(E)dE + \int_{Epi} \phi_{Epi}(E)\sigma_{Epi}(E)dE \right] \quad (2\text{-}11)$$

The thermal energy group is comprised of neutrons whose energy is below 0.5 eV. Below this energy neutron cross-sections are closely proportional to the inverse of the square-root of the neutron energy, $\frac{1}{\sqrt{E}}$. A neutrons energy can also be defined as its kinetic energy; the thermal cross-sections can be said to have a $\frac{1}{v}$ relationship, where v is the neutron's velocity. Thermal neutron

fluxes and cross-sections are typically resolved to discrete values, simplifying the integral seen in Eq. 2-11 to:

$$R_{Th} = N\phi_{Th}\sigma_{Th} \tag{2-12}$$

In contrast, the integral for the epithermal reaction rate is more difficult to solve. Inside the epithermal energy region many nuclides have large resonance peaks where neutron absorption is far more likely, with some isotopes having hundreds of resonances, as seen in Fig. 2-2. To more easily solve equations involving epithermal energy neutrons, a resonance integral, *I*, can be used for simplification. A resonance integral is an index of the epithermal neutron absorption by a material in a neutron flux. Most nuclear reactors that operate using thermal neutrons, like the TRIGA Mark II reactor used in this research, has some epithermal flux—present due to the slowing of fast energy neutrons to thermal energies. Similar to thermal flux, epithermal neutron flux behaves closely as a function of $\frac{1}{E}$ inside of the epithermal region; resonance integrals can be defined with respect to this flux distribution, seen in Eq. (2-13) (Baumann, 1963).

$$I_o = \int_{Epi} \frac{\sigma(E)}{E} dE \tag{2-13}$$

The lower bound energy used in Eq. (2-13) is defined as the lowest energy that is in the epithermal range, or the effective Cadmium cut-off energy: 0.5 eV. The upper bound of the integral is the end of the epithermal energy region: 0.5 MeV. By defining the resonance integral to have a $\frac{1}{E}$ relationship, the neutron flux within the epithermal region can be—instead of varying with energy—made to be a constant within the integral:

$$R_{Epi} = N\phi_{Epi} \int_{Epi} \frac{\sigma(E)}{E} dE \tag{2-14}$$

The epithermal reaction rate can be simplified to:

$$R_{Epi} = N\phi_{Epi}I_o \quad (2\text{-}15)$$

Applying Eq. (2.15) to Eq. (2-10), the reaction rate within a sample can be simplified to:

$$R_n = N\phi_{Th}\sigma_{Th} + N\phi_{Epi}I_o \quad (2\text{-}16)$$

It is useful to combine the thermal and epithermal fluxes and cross-sections, to more easily make NAA calculations. Doing so integrates the product of the neutron absorption cross-section and the neutron flux over the desired energy range. This result, $\phi\sigma_o$, is the total neutron flux multiplied by the average neutron cross-section for a specific energy range. The reaction rate within a sample can now be defined as:

$$R_n = N\phi\sigma_o \quad (2\text{-}17)$$

The purpose of NAA, is to identify gamma-rays that are released by radionuclides as they decay. The rate of change in the total amount of a radionuclide is therefore a function of its production and its decay

$$\frac{dN'}{dt} = N\phi\sigma_o - \lambda N' \quad (2\text{-}18)$$

where N' is the total amount the new radionuclide, and λ is its decay constant. The integration of Eq. (2-18) over a given time period, t_i, results in the total amount of a nuclide present during an irradiation of time t_i.

$$N'(t) = \frac{N\phi\sigma_o}{\lambda}(1 - e^{-\lambda t_i}) \quad (2\text{-}19)$$

Counting of radioactive samples takes place after irradiation which results in further decay of the sample. Often, samples are more radioactive than desired, and will over-saturate a detector when counted, which results in poor data collection due to high dead-time in the detector. A decay time

correction factor, t_d, can be implemented to allow for the sample to decay to a more reasonable level of activity before it's counted. This correction allows for correcting the measured value to determine the original activity of the sample. Similarly, a counting time correction factor, t_c, accounts for the sample decaying during the time the sample is being counted. These two correction factors were added to Eq. (2-19) in Eq. (2-20).

$$N'(t) = \frac{N\phi\sigma_o}{\lambda} \cdot (1 - e^{-\lambda t_i}) \cdot e^{-\lambda t_d} \cdot (1 - e^{-\lambda t_c}) \quad (2\text{-}20)$$

To ultimately determine the concentrations of elements within a sample there are several additional correction factors that need to be added. Firstly, the gamma-ray that is measured by the detector is specific to a stable isotope of an element, which has its own isotopic abundance, θ. Secondly, each gamma-ray has its own specific intensity, I_γ, which must be added. Lastly, the detectors efficiency, ξ, must be considered.

$$N'(t) = \frac{N\phi\sigma_o}{\lambda} \cdot (1 - e^{-\lambda t_i}) \cdot e^{-\lambda t_d} \cdot (1 - e^{-\lambda t_c}) \cdot \theta \cdot I_\gamma \cdot \xi \quad (2\text{-}21)$$

The product of λ and $N'(t)$ is the activity of a sample at time *t*, $A'(t)$. Solving for *N* results in determining the total number of atoms of a specific nuclide within the sample.

$$N = \frac{A'(t)}{\phi\sigma_o} \cdot \frac{1}{\theta I_\gamma \xi} \cdot (1 - e^{-\lambda t_i})^{-1} \cdot e^{\lambda t_d} \cdot (1 - e^{-\lambda t_c})^{-1} \quad (2\text{-}22)$$

Dividing by Avogadro's Number, N_A, and multiplying by the atomic mass, M, of the element that is being inspected results in the total mass of the element, m, present within the sample.

$$m = \frac{A'(t)}{\phi\sigma_o} \cdot \frac{1}{\theta I_\gamma \xi} \cdot \frac{M}{N_A} \cdot (1 - e^{-\lambda t_i})^{-1} \cdot e^{\lambda t_d} \cdot (1 - e^{-\lambda t_c})^{-1} \quad (2\text{-}23)$$

An experimental method, known as the comparator method, can be implemented to sidestep evaluating Eq. (2-23) using an irradiated standard as a comparator (Kafala, 2007). By irradiating

a standard reference material with known concentrations, a reference activity measurement can be made. If the standard was irradiated and counted in identical conditions—like irradiation times, count times, and detector geometries—a ratio can be made to determine the concentration of the sample:

$$\frac{m_{st}}{m_{sm}} = \frac{A\prime_{st}(t)}{A\prime_{sm}(t)} \tag{2-24}$$

where *st* denotes the standard and *sm* denotes the sample. By adjusting Eq. (2-24) the mass of the inspected element can be ascertained:

$$m_{sm} = m_{st}\frac{A\prime_{sm}(t)}{A\prime_{st}(t)} \tag{2-25}$$

The comparator method assumes a standardized neutron flux throughout the entire sample. In the irradiation of most samples the neutron flux is only slightly perturbed by neutron absorption within the material, and it remains homogeneous throughout. For samples that contain elements with large cross-sections this perturbation can have drastic effects on the neutron flux within the sample and effect the total activation. The result is a sample whose calculated isotopic composition is much less than expected. Two samples with identical concentrations of ^{157}Gd, with a thermal absorption cross-section above 250000 barns, and either isotope of stable Cerium whose cross-sections are both less than 1 barn, will have vastly differing measurements due to the change in average neutron flux.

There have been many attempts to develop methods to address neutron self-shielding within samples. Both correction factors and general equations have been developed to improve NAA measurements. Correction factors work by using a reference sample with a small concentration of the desired element, to minimize the self-shielding effects, and extrapolating data for comparison

with experimental measurements made from higher concentrations. The desired result is a numerical quantity, f, that accounts for the change in average neutron flux, ϕ_{avg}, with respect to the assumed neutron flux, ϕ_{∞}, shown in Eq. (1-3).

The first algorithms for modeling neutron fluxes were developed to calculate the perturbed-to-unperturbed thermal reaction rate. Early attempts at universal self-shielding equations focused on thermal neutrons and solving for the thermal self-shielding factor, G_{th}, for various sample geometries (Stewart, 1958)

The equation for the activity produced by a sample after an irradiation that accounts for neutron self-shielding is given by:

$$A = N_o \sigma_{th} \phi_{th} (G_{th} + G_{epi} \frac{Q_o}{f})(1 - e^{-\lambda t_i}) \quad (2\text{-}26)$$

In Eq. (2-26), N_o is the number of target nuclei, $Q_o$is the ratio of the resonance integral to the thermal neutron absorption cross-section, f is equal to $\frac{\varphi_{th}}{\varphi_{epi}}$, where φ_{th} and φ_{epi} are the unperturbed thermal and epithermal fluxes inside the sample, and G_{th} and G_{epi} are the thermal and epithermal self-shielding factors.

Self-shielding factors have evolved since their introduction by Zweifel in the 1950s. Research into the area by Gonclaves (2004) proposed the use sigmoid function to solve for these parameters. The evolution of that work eventually resulted in the equation for the thermal self-shielding facto, G_{th},

$$G_{th} = \frac{1}{1+\left(\frac{N_{Av} k_{th}}{r(r+h)} \Sigma \frac{m_i \sigma_{abs,i}}{M_{at,i}}\right)^{0.964}} \quad (2\text{-}27)$$

and the equation for the epithermal self-shielding factor, G_{epi},

$$G_{epi} = \frac{0.94}{1+\left(\frac{mN_{Av}k_{epi}\sigma_{abs,epi}}{r(r+h)M_{at,i}}\right)^{0.82}} + 0.06 \quad (2\text{-}28)$$

In these equations. m is the mass of an element, N_{Av} is Avogadro's number, k_{th} and k_{epi} are the thermal and epithermal self-shielding constants, r and h are the radius and height of a cylindrical sample, and M is the atomic mass of an element. Additional experiments found the thermal and epithermal self-shielding constants to be on average 0.91 and 1 (Chilian, 2008). The equation for the epithermal self-shielding factor ignores shielding by other elements in a sample as it is usually negligible due to the discrete resonances usually will not overlap.

The total effective self-shielding factor, G_{eff}, is a weighted average of Eqs. 2-28 and 2-29, as the amount of thermal and epithermal neutrons within a reactor is not equal; epithermal neutrons make up 5-10% of total neutrons within the RSR in UT's TRIGA reactor (Graham, 2011).

$$G_{eff} = \frac{f}{f+Q_o}G_{th} + \frac{Q_o}{f+Q_o}G_{epi} \quad (2\text{-}29)$$

Combining Eqs. (2-28), (2-29) and (2-30) gives:

$$G_{eff} = \frac{f}{f+Q_o}\left[\frac{1}{1+\left(\frac{N_{Av}k_{th}}{r(r+h)}\Sigma\frac{m_i\sigma_{abs,i}}{M_{at,i}}\right)^{0.964}}\right] + \frac{Q_o}{f+Q_o}\left[\frac{0.94}{1+\left(\frac{mN_{Av}k_{epi}\sigma_{abs,epi}}{r(r+h)M_{at,i}}\right)^{0.82}} + 0.06\right] \quad (2\text{-}30)$$

The epithermal neutron absorption cross-section, $\sigma_{abs,epi}$, is a parameter defined as:

$$\sigma_{abs,epi} = 0.1945\theta\frac{\sum w_i\left[\sigma_{tot,i}(E_{res,i})\sqrt{\frac{\Gamma_\gamma}{\Gamma}}\right]}{\sum w_i} \quad (2\text{-}31)$$

In Eq. (2-31), Γ and Γ_γ is the total and radiative resonance width, θ is the isotopic abundance, and $\sigma_{tot,i}(E_{res,i})$ is the total cross-section at the peak of resonance i. The weighting factor w_i is defined as:

$$w_i = \left[\frac{\Gamma_\gamma}{E_{res}^2}\frac{(2J+1)\Gamma_n}{(2I+1)\Gamma}\right] \quad (2\text{-}32)$$

where Γ_n is the neutron resonance width, and *J* and *I* are the spins of the resonance state and target nucleus. The weighting factor is proportional to $\frac{1}{E_{res}^2}$, which gives greater relative weight to resonances that appear at lower energies (Salgado, 2004).

Chilian continued this process by creating a computer code that can automatically produce self-shielding factors based upon a sample's dimensions and isotopic composition. This computer code utilizes the aforementioned method of calculating self-shielding factors, G_{eff}.

Using the effective self-shielding factor, G_{eff}, as a correction factor, it can be added to Eq. (2-21). The resulting equation calculates the total number of activated nuclei in the sample after correcting for self-shielding effects.

$$N'(t) = \frac{N\phi\sigma_o}{\lambda} \cdot (1 - e^{-\lambda t_i}) \cdot e^{-\lambda t_d} \cdot (1 - e^{-\lambda t_c}) \cdot \theta \cdot I_\gamma \cdot \xi \cdot G_{eff} \quad (2\text{-}33)$$

By multiplying by the decay constant of the produced radionuclide, the total activity after an irradiation and some decay and counting time is

$$A'(t) = N\phi\sigma_o \cdot (1 - e^{-\lambda t_i}) \cdot e^{-\lambda t_d} \cdot (1 - e^{-\lambda t_c}) \cdot \theta \cdot I_\gamma \cdot \xi \cdot G_{eff} \quad (2\text{-}34)$$

To analyze the results obtained from the count of each sample, the comparison method can be used to compare the self-shielding effects in different samples. By setting sample with the lowest concentration of neutron absorbing materials, and therefore the lowest amount of self-shielding, as the standard comparator the comparison method can be used for analysis. Applying Eq. (2-25) to each sample, where m_{st} is the lowest concentration sample, concentrations can be determined for each sample. As the true value of each sample is known, a correction factor can be made that

compares the difference between the experimentally determined concentration and the actual concentration, f. This correction factor is comparable to G_{eff}.

II.II MCNP

It is difficult to manually calculate particle transport through media and systems, as the neutron diffusion equation becomes increasingly more difficult to solve when working in three-dimensional space with intricate geometries and in the presence of strong sources or sinks of neutrons. To help solve these problems, Los Alamos National Laboratories created and continuously updates Monte Carlo N-Particle (MCNP) code.

Monte Carlo codes are broad based computational methods that rely on repeated samplings to obtain results. The Monte Carlo process is the implementation of randomness within a system to gain approximate solutions to complex problems.

In MCNP, a neutron, or any other particle of interest, is placed within a system with given starting conditions. The code tracks the particle through the system from its generation to its end. The particle's history can end when it leaves the system, is absorbed, etc. Each time a particle is started in the system the code tracks each of its collisions until it reaches its end, this marks the end of its history. After this, another particle is placed in the system and another history begins. MCNP will run a predetermined number of histories that has been requested by the user, usually until the uncertainties of the results reach a desired limit.

Each MCNP code is called a deck, reminiscent of initial methods of computation which utilized punch cards. Similarly, each function that can be added to a deck—specifying conditions, source

type, or any other system characteristics—are called cards. MCNP decks are broken into three sections: cell cards, surface cards and data cards. Surface and cell cards are used to create the system within the code, with each cell being created from specified surfaces. Data cards are used to define the particle source, which results to measure, how to investigate the measurements, and materials.

Results generated by MCNP are called tallies, which can be representative of several different conditions depending upon the type of tally card that is instituted. Tally cards can be used to calculate the neutron flux within a volume—an F4 tally—or the neutron current through a surface—an F2 tally. The addition tally multiplier card, FM, can add a response function to the measured tally or be used to measure the amount of a specific interaction occurring at or within a cell or surface. Each output produced by MCNP include an associated error that is based upon each of the calculation made within the code. This associated error allows for a quick determination of the accuracy of the data collected from the code. High uncertainty can usually be remedied by increasing the amount of histories that are run.

To accurately model NAA and the self-shielding effects within an NAA, a source representative of the neutron flux spectrum inside the University of Texas (UT) reactor must be determined. A deck modeling UT's TRIGA Mark II reactor can be used to create this source definition. The deck utilizes the data card KCODE to specify that the system defined in the deck has a criticality source. The code uses fissions from previous histories as starting places for future particles. The flux spectrum is then measured at the surface of the experiment facility—using the F2 tally card—where sample irradiation takes place, in this case cell 1301. The code looks specifically at neutron current moving through the surface due to the designator *N*:

```
F2:N    1301
```

C2 0 1

E2 1e-10 400log 20

The C2 card shown above measures the directionality of the current of neutrons entering surface 1301. Similarly, The E2 card places the particles moving through surface 1301 into different energy bins between $1 \times 10^{-10} MeV$ and $20\ MeV$. To increase accuracy additional energy bins were placed within the epithermal and thermal energy ranges.

This spectrum can be exported to a separate deck that models the sample. In the second deck the source is defined with an energy spectrum resembling that found from the first. This is done using the ERG parameter for the SDEF—source definition—card.

SDEF SUR=201 PAR=1 ERG=d1 DIR=1 NRM=-1

In the SDEF card there are several conditions that are stated that signify how the source behaves in the system. The SUR parameter means that the source is emanating from the surface 201. The PAR parameter signifies that particle type 1, neutrons, is leaving the surface. The ERG parameter is stating that the neutrons have an energy distribution, d1. The flux tallies for each energy found from the reactor code were used for defining the d1 distribution. The DIR and NRM parameters show that the neutrons are leaving the surface inwardly normal to the surface. An F4 tally card is added to the deck to measure the total neutron flux within the cell that defines the sample undergoing irradiation: cell 2. The addition of an FM4 card, with the 102 reaction parameter, calculates the total number of radiative capture reaction occurring within the cell specified in the F4 tally. Due to the utilization of the FM4 card, the tallies produced from MCNP will be in units of $\frac{neutrons}{cm^3 \cdot atom \cdot source\ particle}$.

F4:N 2

FM4 (-3.33543E-07 3 102)

When calculating these reactions, MCNP refers to a library of cross-sections data within the program. Depending upon the materials that are listed and the types of reactions that are occurring, different libraries may need to be called order to use the correct cross-section data. These are specified by including a string of number at the end of the material ID. For the purposes of this research, the libraries that are to be used are the ENDF neutron continuous-energy cross-section. To call this library, each material ID will be followed by: .80c. For example, to use this cross-section library when using Lanthanum-139 the material would be listed as:

M3 57139.80c

Unfortunately, the ENDF libraries do not include neutron continuous-energy cross-section data for Ytterbium. Thus, MCNP cannot be used to verify the self-shielding factors found experimentally. Instead, Ytterbium will solely be verified using values received from Dr. Chilian, (Slowpoke Reactor, Ecole Polytechnique, Montreal, Canada) using her self-shielding calculation program.

III Experimental

The objective of this research is to analyze the effects of neutron self-shielding in samples containing lanthanides when conducting NAA. The samples were prepared using different liquid standards which were diluted to varying concentrations. Each standard was an aqueous solution of a different lanthanide and had a concentration of 10000 μg/g. The concentrations of each sample varied from 10 to 10000 μg/g, with each lanthanide element—with the exception of promethium, which does not occur naturally—having a total of 10 samples. The procedure for the preparation, irradiation and measurement of each element was as follows:

1. Pipette out a set volume of standard from the standard container and discharge it into a small 2/5 dram vial
2. Fill the 2/5 dram vial with rare-earth standard so that total volume within the vial is 1 mL
3. Steps 1 and 2 should be completed until there are 10 total samples containing approximate concentrations of: 10000, 7500, 5000, 2500, 1000, 500, 250, 100, 50 and 10 μg/g
4. Heat seal each 2/5 dram vial in a thin plastic bag
5. Insert each 2/5 dram vial into a larger 2 dram vial
6. Place each vial into an RSR vial
7. Insert each RSR vial into the rotary specimen rack (Figure 3-1), ensuring that the samples are evenly distributed between the sample slots
8. Irradiate the samples in the RSR until the samples are of an appreciable activity. Each set of samples were irradiated for different power levels—100, 500, or 950 kW—depending on their absorption cross-sections and half-lives

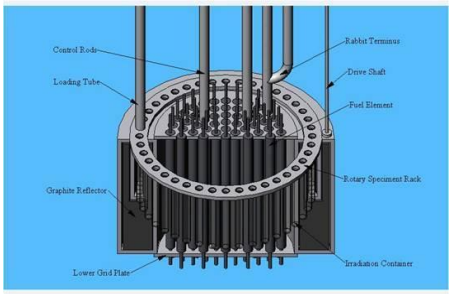

Figure 3-1: Rotary Specimen Rack (Landsberger, 2019)

9. Remove the samples from the core and let decay until the samples are ready to be counted.
10. Using a High Purity Germanium (HPGe) detector, measure the activity of each sample. Each sample was counted until a total number of counts for the peak of interest has reached 10,000—done by increasing the count time for samples with lower activities
11. Upon completion of each count, ensure that the deadtime of the detector was limited to below 30%
12. After collecting the data from each set of counts, correct the net counts by accounting for decay and count times to acquire measured activation rates for each sample.

Each step of the previously listed procedure was to be conducted for each of the following elements: lanthanum, cerium, neodymium, praseodymium, samarium, europium, gadolinium, terbium, dysprosium, holmium, erbium, thulium, ytterbium, and lutetium.

IV Results and Discussion

IV.I Self-Shielding Factor Determination

Neutron self-shielding correction factors were calculated by experimentally measuring the activities of samples of varying concentrations and comparing these values to two different computer models. These models, explained in the previous sections, were used as comparison tools to evaluate the perceived accuracy of the experimental data.

The experiment called for the irradiation of samples of 14 different elements—10 samples of varying concentrations for each element—equaling a total of 140 distinct samples. The elements chosen for irradiation comprised of all the naturally occurring elements that are a part of the lanthanide group of elements. With the exception of promethium, which is not naturally occurring, samples of all elements between lanthanum and lutetium were investigated. Upon irradiation each sample was counted until a total of at least 10,000 counts in the peak of interest was measured. By dividing the total number of counts by the counting time, it was possible to determine the activity of each sample. The activity of each sample was then corrected based upon its counting and decay time with respect to the first sample measured of each element.

The total measured activity for each sample can be seen in Tables 4-1 and 4-2. The concentrations listed are the desired concentrations, not actual values for each sample; the standards used were not exactly at 1% concentration, but the same dilution methods were used throughout the experiment. For more precise values of each sample refer to Appendix A for charts of each elements.

Each element that was investigated during this experiment expressed a negative concavity second order polynomial relationship. For elements with large cross-sections, like gadolinium, the

polynomial was significantly more pronounced, meaning that the calculated activity at higher concentrations showed significant deviations from a linear relationship. For elements with low cross-sections, like ytterbium, the polynomial expression was much more representative of a linear relationship as concentrations of the rare earth element were increased within the solution. Graphs of the activities of both sets of samples—gadolinium and ytterbium—can be seen in Figure 4-1 and Figure 4-2. Graphs for the other tested elements can be seen in Appendix B.

Table 4-1: Activity in Becquerels of Each Sample

µg/g	La	Ce	Nd	Pm	Sm	Eu
10000	3205.5	459.9	430.5	552.3	3207.1	1435.0
7500	2362.9	349.0	335.0	440.3	2470.3	1115.3
5000	1628.1	247.5	226.9	300.0	1809.0	783.5
2500	826.4	114.6	114.1	149.8	974.2	347.6
1000	364.8	51.2	46.7	64.3	384.1	172.8
500	168.5	24.9	11.1	32.3	270.7	87.6
250	83.5	14.1	22.1	15.2	200.0	42.9
100	31.5	6.1	4.5	6.0	112.6	16.7
50	15.8	-	-	3.1	59.6	8.7
10	3.9	-	-	0.7	15.1	1.9

Table 4-2: Activity in Becquerels of Each Sample Continued

Gd	Tb	Dy	Ho	Er	Tm	Yb	Lu
169.5	185.5	26023.8	3687.1	1453.9	2244.4	716.1	2739.5
145.5	142.7	20084.0	2802.0	1116.9	1707.4	541.2	2063.9
111.4	94.1	13368.0	1857.1	730.3	1116.2	360.6	1357.5
69.0	47.3	6887.7	962.5	366.7	564.9	179.9	702.4
156.3	19.5	2582.6	413.1	150.0	247.2	76.5	284.6
16.9	10.1	1423.9	212.1	75.5	117.0	41.0	143.0
8.5	4.6	701.2	95.8	37.3	59.7	18.4	69.9
4.1	1.5	***702.4***	38.5	17.1	15.7	7.2	26.0
2.3	0.9	142.4	18.5	2.3	11.2	3.6	***3.8***
1.0	0.2	29.9	4.4	2.5	2.3	0.8	***0.8***

To determine the self-shielding effects for each Gadolinium concentration, the activity and concentration of each sample needed to be compared to a standard reference value. For this experiment, each set of samples were compared to the activity of the sample with the lowest concentration. With the exception of cerium and neodymium, which used the comparison value of 100 µg/g, each element was compared to the sample with 10 µg/g concentration.

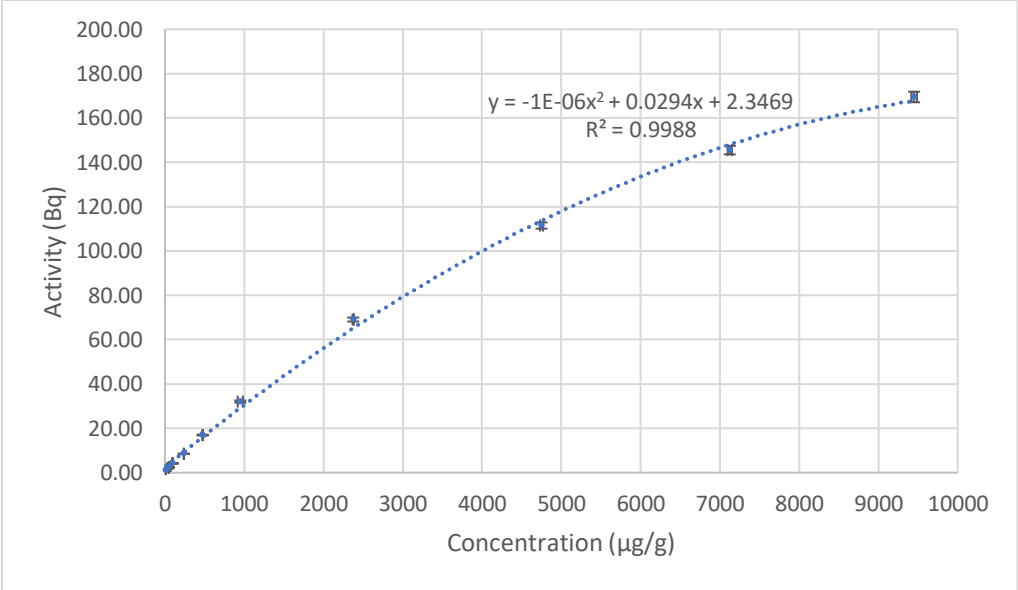

Figure 4-1: Gadolinium Concentration vs Activity

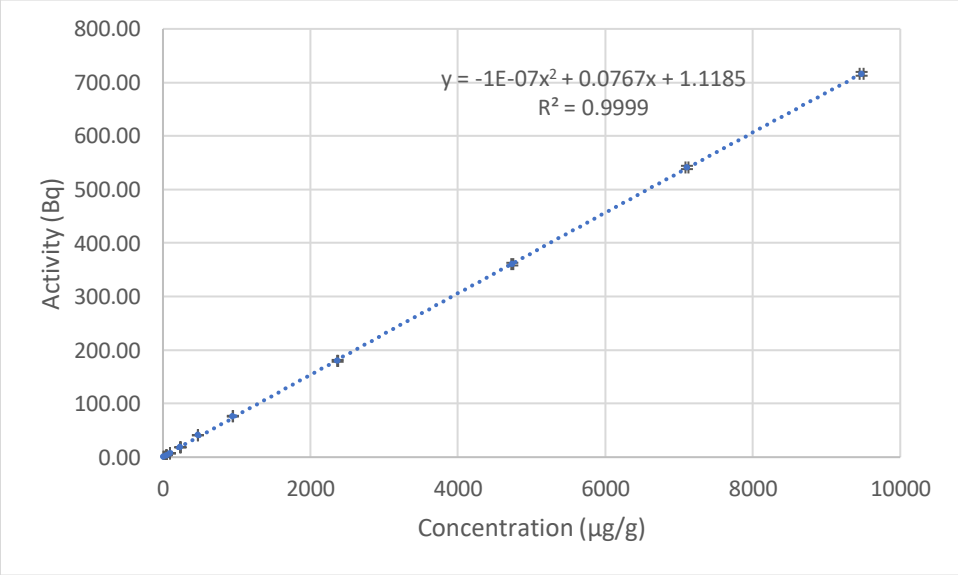

Figure 4-2: Ytterbium Concentration vs Activity

The comparisons of the samples began with normalizing a sample's concentration to that of the standard. For example, the normalized value of a sample with a concentration of 10,000 µg/g would be the quotient of 10,000 µg/g and 10 µg/g, which is 1,000. The activity of each sample is similarly normalized. The normalized activities were then divided by the normalized concentrations to determine the self-shielding factor. Tables 4-3 and 4-4 show the calculated self-shielding factors that were calculated by this normalization method. More comprehensive tables for the determination of these values for each element can be found in Appendix C.

Table 4-3: Calculated Self-Shielding Factors

µg/g	La	Ce	Nd	Pr	Sm	Eu
10000	0.9639	0.903	0.967	0.925	0.6862	0.741
7500	0.9474	0.914	0.999	0.984	0.7299	0.768
5000	0.9791	0.972	1.015	1.005	0.7766	0.81
2500	0.994	0.9	1.021	1.004	0.8659	0.718
1000	1.0969	1.005	1.044	1.077	0.8567	0.941
500	1.0132	0.978	0.991	1.083	0.8559	0.954
250	1.0042	0.989	0.988	1.022	0.9079	0.93
100	0.9964	1	1	1	0.92	0.907
50	1.0004	-	-	-	0.968	0.937
10	1	-	-	-	1	1

Table 4-4: Calculated Self-Shielding Factors Continued

Gd	Tb	Dy	Ho	Er	Tm	Yb	Lu
0.388	0.969	0.871	0.957	0.973	0.963	0.9	0.979
0.468	0.994	0.896	0.97	0.997	0.977	0.91	0.984
0.538	0.991	0.894	0.964	0.978	0.958	0.91	0.971
0.666	0.988	0.922	0.999	0.982	0.969	0.91	1.004
0.419	1.018	0.864	1.072	1.004	1.061	0.96	1.017
0.814	1.05	0.953	1.101	1.01	1.004	1.03	1.022
0.817	0.95	0.938	0.994	1	1.024	0.93	1
1	0.799	***2.35***	1	-	***0.67***	0.91	-
-	0.9	0.953	-	-	0.958	0.91	-
-	1	1	-	-	1	1	-

As seen in Tables 4-3 and 4-4, there are some calculated self-shielding factors, specifically for lutetium, that are not consistent with expected values. For these elements the values were significantly larger than expected. With a cross-section of 6.6 barns, it was expected that the second order polynomial for Lutetium would have much less curvature than that of other elements.

Additionally, the values calculated for lutetium make a significant jump between 50 and 100 µg/g. These errors are indicative of an error in the preparation of the 50 and 10 µg/g samples; using a different comparison concentration can adjust these values to make them more representative of what is occurring within the solution during irradiation.

There were several individual samples for which the calculated self-shielding value deviated from the trends expressed by the rest of the samples in each set. These values are bolded in Tables 4-3 and 4-4. All of these values are for samples which contained 100 µg/g of the lanthanide or less. As stated previously, this is indicative of an error when preparing these samples. All samples

containing 250 µg/g or less were created by diluting the standard two times and filling a 50 mL beaker with deionized water. Both of these actions would increase the potential error in these samples' results.

Other elements which showed a divergence from the expected values include: praseodymium, gadolinium, holmium, and erbium. For these elements, different samples were used as the standards. For praseodymium, gadolinium and holmium, the samples with a concentration of 100 µg/g were used as the comparison standard. For erbium and lutetium, the samples with a concentration of 250 µg/g were used. Using these new standards, new self-shielding values were calculated. These new self-shielding factors can be seen in Table 4-5.

Table 4-5: Alternative Self-Shielding Factors for Praseodymium, Gadolinium, Holmium, Erbium and Lutetium

µg/g	Pr	Gd	Ho	Er	Lu
10000	0.925	0.388	0.957	0.973	0.979
7500	0.984	0.468	0.970	0.997	0.984
5000	1.005	0.538	0.964	0.978	0.971
2500	1.004	0.666	0.999	0.982	1.004
1000	1.077	0.419	1.072	1.004	1.017
500	1.083	0.814	1.101	1.010	1.022
250	1.022	0.817	0.994	1.000	1.000
10	1.000	1.000	1.000	-	-

The results from the experiments clearly show a relationship between the cross-sections of the isotopes present in the solution and the self-shielding effects exhibited by the samples. Elements with large cross-sections, like gadolinium and europium, exhibit significant self-shielding effects that quickly manifest as the concentrations are increased within the samples. Conversely, elements with low cross-sections exhibit little to no self-shielding effects.

The self-shielding factors represent the average neutron flux moving through the sample compared to what the flux is in the surrounding environments. For application during NAA, any counting data ascertained during a count would be divided by these neutron self-shielding factors as a correction factor, similar to decay and counting time corrections.

IV.II MCNP Self-Shielding Verification

After compiling a list of self-shielding factors from the experimental data, the results were evaluated using data sets generated using MCNP. To calculate these values, two decks needed to be created. To more accurately model the irradiation of the samples within the core the first code models the reactor and its experiment facilities and utilized KCODE to compile an energy spectrum with a corresponding flux tally. This energy spectrum was reflective of the neutron flux entering the RSR sample rack. The flux spectrum that was created by this code can be seen in Figure 4-3, and a more extensive summary of this code can be seen in Appendix H.

The energy spectrum seen above was then copied into a second MCNP deck. This second deck can be seen in Appendix H. This code must be run for each sample, as parameters within the code need to be changed to be representative of each sample.

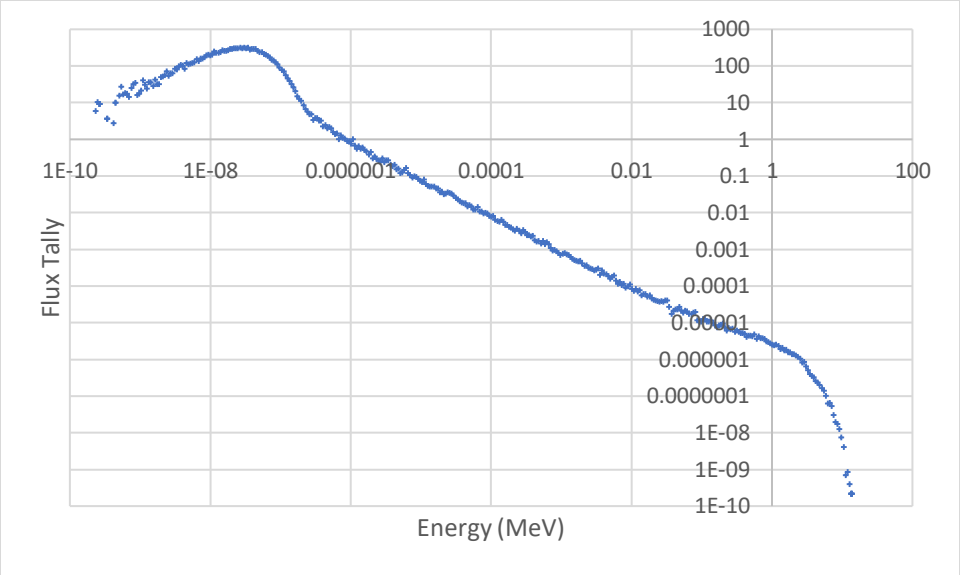

Figure 4-3: Energy Spectrum within Reactor RSR Created using MCNP KCODE

In preparation for each element there were a few parameters that needed to be added or removed from the code. First, the number of materials within the code need to reflect the number of isotopes of each element. When changing the deck from calculating the neutron absorption in a sample of lanthanum to a sample of samarium the material's list would change from:

```
M1    6000.60c    1              $C
      1001.60c    2              $H      HDPE
c
M2    57139.80c      7500        $La
      1001.60c       1985000     $H
      8016.60c       992500      $O
c
M3    57139.80c      7500        $La
```

To:

```
M1    6000.60c    1          $C
      1001.60c    2          $H      HDPE
```

```
c
M2    62144.80c      307
      62147.80c     1499
      62148.80c     1124
      62149.80c     1382
      62150.80c      738
      62152.80c     2675
      62154.80c     2275
      1001.60c   1985000     $H
      8016.60c    992500     $O
c
M3    62144.80c      307
M4    62147.80c     1499
M5    62148.80c     1124
M6    62149.80c     1382
M7    62150.80c      738
M8    62152.80c     2675
M9    62154.80c     2275
```

Additionally, when changing the concentration of the lanthanide within the sample, the atomic fraction of hydrogen and oxygen needs to be changed relative to the amount of the lanthanide in the sample. For example, when there are 10 atoms of lanthanide in the solution, there would be 999990 atoms of Oxygen and 1999980 atoms of hydrogen. When adjusting the concentration to 10000 atoms of the lanthanide, the amount of oxygen would be changed to 990000 atoms, and the amount of hydrogen would be changed to 1980000 atoms.

To allow for the evaluation of the absorption of neutrons in each isotope within the sample, a second change needed to be made. The previous change allowed for the specific calling of each isotope for its tallying of neutron absorption when the deck is run. The second change, shown below, instructs the code to tally the number of absorptions occurring in each isotope. As in the previous example, the original case evaluates a sample of lanthanum and the change is made to evaluate a sample of samarium.

```
FM4      (-0.000245767 3 102)
```

To:

```
FM4      (-0.000331095 3 102) (-0.000331095 4 102)
         (-0.000331095 5 102) (-0.000331095 6 102)
         (-0.000331095 7 102) (-0.000331095 8 102)
         (-0.000331095 9 102)
```

As there is only one stable isotope of Lanthanum, La-139, there is only one set of tally multipliers (FM4). For Samarium code, shown second, there are a total of seven sets of tally multipliers, one for each isotope of Samarium.

In each set of multipliers, the first term is representative of the total number of atoms of the element multiplied by one barn. The second term indicates to the multiplier which material to analyze. The last term, 102, instructs MCNP to analyze the radiative capture cross-section of these elements, and does not change when analyzing different samples in MCNP. When changing the code to represent a different sample, the first term needs to be adjusted in order to indicate the change in the number of atoms within the sample. The second term corresponds to the material numbers of the isotopes that are being investigated.

The final change that needed to be made between each run was pertaining to the density of the cell which represented the rare-earth solution. The density of the cell slightly adjusts how neutrons diffuse through the cell, and thus requires changing for different samples.

2 2 -1.035873 +5 -6 -103 Vol=9.76264

To:

2 2 -1.062430 +5 -6 -103 Vol=9.76264

With the changes made, each sample can be analyzed using MCNP. MCNP outputs the tally values in strings corresponding to each tally multiplier set. The summation of these can be used to determine the total number of absorptions within the sample by the element. The results of the code can be seen in Tables 4-6 and 4-7.

Table 4-6: Total MCNP Tally for each Sample

µg/g	La	Ce	Pr	Nd	Sm	Eu
10000	4.32E-06	6.29E-06	5.69E-06	1.90E-04	7.79E-03	1.80E-03
7500	3.29E-06	4.74E-06	4.30E-06	1.40E-04	7.15E-03	1.60E-03
5000	2.22E-06	3.18E-06	2.89E-06	9.68E-05	6.17E-03	1.31E-03
2500	1.13E-06	1.60E-06	1.46E-06	4.88E-05	4.35E-03	8.39E-04
1000	4.55E-07	6.42E-07	5.87E-07	1.96E-05	2.31E-03	4.08E-04
500	2.28E-07	3.21E-07	2.94E-07	9.84E-06	1.29E-03	2.20E-04
250	1.14E-07	1.61E-07	1.47E-07	4.92E-06	6.85E-04	1.14E-04
100	4.58E-08	6.44E-08	5.88E-08	9.85E-07	2.85E-04	4.68E-05
250	2.29E-08	3.22E-08	2.94E-08	9.86E-07	1.44E-04	2.36E-05
100	4.58E-09	6.44E-09	5.89E-09	1.97E-07	2.91E-05	4.76E-06

As mentioned in Section II.II, the ENDF cross-section libraries that are used for MCNP do not include neutron continuous-energy cross-section data for ytterbium. Consequently, it is impossible to take a tally of ytterbium by standard means. Summarily, self-shielding factors of ytterbium cannot be calculated via MCNP.

Table 4-7: Total MCNP Tally for each Sample Continued

Gd	Tb	Dy	Ho	Er	Tm	Yb	Lu
8.57E-03	1.74E-05	1.46E-03	3.95E-05	4.30E-04	6.36E-05	-	2.04E-05
8.38E-03	1.33E-05	1.16E-03	3.03E-05	3.28E-04	4.92E-05	-	1.56E-05
8.03E-03	9.01E-06	8.28E-04	2.07E-05	2.25E-04	3.41E-05	-	1.07E-05
7.12E-03	4.61E-06	4.44E-04	1.06E-05	1.15E-04	1.80E-05	-	5.46E-06
5.36E-03	1.87E-06	1.86E-04	4.31E-06	4.67E-05	7.58E-06	-	2.22E-06
3.79E-03	9.41E-07	9.42E-05	2.17E-06	2.35E-05	3.88E-06	-	1.12E-06
2.39E-03	4.71E-07	4.75E-05	1.09E-06	1.18E-05	1.96E-06	-	5.60E-07
1.13E-03	1.89E-07	1.91E-05	4.36E-07	4.71E-06	7.92E-07	-	2.24E-07
6.03E-04	9.45E-08	9.56E-06	2.18E-07	2.36E-06	3.97E-07	-	1.12E-07
1.27E-04	1.89E-08	1.91E-06	4.36E-08	4.71E-07	7.96E-08	-	2.24E-08

Using a similar method of determining self-shielding factors from the experimental data, self-shielding factors were generated from the MCNP data. For each element the tally at each concentration was normalized against the lowest tally value, the 100 µg/g tally. Additionally, each concentration was normalized to 100 µg/g before using it to divide the normalized tallies. The self-shielding factors calculated from the two MCNP decks can be seen in Tables 4-8 and 4-9.

Table 4-8: MCNP Calculated Self-Shielding Factors

µg/g	La	Ce	Pr	Nd	Sm	Eu
10000	0.943	0.978	0.967	0.964	0.267	0.379
7500	0.958	0.981	0.975	0.946	0.327	0.449
5000	0.971	0.987	0.983	0.982	0.423	0.549
2500	0.985	0.994	0.991	0.991	0.597	0.705
1000	0.994	0.998	0.997	0.996	0.791	0.858
500	0.997	0.999	0.998	0.998	0.885	0.923
250	0.999	0.999	0.999	0.999	0.940	0.960
100	0.999	1.000	1.000	0.999	0.977	0.984
250	1.000	1.000	1.000	1.000	0.990	0.992
100	1.000	1.000	1.000	1.000	1.000	1.000

Table 4-9: MCNP Calculated Self-Shielding Factors Continued

Gd	Tb	Dy	Ho	Er	Tm	Yb	Lu
0.067	0.919	0.762	0.906	0.913	0.799	-	0.910
0.088	0.935	0.810	0.925	0.927	0.824	-	0.929
0.126	0.953	0.865	0.946	0.954	0.856	-	0.949
0.224	0.975	0.928	0.971	0.976	0.906	-	0.974
0.421	0.989	0.970	0.988	0.990	0.952	-	0.989
0.595	0.995	0.984	0.994	0.995	0.974	-	0.994
0.751	0.997	0.992	0.997	0.997	0.987	-	0.997
0.889	0.999	0.997	0.999	0.999	0.995	-	0.999
0.948	1.000	0.999	1.000	0.999	0.998	-	1.000
1.000	1.000	1.000	1.000	1.000	1.000	-	1.000

Like the trends of the results found experimentally, the MCNP results for elements with large cross-sections show extreme decreases in the neutron self-shielding factors. Elements like gadolinium, samarium, and europium all have self-shielding factors of more than 60%. Table 4-0 shows the percent difference between the self-shielding factors calculated by MCNP and the self-shielding factors found experimentally.

Table 4-10: Percent Difference between MCNP Self-Shielding Factors and Experimental Self-Shielding Factors

µg/g	La	Ce	Pr	Nd	Sm	Eu
10000	2.2163	7.6687	0	4.0456	157	95.515
7500	1.1113	6.8298	2.4615	4.0169	123.2	71.047
5000	0.8372	1.5198	3.2553	2.3422	83.599	47.541
2500	0.9151	9.4567	3.0272	1.3118	45.045	1.844
1000	10.354	0.7014	4.7141	8.1325	8.3103	9.6737
500	1.6236	2.1021	0.7014	8.517	3.2862	3.3586
250	0.5186	1.001	1.1011	2.3023	3.4155	3.125
100	0.2615	0	0	0.0300	6.3156	7.8252
250	0.0433	-	-	-	2.2232	5.5444
100	0	-	-	-	0	0

Table 4-11: Percent Difference between MCNP Self-Shielding Factors and Experimental Self-Shielding Factors Continued

Gd	Tb	Dy	Ho	Er	Tm	Yb	Lu
479.1	5.4407	14.304	5.6291	6.5717	20.526	-	7.5824
431.82	6.3102	10.617	4.8649	7.5512	18.568	-	5.9203
326.98	3.9874	3.3526	1.9027	2.5157	11.916	-	2.3182
197.32	1.3333	0.6466	2.8836	0.6148	6.9536	-	3.0801
0.4751	2.9323	10.928	8.502	1.4141	11.45	-	2.8311
36.807	5.5276	3.1504	10.765	1.5075	3.0801	-	2.8169
8.7883	4.7141	5.4435	0.3009	0.3009	3.7487	-	0.3009
12.486	20.02	135.71	0.1001	-	32.362	-	-
-	10	4.6046	-	-	4.008	-	-
-	0	0	-	-	0	-	-

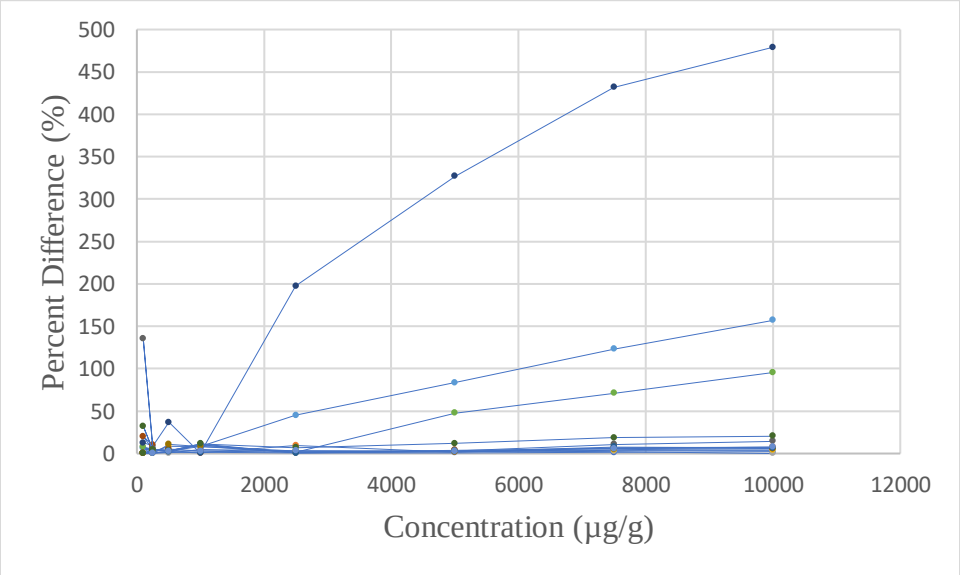

Figure 4-4: Percent Difference between MCNP Self-Shielding Factors and Experimental Self-Shielding Factors

For most of the elements the percent difference between the two sets of data either slowly increases or remains steady as concentration is increased. This trend remains true with exception of samarium, europium, and gadolinium, as the values found from MCNP quickly decrease away

from the experimental data and continues to do so as the concentration is increased. This can be seen in Figure 4-4.

To allow for closer inspection of the difference between the two data sets samarium, europium, and gadolinium were removed in Figure 4-5

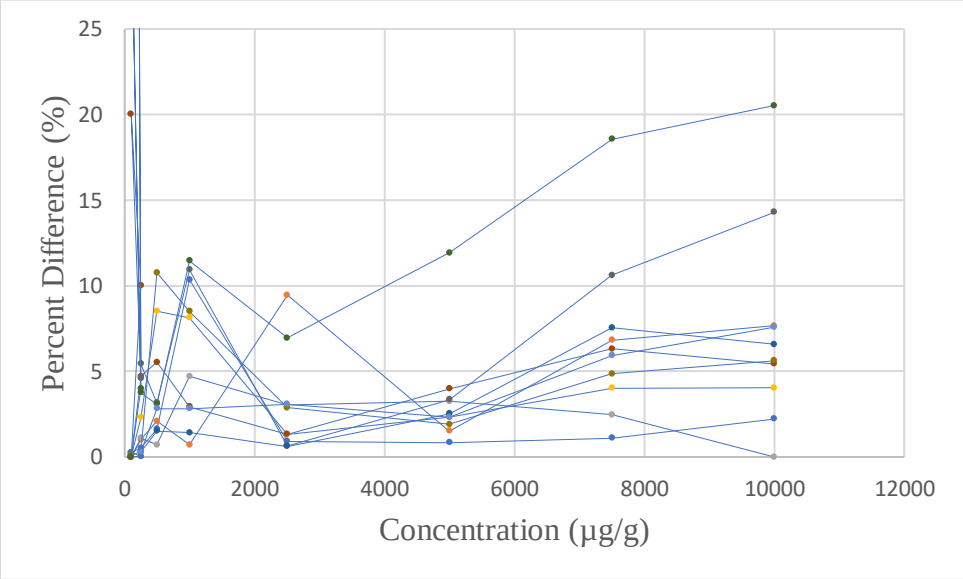

Figure 4-5: Percent Difference Between MCNP Self-Shielding Factors and Experimental Self-Shielding Factors

IV.III Chilian Self-Shielding Factors

Section II.I discusses the many equations that can be used to calculate the self-shielding effects within a sample. Many of these equations have been developed by Dr. Chilian who has contributed significant research into the effects of self-shielding factors. The most recent developments in her research have allowed for the implementation of a computer code that can calculate self-shielding effects of materials based upon their composition and dimensions.

Taking the dimensions of the sample vials that are used for irradiation by The University of Texas and using the code developed by Chilian, a set of self-shielding factors were compiled. The self-shielding factors that were calculated are for individual isotopes of each element that have the largest cross-sections, and thus represent the largest contributors to self-shielding effects in a sample. These values can be seen in Tables 4-12 and 4-13.

Table 4-12: Self-Shielding Factors Calculated from Chilian Computer Code

µg/g	La-139	Ce-140	Ce-142	Pr-141	Nd-146	Sm-152	Sm-154	Eu-151	Gd-152
10000	0.998	1.000	1.000	0.998	0.998	0.806	0.877	0.872	0.440
7500	0.998	1.000	1.000	0.998	0.999	0.842	0.903	0.899	0.505
5000	0.999	1.000	1.000	0.999	0.999	0.883	0.932	0.929	0.598
2500	0.999	1.000	1.000	0.999	0.999	0.932	0.963	0.962	0.741
1000	1.000	1.000	1.000	1.000	1.000	0.968	0.984	0.984	0.872
500	1.000	1.000	1.000	1.000	1.000	0.982	0.992	0.992	0.930
250	1.000	1.000	1.000	1.000	1.000	0.990	0.996	0.996	0.963
100	1.000	1.000	1.000	1.000	1.000	0.995	0.998	0.998	0.984
250	1.000	1.000	1.000	1.000	1.000	0.997	0.999	0.999	0.992
100	1.000	1.000	1.000	1.000	1.000	0.999	1.000	1.000	0.998

Table 4-13: Self-Shielding Factors Calculated from Chilian Computer Code

Gd-158	Tb-159	Dy-164	Ho-165	Er-171	Tm-170	Yb-169	Yb-175	Lu-176
0.796	0.973	0.970	0.974	0.992	0.939	0.998	0.998	0.997
0.821	0.978	0.977	0.979	0.994	0.950	0.999	0.999	0.998
0.855	0.984	0.985	0.985	0.996	0.963	0.999	0.999	0.998
0.907	0.991	0.992	0.991	0.998	0.978	1.000	0.999	0.999
0.954	0.996	0.997	0.996	0.999	0.989	1.000	1.000	1.000
0.975	0.998	0.998	0.998	0.999	0.994	1.000	1.000	1.000
0.987	0.999	0.999	0.999	1.000	0.997	1.000	1.000	1.000
0.994	0.999	1.000	0.999	1.000	0.998	1.000	1.000	1.000
0.997	1.000	1.000	1.000	1.000	0.999	1.000	1.000	1.000
0.999	1.000	1.000	1.000	1.000	1.000	1.000	1.000	1.000

IV.IV Comparison and Discussion

When comparing the three values of self-shielding factors, it is apparent that for elements with low cross-sections all three results produced consistent values. Elements with lower absorption cross-sections (e.g. lanthanum, cerium, praseodymium, neodymium, terbium, holmium, erbium, thulium, ytterbium and lutetium) showed remarkable similarities in their self-shielding factors. In comparison, elements with isotopes that have larger cross-sections (e.g. samarium, europium, gadolinium, and dysprosium) showed large differences among the three different methods.

Comparing the experimental or MCNP self-shielding factors to those of the calculated from the Chilian software, it is expected that there will be a discrepancy since it does not consider all the isotopes in the sample at the same time. Elements that only have one isotope, like Terbium, are not simplifications, and so the Chilian values are close to those found experimentally.

Table 4-14: Percent Difference between Chilian Computer Code and Experimental Self-Shielding Factors

PPM	La-140	Ce-141	Ce-143	Pr-142	Nd-147	Sm-153	Sm-155	Eu-152	Gd-153
10000	3.417	9.700	9.700	7.315	3.106	14.864	21.756	15.023	11.818
7500	5.075	8.600	8.600	1.403	0.000	13.319	19.175	14.572	7.327
5000	1.989	2.800	2.800	0.601	1.602	12.047	16.671	12.809	10.033
2500	0.499	10.000	10.000	0.501	2.202	7.090	10.081	25.364	10.121
1000	9.692	0.500	0.500	7.700	4.400	11.494	12.934	4.370	51.950
500	1.319	2.200	2.200	8.300	0.900	12.839	13.718	3.831	12.473
250	0.418	1.100	1.100	2.200	1.200	8.293	8.846	6.627	15.161
100	0.361	0.000	0.000	0.000	0.000	8.010	8.287	9.118	1.626
50	0.043	-	-	-	-	2.910	3.104	6.206	-
10	0.000	-	-	-	-	0.100	0.000	0.000	-

Table 4-15: Percent Difference between Chilian Computer Code and Experimental Self-Shielding Factors Continued

Gd-159	Tb-160	Dy-165	Ho-166	Er-171	Tm-170	Yb-169	Yb-175	Lu-177
51.256	0.411	10.206	1.745	1.915	2.556	9.619	9.619	1.805
42.996	1.636	8.291	0.919	0.302	2.842	9.009	9.009	1.403
37.076	0.711	9.239	2.132	1.807	0.519	9.109	9.109	2.705
26.571	0.303	7.056	0.807	1.603	0.920	9.400	9.309	0.501
56.080	2.209	13.340	7.631	0.501	7.280	3.600	3.600	1.700
16.513	5.210	4.509	10.321	1.101	1.006	3.200	3.200	2.200
17.224	4.905	6.106	0.501	0.000	2.708	7.200	7.200	0.000
0.604	20.020	135.000	0.100	-	32.565	9.500	9.500	-
-	10.000	4.700	-	-	4.104	9.400	9.400	-
-	0.000	0.000	-	-	0.000	0.000	0.000	-

As seen in Table 4-14 and 4-15, the majority**,** 88.9%, of the self-shielding factors for 10,000µg/g concentration calculated using the Chilian software were within 20% difference of values calculated experimentally. Of those, 66.7% were found to be within 10%, and 38.9% were within 5% difference. In comparison, 69.2% of the values found experimentally were within 20% of the self-shielding factors that were found using MCNP. Of that, 53.8% were within 10%, and 15.4% were within 5%.

Like the self-shielding factors calculated using MCNP, self-shielding factors for Samarium, Europium, and Gadolinium calculated using the Chilian Computer Code showed noticeable differences to the values found experimentally. These differences, for the aforementioned three elements, as well as all other elements, were noticeably less significant than between the MCNP and experimental values. The percent differences between the self-shielding factors found experimentally and those found using the Chilian Computer Code can be seen in Figure 4-5.

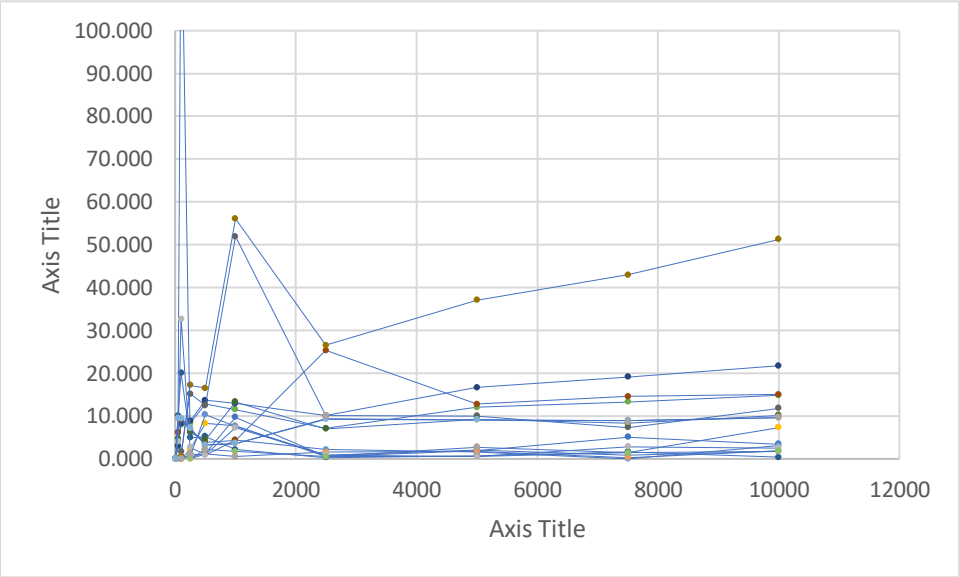

Figure 4-6: Percent Difference between Chilian Computer Code Self-Shielding Factors and Experimental Self-Shielding Factors

Table 4-16: Percent Difference between MCNP Self-Shielding Factors and Chilian Computer Code

PPM	La-140	Ce-141	Ce-143	Pr-142	Nd-147	Sm-153	Sm-155	Eu-152
10000	5.511	2.200	2.200	3.106	3.407	66.873	69.555	56.537
7500	4.008	1.900	1.900	2.305	5.305	61.164	63.787	50.056
5000	2.803	1.300	1.300	1.602	1.702	52.095	54.614	40.904
2500	1.401	0.600	0.600	0.801	0.801	35.944	38.006	26.715
1000	0.600	0.200	0.200	0.300	0.400	18.285	19.614	12.805
500	0.300	0.100	0.100	0.200	0.200	9.878	10.786	6.956
250	0.100	0.100	0.100	0.100	0.100	5.051	5.622	3.614
100	0.100	0.000	0.000	0.000	0.030	1.809	2.104	1.403
50	0.000	-	-	-	-	0.702	0.901	0.701
10	0.000	-	-	-	-	0.100	0.000	0.000

Table 4-17: Percent Difference between MCNP Self-Shielding Factors and Chilian Computer Code

Gd-153	Gd-159	Tb-160	Dy-165	Ho-166	Er-171	Tm-170	Lu-177
84.773	91.583	5.550	21.443	6.982	7.964	14.909	8.726
82.574	89.281	4.397	17.093	5.516	6.740	13.263	6.914
78.930	85.263	3.150	12.183	3.959	4.217	11.111	4.910
69.771	75.303	1.615	6.452	2.018	2.204	7.362	2.503
51.720	55.870	0.703	2.708	0.803	0.901	3.741	1.100
36.022	38.974	0.301	1.403	0.401	0.400	2.012	0.600
22.015	23.911	0.200	0.701	0.200	0.300	1.003	0.300
9.654	10.563	0.000	0.300	0.000	-	0.301	-
-	-	0.000	0.100	-	-	0.100	-
-	-	0.000	0.000	-	-	0.000	-

As seen in Tables 4-16 and 4-17, the differences between the Chilian values and those found using MCNP are much greater than the differences between those found experimentally and either of the two computer models. When comparing the differences between the experimental, Chilian, and MCNP self-shielding factors, the general trend is that the Chilian values were the largest, then the values found experimentally, with values produced from MCNP being the smallest.

A secondary method of comparison is shown in Appendix F. In Figures F-1 through F-14, the ratio of self-shielding factors created using the computer models to those calculated from the experimental data. In the graphs closer the value is to 1, the closer the two values are to each other.

IV.V Error Propagation

The error of the data was determined by propagating uncertainty from the standard concentration and the activity in the counting data. The general uncertainty equation, Eq. (4-1), was applied to each case of error propagation.

$$s_f = |f| \sqrt{\left(\frac{\partial x}{x}\right)^2 + \left(\frac{\partial y}{y}\right)^2 + \cdots} \quad (4\text{-}1)$$

Applying Eq. (4-1) to the formula that was used to calculate activity:

$$A = (Counts)/(Count\_Time) \quad (4\text{-}2)$$

The uncertainty of the activity in each sample was calculated using the equation

$$s_A = |A| \sqrt{\left(\frac{\partial C}{C}\right)^2 + \left(\frac{\partial T}{T}\right)^2} \quad (4\text{-}3)$$

In equation 4-3, $\frac{\partial A}{\partial C}$ represents the partial derivatives of the activity formula with respect to the total counts, $\frac{\partial A}{\partial T}$ is the partial derivative of the activity formula with respect to the time, and s_C and s_T are their uncertainties respectively. As there is no uncertainty in the count time $\frac{\partial A}{\partial T} = 0$. Thus,

$$s_A = |A| \sqrt{\left(\frac{\partial C}{C}\right)^2} \quad (4\text{-}4)$$

To calculate the uncertainty of the self-shielding factors it was first necessary to calculate the uncertainty of each of the relation value. This is shown in Eqs. (4-5) through (4-10). In these equations 'CR' represents the concentration relation, 'AR' represents the activity relation and 'SSF' represents the self-shielding factor. Additionally, 'C_1' and 'C_2' are two concentration that are being related, and 'A_1' and 'A_2' are two activities being related.

$$s_{CR} = |CR| \sqrt{\left(\frac{\partial C_1}{C_1}\right)^2 + \left(\frac{\partial C_2}{C_2}\right)^2} \quad (4\text{-}4)$$

$$s_{AR} = |AR| \sqrt{\left(\frac{\partial A_1}{A_1}\right)^2 + \left(\frac{\partial A_2}{A_2}\right)^2} \quad (4\text{-}5)$$

$$s_{SSF} = |SSF| \sqrt{\left(\frac{\partial CR_1}{CR_1}\right)^2 + \left(\frac{\partial AR_2}{AR_2}\right)^2} \quad (4\text{-}6)$$

V Conclusion

This investigation has produced useful information that can provide a basis for the general use of correction factors for rare-earth elements. Using data collected from the irradiation and subsequent counting of aqueous samples of rare-earth elements, a series of correction factors have been produced for each element in the lanthanide series (Tables 4-3 and 4-4): Lanthanum (Z=57) to Lutetium (Z=71). These correction factors are for samples with compositions that vary between 10 and 10000 μg/g of the lanthanide.

These results were compared to two computer models to verify the accuracy of the data that was collected experimentally. These two computer codes—MCNP and Chilian's self-shielding code—were used to create their own, independent sets of correction factors (Tables 4-8 and 4-9 and Tables 4-12 and 4-13). With the exception of several elements—Samarium, Europium, and Gadolinium—the results collected between each of the three data sets were similar, with most being within 10% difference of their counterpart calculated in each model (Tables 4-10 and 4-11 and Tables 4-14 through 4-17). For the data collected for the previously listed elements, their large cross-sections make it difficult to fully account how these elements behave computationally. Therefore, the differences that these models express in comparison to experimental data increases as the concentration is increased in the samples.

There are several erroneous values present in the experimental data that can be attributed to experimental error when preparing the samples. When using the 10 μg/g sample as a comparator, there is larger opportunity for error as the samples are prepared using previously prepared samples. This was counter-acted by using a different sample as the comparator, which has shown to reduce error and improve the quality of the data (Table 4-5).

It is recommended that there be further investigation into elements like samarium, europium, and gadolinium either through refinement of the codes used in this experiment or reproduction of the experiment itself. Reaction libraries for Ytterbium can be added to MCNP in order to utilize it to investigate the self-shielding factors of Ytterbium; this can be done using the NJOY software. Additionally, an investigation into rare-earth's behavior in materials other than aqueous solutions should be pursued. The self-shielding factors produced by this research are limited in scope, as they are specifically applicable for for samples that are aqueous, homogenous and have relatively low concentrations. As most rare-earths are collected during mineral extraction during large scale mining processes, additional study into how these elements behave during NAA in a variety of concentrations in solid, non-homogenous samples should be investigated.

In conclusion, this research has shown that neutron self-shielding factors express a decreasing trend as concentration increases. The results show a clear relationship between the cross-sections of the isotopes present in the solution and the self-shielding effects that manifest within the samples. While elements with small absorption cross-sections expressed verifiable—via computer computational models—correction factors, elements such as those listed previously in this section—with large absorption cross-sections—showed a wide variance between each of the calculated and experimentally determined values.

References

Baumann, N. P. (1963). “Resonance Integrals and Self-Shielding Factors for Detector Foils”. Aiken, SC: E.I. du Pont de Nemours & Company, Savannah River Laboratory.

Chilian, C., Kassakov, M., St-Pierre, J., Kennedy, G. (2006). “Extending NAA to materials with high concentration of neutron absorbing elements”. *Journal of Radioanalytical and Nuclear Chemistry,* 270(2), 417-423.

Chilian, C., St-Pierre, J., & Kennedy, G. (2008). “Complete thermal and epithermal neutron self-shielding corrections for NAA using a spreadsheet”. *Journal of Radioanalytical and Nuclear Chemistry*,*278*(3), 745-749. doi:10.1007/s10967-008-1604-8

De Soete, D., Gijbels, R. and Hoste, J., “Neutron Activation Analysis”, Wiley-Interscience: London (1972).

Frontasyeva, L.I. Smirnov, E. Steinnes, S. M. Lyapunov, V.D. Cherchintsev, J. (2004) Radioanal. Nucl. Chem., 259 19.

Graham, J. T. (2011). “Characterizations of Neutron Flux Spectra for Radiation Effects Studies”. Master’s Thesis, University of Texas at Austin, 2011.

Hevesy, G. and Levi, H. (1936). “Det. Kgl Dansk Videnskabernes Selskab”, *Mathematisk – Fysiske Meddelelser*, 14, 3.

Kafala, S. I., & MacMahon, T. D. (2007). “Comparison of Neutron Activation Analysis Methods”. *Journal of Radioanalytical and Nuclear Chemistry*, *271*(2), 507–516. doi: https://doi.org/10.1007/s10967-007-0238-6

Kirstein, Erik S. (2011). “Neutron Absorption Self-Shielding Factors in Activation Analysis”. Master's Thesis, University of Illinois at Urbana-Champaign, 1997.

Koskinas, M. F., Lacerda, F. W., Matos, I. T., Nascimento, T. S., Yamazaki, I. M., Takeda, M. N., & Dias, M. S. (2014). “Determination of gamma-ray emission probabilities per decay of Ga-68”. *Applied Radiation and Isotopes*, *87*, 118–121. doi: 10.1016/j.apradiso.2013.11.003

Lamarsh, J.R., “Introduction to Nuclear Engineering”, Addison-Wesley Publishing Company: Reading, Massachusetts (1983).

Landsberger, S., “Updated of Uranium Fission Interferences in Neutron Activation Analysis,” Chem. Geol., 77, 65-70 (1989)

Landsberger, S. (2019, October). jpg.

Leal, A.s., M.â.b.c. Menezes, P. Vermaercke, L. Sneyers, and C.e.m. Jensen. "Investigation of Chemical Impurities in Formulations, Phytotherapics and Polyvitaminic Medicines by K0-instrumental Neutron Activation Analysis." *Nuclear Instruments and Methods in Physics Research Section A: Accelerators, Spectrometers, Detectors and Associated Equipment*564, no. 2 (August 15, 2006): 729-32. doi:10.1016/j.nima.2006.04.010.

Lim, C. S. "Recent Developments in Neutron-induced Gamma Activation for On-line Multielemental Analysis in Industry." *Journal of Radioanalytical and Nuclear Chemistry*262, no. 2 (February 14, 2004): 525-32. doi:10.1023/b:jrnc.0000046791.73058.f5.

NDC, Updated October 2009, “Evaluated Nuclear Data Files (ENDF) Retrieval and Plotting” Version 3.1, National Nuclear Data Center, USA.

Salgado, J., Gonçalves, I. F., & Martinho, E. (2004). “Development of a Unique Curve for Thermal Neutron Self-Shielding Factor in Spherical Scattering Materials”. *Nuclear Science and Engineering,148*(3), 426-428. doi:10.13182/nse04-a2468

Salgado, J., Martinho, E., & Gonçalves, I. F. (2004). “The calculation of neutron self-shielding factors of a group of isolated resonances”. *Journal of Radioanalytical and Nuclear Chemistry,260*(2), 317-320. doi:10.1023/b:jrnc.0000027103.05680.98

Sayre, E. V., and Dodson, R. W., 1957. “Neutron activation study of Mediterranean potsherds”, *American Journal of Archaeology*, 61, 35-41.

Smith, A. R. "Low-Background Instrumental Neutron Activation Analysis of Silicon Semiconductor Materials." *Journal of The Electrochemical Society*143, no. 1 (January 1996): 339-46. doi:10.1149/1.1836433.

Speakman, R. J., and M. D. Glascock. "Acknowledging Fifty Years Of Neutron Activation Analysis In Archaeology." *Archaeometry*49, no. 2 (May 15, 2007): 179-83. doi:10.1111/j.1475-4754.2007.00294.x.

Stewart, J. C., Zweifel, P. F. (1958). “A Review of Self-Shielding and Doppler Effects in the Absorption of Neutrons”. Proc. U. N. Intern. Cof. Peaceful Uses Atomic Energy, 2nd, Geneva, 16, 652-56.

Tzaphlidou, V.Zaichick, (2002) Appl. Radiation Isotopes, 57 779.

Witkowska, E. "Some Applications of Neutron Activation Analysis: A Review." *Journal of Radioanalytical and Nuclear Chemistry*265, no. 1 (2005): 141-50.

APPENDIX A: COUNTING DATA

Table A-1: Lanthanum Counting Data

µg/g	±	C_T	Start Count Time	C_NET	±	A	±	C_TC	D_T	D_TC
9499.53	21	45.6	11:20	98826	570	3205.52	12.5	1.0002	81621	1.4771
7124.64	15.75	60	11:18	96025	563	2362.87	9.38	1.0003	81458	1.4760
4749.76	10.5	31.6	11:08	34995	187	1628.08	5.91	1.0002	80860	1.4718
2374.88	5.25	30.4	11:12	17036	144	826.42	4.74	1.0001	81108	1.4735
949.953	2.1	135	12:26	49286	358	364.79	2.66	1.0006	-830	0.9960
474.976	1.05	104	12:40	17583	155	168.47	1.48	1.0005	0	1.0000
237.488	0.525	146	12:44	12156	116	83.49	0.80	1.0007	222	1.0011
90.2139	0.21	397	12:48	12426	118	31.47	0.30	1.0019	460	1.0022
45.1062	0.105	656	12:56	10282	107	15.80	0.16	1.0031	957	1.0046
11.2767	0.021	2695	13:09	10415	112	3.95	0.04	1.0130	1760	1.0084

Table A-2: Cerium Counting Data

µg/g	±	C_T	Start Count Time	C_NET	±	A	±	C_TC	D_T	D_TC
8959	23	59.94	12:14	27565	193	459.88	3.22	1.0000	0	1.0000
6719.09	17.25	59.76	12:17	20857	171	349.02	2.86	1.0000	179	1.0000
4479.40	11.5	60.02	12:19	14853	147	247.47	2.45	1.0000	309	1.0001
2239.70	5.75	98.78	12:23	11324	133	114.64	1.35	1.0000	538	1.0001
895.90	2.3	196.74	12:26	10067	140	51.17	0.71	1.0000	721	1.0002
447.94	1.15	404.3	12:32	10068	170	24.90	0.42	1.0001	1066	1.0003
250.845	0.644	733.9	12:40	10346	211	14.10	0.29	1.0002	1559	1.0004
107.505	0.276	1813.08	12:55	11075	304	6.11	0.17	1.0004	2456	1.0006
53.753	0.138	-	-	-	-	-	-	-	-	-
8.958	0.023	-	-	-	-	-	-	-	-	-

Table A-3: Praseodymium Counting Data

µg/g	±	C_T	Start Count Time	C_NET	±	A	±	C_TC	D_T	D_TC
9483	27	30.4	12:13:36 PM	16786	138	552.34	4.54	1.0003	0	1.0000
7112.2	22.5	50.89	12:16:30 PM	22356	157	439.55	3.09	1.0005	179	1.0018
4741	15	45.16	12:19:36 PM	13492	120	298.92	2.66	1.0005	309	1.0031
2370.74	7.50	74.54	12:21:28 PM	11102	109	149.07	1.46	1.0008	538	1.0054
948.3	3.0	159.46	12:23:52 PM	10168	102	63.88	0.64	1.0016	721	1.0073
474.15	1.50	313.46	12:27:30 PM	10017	101	32.07	0.32	1.0032	1066	1.0108
237.07	0.75	671.1	12:33:49 PM	10041	102	15.07	0.15	1.0068	1559	1.0158
94.83	0.30	1742.44	12:46:16 PM	10020	106	5.86	0.06	1.0177	2456	1.0250
47.41	0.15	3740.26	1:08:23 PM	10673	108	3.06	0.03	1.0384	3287	1.0337
9.48	0.03	28745.32	2:39:18 PM	14046	128	0.71	0.00	1.3357	8742	1.0920

Table A-4: Neodymium Counting Data

µg/g	±	C_T	Start Count Time	C_NET	±	A	±	C_TC	D_T	D_TC
9560	31	45.50	1:31:37 PM	19585	149	430.54	3.27	1.0000	276	1.0002
7200	23	43.32	1:33:19 PM	14510	131	335.05	3.02	1.0000	378	1.0003
4800	16	45.22	1:34:55 PM	10262	111	227.02	2.45	1.0000	474	1.0003
2399.9	7.8	89.58	1:27:01 PM	10221	114	114.11	1.27	1.0001	0	1.0000
960.0	3.1	216.50	1:39:06 PM	10100	117	46.68	0.54	1.0002	725	1.0005
239.99	0.78	944.92	1:43:47 PM	10464	149	11.09	0.16	1.0007	1006	1.0007
480.00	1.60	1006.10	2:00:40 PM	22215	189	22.13	0.19	1.0007	2019	1.0015
96.00	0.31	3127.28	2:18:34 PM	13951	225	4.48	0.07	1.0023	3093	1.0023
48.00	0.16	-	-	-	-	-	-	-	-	-
9.600	0.031	-	-	-	-	-	-	-	-	-

Table A-5: Samarium Counting Data

µg/g	±	C_T	Start Count Time	C_NET	±	A	±	C_TC	D_T	D_TC
9529	26	36.14	10:41:46 AM	115905	388	8909.35	10.74	1.0002	245573	2.7776
7147	19.5	60.22	10:49:15 AM	153761	444	7107.10	7.37	1.0003	246022	2.7828
4764	13	90.00	10:53:56 AM	162807	452	5041.72	5.02	1.0004	246303	2.7860
2382.2	6.5	90.00	10:57:47 AM	90676	330	2810.71	3.67	1.0004	246534	2.7887
952.9	2.6	27.98	2:42:57 PM	31011	197	1112.36	7.04	1.0001	844	1.0035
476.45	1.30	71.36	2:45:49 PM	39472	224	555.65	3.14	1.0003	1016	1.0042
238.22	0.68	50.46	2:40:55 PM	14823	125	294.69	2.48	1.0002	722	1.0030
90.49	0.21	98.58	2:37:31 PM	11097	128	112.86	1.30	1.0004	518	1.0022
45.25	0.13	698.18	2:22:41 PM	41609	191	59.68	0.27	1.0029	-372	0.9985
11.312	0.021	3600	2:28:53 PM	54661	267	15.41	0.07	1.0151	0	1.0000

Table A-6: Europium Counting Data

µg/g	±	C_T	Start Count Time	C_NET	±	A	±	C_TC	D_T	D_TC
9979	37	30.00	-	43050	260	1435.00	8.67	-	-	-
7484	28	30.00	-	33459	228	1115.30	7.60	-	-	-
4990	19	30.00	-	23504	189	783.47	6.30	-	-	-
2495.0	9.3	60.00	-	20854	177	347.57	2.95	-	-	-
947.0	3.5	90.00	-	15556	155	172.84	1.72	-	-	-
473.0	1.8	300.00	-	26266	199	87.55	0.66	-	-	-
238.00	0.88	600.00	-	25745	197	42.91	0.33	-	-	-
95.00	0.35	1800.00	-	30073	215	16.71	0.12	-	-	-
47.90	0.18	1200	-	10447	125	8.71	0.10	-	-	-
9.540	0.035	6500	-	12027	138	1.85	0.02	-	-	-

Europium has a half-life of 13.57 years, so it was assumed that any correction factor would be effectively 1, and they are therefore neglected

Table A-7: Gadolinium Counting Data

µg/g	±	C_T	Start Count Time	C_NET	±	A	±	C_TC	D_T	D_TC
9450	36	63.30	10:04:30 AM	10721	151	169.48	2.39	1.0007	0	1.0000
7125	27	70.56	10:06:04 AM	10249	135	145.50	1.91	1.0007	94	1.0010
4750	18	91.44	10:07:58 AM	10162	128	111.48	1.40	1.0010	208	1.0022
2374.9	9.0	146.44	10:10:00 AM	10067	130	69.09	0.89	1.0015	330	1.0034
949.9	32.4	318.39	10:13:22 AM	10125	152	32.08	0.48	1.0033	532	1.0056
475.0	2.7	624.30	10:19:17 AM	10416	112	16.95	0.18	1.0065	887	1.0093
237.49	0.90	1297.20	10:30:06 AM	10719	115	8.51	0.09	1.0136	1536	1.0161
90.21	0.36	3225.46	10:52:12 AM	12613	134	4.17	0.04	1.0342	2862	1.0303
45.10	0.18	5450	11:46:36 AM	11293	120	2.34	0.02	1.0584	6126	1.0659
11.28	0.036	28590.5	1:18:02 PM	18536	156	0.99	0.01	1.3470	11612	1.1286

Table A-8: Terbium Counting Data

µg/g	±	C_T	Start Count Time	C_NET	±	A	±	C_TC	D_T	D_TC
9570	36	54.28	11:47:40 AM	10070	105	185.52	1.93	1.0000	177	1.0000
7177	27	73.30	11:44:43 AM	10459	107	142.69	1.46	1.0000	0	1.0000
4749	18	113.84	11:55:19 AM	10718	109	94.14	0.96	1.0000	636	1.0001
2392.4	9.0	221.06	11:50:02 AM	10460	106	47.32	0.48	1.0000	319	1.0000
957.0	3.6	521.58	11:58:19 AM	10172	105	19.50	0.20	1.0001	816	1.0001
478.5	1.8	1559.46	12:09:08 PM	15673	131	10.05	0.08	1.0002	1465	1.0002
239.77	0.75	5601.94	1:37:03 PM	25525	170	4.56	0.03	1.0006	6740	1.0007
95.91	0.30	6703.56	1:26:02 PM	10378	125	1.53	0.02	1.0007	92479	1.0103
47.95	0.15	86400	11:52:51 PM	77130	303	0.86	0.00	1.0096	389288	1.0441
9.590	0.030	86400	3:22:40 PM	16604	145	0.19	0.00	1.0096	99477	1.0111

Table A-9: Dysprosium Counting Data

µg/g	±	C_T	Start Count Time	C_NET	±	A	±	C_TC	D_T	D_TC
9371	27	30.08	8:04:16 PM	47245	231	26023.75	7.68	1.0025	34003	16.5278
7029	27	59.28	7:41:58 PM	80049	299	20083.97	5.04	1.0049	32665	14.8006
4686	18	30.04	6:07:38 PM	43171	220	13368.04	7.32	1.0025	27005	9.2790
2342.8	9.0	30.12	3:56:46 PM	42625	218	6887.74	7.24	1.0025	19153	4.8550
937.1	3.6	27.22	10:58:02 AM	63377	270	2582.56	9.92	1.0022	1229	1.1067
468.6	1.8	27.64	10:54:31 AM	36104	201	1423.90	7.27	1.0023	1018	1.0876
234.28	0.90	30.88	10:52:49 AM	20026	149	701.20	4.83	1.0026	916	1.0785
93.71	0.36	29.86	10:51:15 AM	19549	147	702.35	4.92	1.0025	822	1.0702
46.86	0.18	72.1	10:37:33 AM	10204	112	142.37	1.55	1.0060	0	1.0000
9.371	0.036	374.92	10:40:38 AM	10701	129	29.89	0.34	1.0314	185	1.0154

Table A-10: Holmium Counting Data

µg/g	±	C_T	Start Count Time	C_NET	±	A	±	C_TC	D_T	D_TC
9511	27	20.56	11:41:59 AM	75796	336	3687.12	16.34	1.0001	0	1.0000
7134	28	20.22	11:44:49 AM	56580	276	2802.04	13.65	1.0001	170	1.0012
4756	19	19.66	11:46:50 AM	36430	258	1857.14	13.12	1.0001	291	1.0021
2377.9	9.3	30.58	11:49:48 AM	29329	229	962.54	7.49	1.0002	469	1.0034
951.1	3.7	60.20	11:51:36 AM	24755	180	413.10	2.99	1.0004	577	1.0042
475.6	1.9	60.44	11:55:29 AM	12737	132	212.06	2.18	1.0004	810	1.0058
237.79	0.93	152.14	11:57:40 AM	14457	146	95.77	0.96	1.0011	941	1.0068
95.11	0.37	395.80	12:01:11 PM	15083	154	38.53	0.39	1.0028	1152	1.0083
47.56	0.19	975.22	12:09:52 PM	17697	213	18.49	0.22	1.0070	1673	1.0121
9.511	0.037	2511.76	12:30:20 PM	10667	121	4.42	0.05	1.0182	2901	1.0210

Table A-11: Erbium Counting Data

µg/g	±	C_T	Start Count Time	C_NET	±	A	±	C_T C	D_T	D_T C
9534	27	59.94	10:35:19 AM	87015	309	1453.93	5.16	1.0015	0	1.0000
7150	23	60.40	10:38:57 AM	66984	269	1116.94	4.45	1.0015	218	1.0056
4767	16	59.62	10:41:21 AM	43070	216	730.25	3.62	1.0015	362	1.0093
2383.4	7.8	59.76	10:44:47 AM	21563	150	366.68	2.51	1.0015	568	1.0147
953.4	3.1	90.72	10:46:58 AM	13337	121	150.02	1.33	1.0023	699	1.0181
476.7	1.6	180.58	10:49:38 AM	13268	119	75.46	0.66	1.0046	859	1.0222
238.34	0.78	370.46	10:53:55 AM	13318	125	37.35	0.34	1.0095	1116	1.0290
101.86	13.95	631.22	11:01:27 AM	10173	107	17.05	0.17	1.0163	1568	1.0410
45.27	6.20	5515.62	11:22:35 AM	10060	1.82	2.26	0.00	1.1518	2836	1.0754
11.317	1.550	99939.48	1:01:31 PM	15471	202	2.51	0.00	12.9384	8772	1.2520

Table A-12: Thulium Counting Data

µg/g	±	C_T	Start Count Time	C_NET	±	A	±	C_T C	D_T	D_T C
9550	36	50.00	12:24:52 PM	112218	359	2244.37	7.18	1.0000	0	1.0000
7163	27	30.14	12:27:20 PM	51460	243	1707.38	8.06	1.0000	148	1.0000
4775	18	30.02	12:28:35 PM	33508	195	1116.21	6.50	1.0000	223	1.0000
2388.0	9.0	29.70	12:30:03 PM	16777	138	564.89	4.65	1.0000	311	1.0000
955.0	0.4	48.18	12:31:32 PM	11909	118	247.18	2.45	1.0000	400	1.0000
477.5	1.8	86.96	12:33:39 PM	10177	110	117.04	1.26	1.0000	527	1.0000
238.76	0.90	3226.30	12:35:42 PM	192533	504	59.69	0.16	1.0002	650	1.0000
95.50	0.36	649.28	1:30:54 PM	10188	123	15.70	0.19	1.0000	3962	1.0002
47.75	0.18	898.86	12:40:00 PM	10036	129	11.17	0.14	1.0001	908	1.0001
9.550	0.036	6106.88	1:58:30 PM	14222	228	2.33	0.04	1.0004	5618	1.0004

Table A-13: Ytterbium Counting Data

µg/g	±	C_T	Start Count Time	C_NET	±	A	±	C_TC	D_T	D_TC
9476	27	60.38	9:56:14 AM	43234	215	716.11	3.56	1.0001	0	1.0000
7107	20	60.44	10:00:28 AM	32689	186	541.18	3.08	1.0001	254	1.0005
4738	14	60.64	10:04:21 AM	21844	150	360.60	2.47	1.0001	487	1.0009
2368.9	6.8	61.82	10:07:02 AM	11108	107	179.93	1.73	1.0001	648	1.0012
947.6	2.7	150.08	10:09:15 AM	11463	108	76.52	0.72	1.0003	781	1.0015
473.8	1.4	304.26	10:13:00 AM	12441	113	40.99	0.37	1.0006	1006	1.0019
236.89	0.68	600.54	10:19:25 AM	11020	109	18.42	0.18	1.0012	1391	1.0027
94.76	0.27	1412.40	10:25:52 AM	10083	111	7.18	0.08	1.0027	1778	1.0034
47.38	0.14	3032.34	10:55:17 AM	10770	125	3.60	0.04	1.0058	3543	1.0068
9.476	0.027	86168.56	10:52:19 AM	57632	290	0.79	0.00	1.1796	3365	1.0065

Table A-14: Lutetium Counting Data

µg/g	±	C_T	Start Count Time	C_NET	±	A	±	C_TC	D_T	D_TC
9607	27	60.22	10:59:47 AM	164961	414	2739.50	6.87	1.0001	0	1.0000
7206	22	26.04	11:03:51 AM	53726	235	2063.87	9.02	1.0000	244	1.0003
4804	15	33.12	11:05:44 AM	44941	215	1357.55	6.49	1.0000	357	1.0004
2401.9	7.3	28.52	11:07:04 AM	20021	143	702.39	5.01	1.0000	437	1.0005
960.7	2.9	36.58	11:08:25 AM	10402	103	284.55	2.82	1.0000	518	1.0006
480.4	1.5	98.28	11:09:54 AM	14043	121	143.01	1.23	1.0001	607	1.0007
240.19	0.73	157.44	11:12:30 AM	10998	108	69.93	0.69	1.0002	763	1.0009
96.07	0.29	985.98	11:16:03 AM	25577	174	26.00	0.18	1.0012	976	1.0012
48.04	0.15	2876.46	11:17:02 AM	10792	153	3.77	0.05	1.0034	1035	1.0012
9.607	0.029	12471.78	12:24:30 PM	10155	240	0.83	0.02	1.0150	5083	1.0061

APPENDIX B: COUNTING DATA GRAPHS

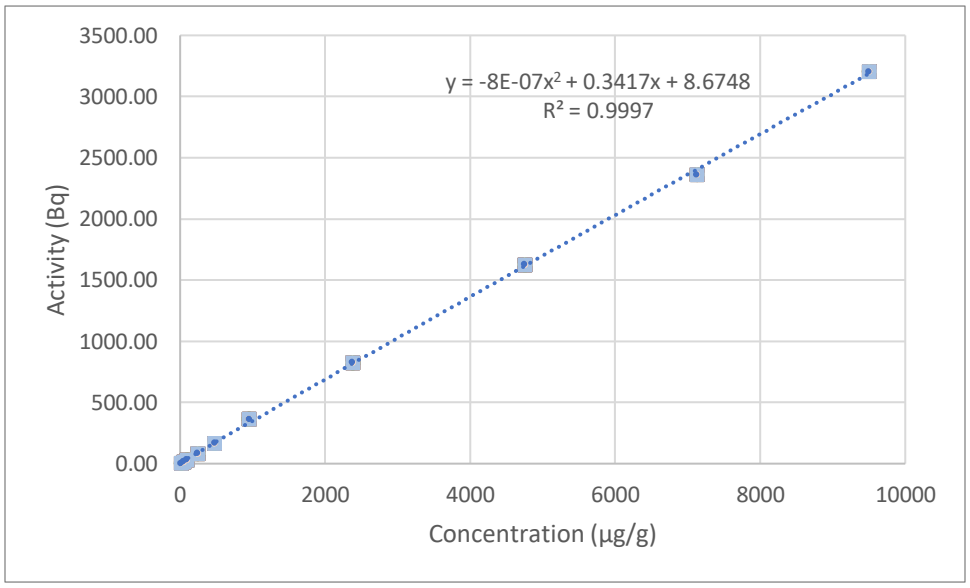

Figure B-1: Lanthanum Counting Data Plot

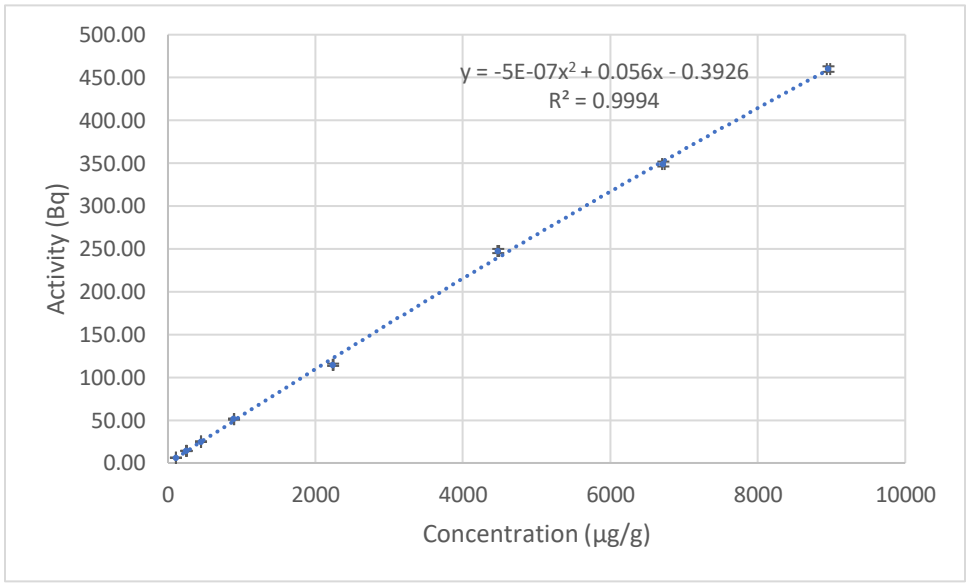

Figure B-2: Cerium Counting Data Plot

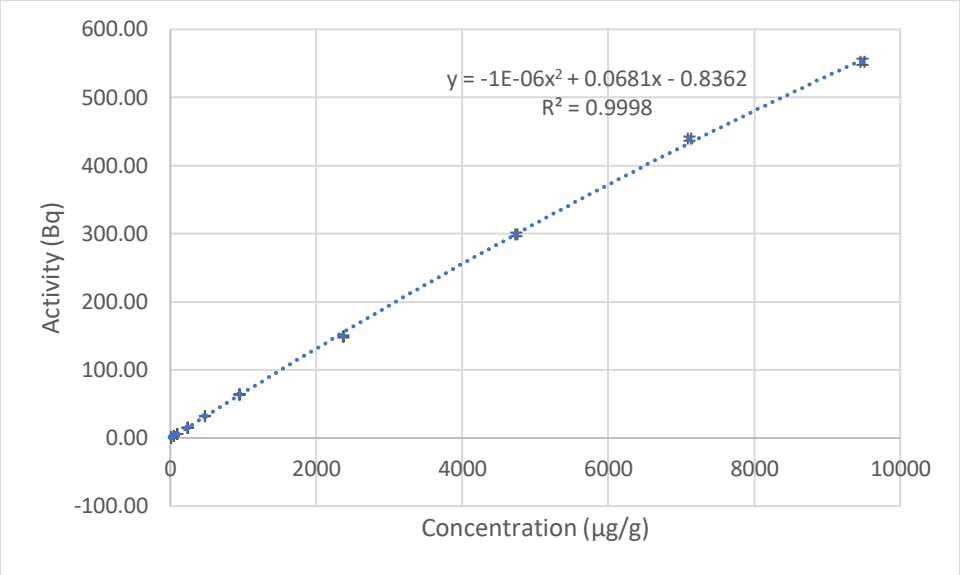

Figure B-3: Praseodymium Counting Data Plot

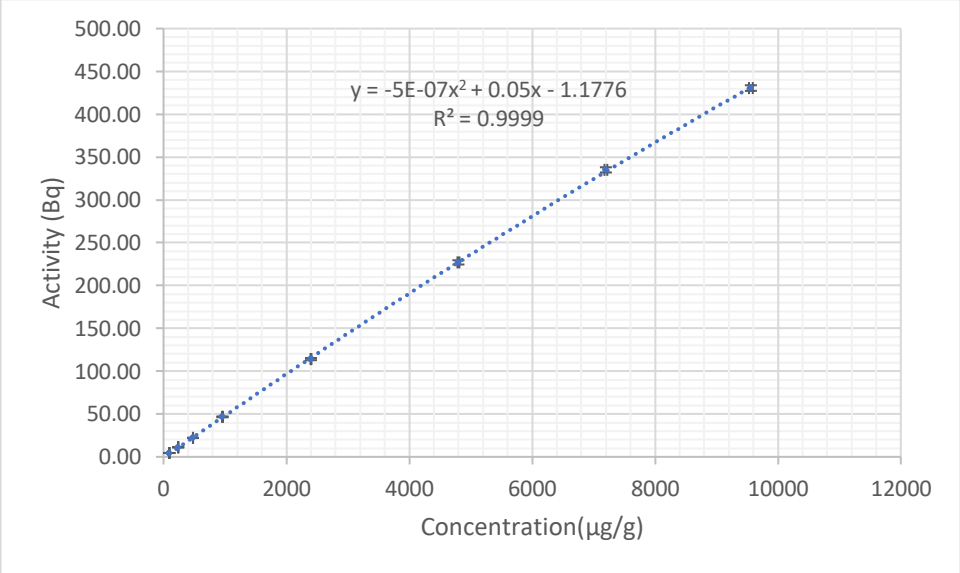

Figure B-4: Neodymium Counting Data Plot

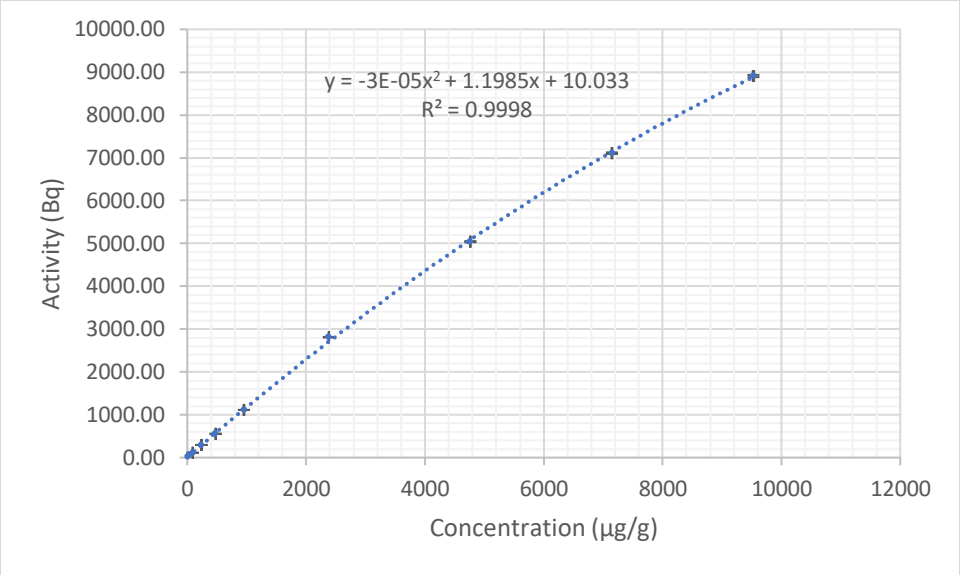

Figure B-5: Samarium Counting Data Plot

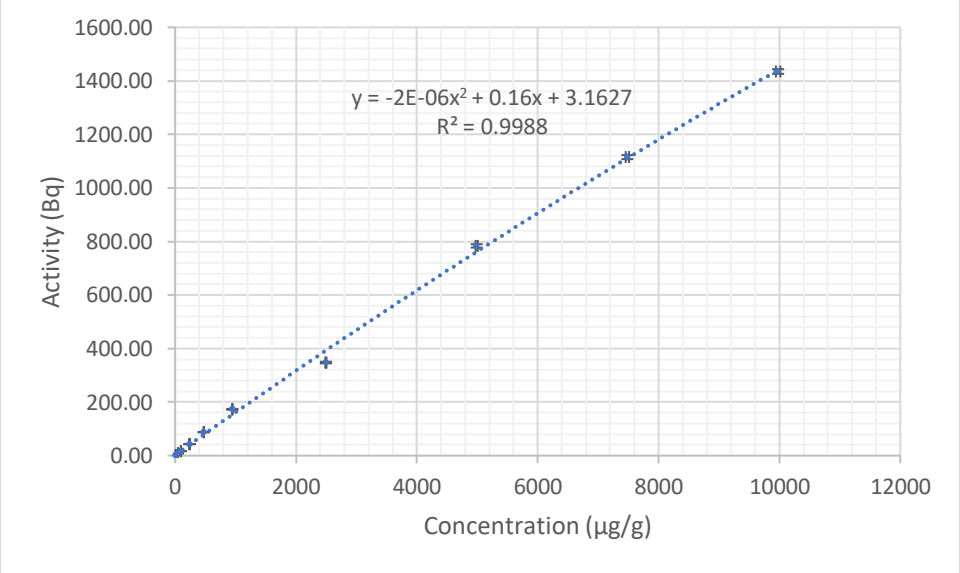

Figure B-6: Europium Counting Data Plot

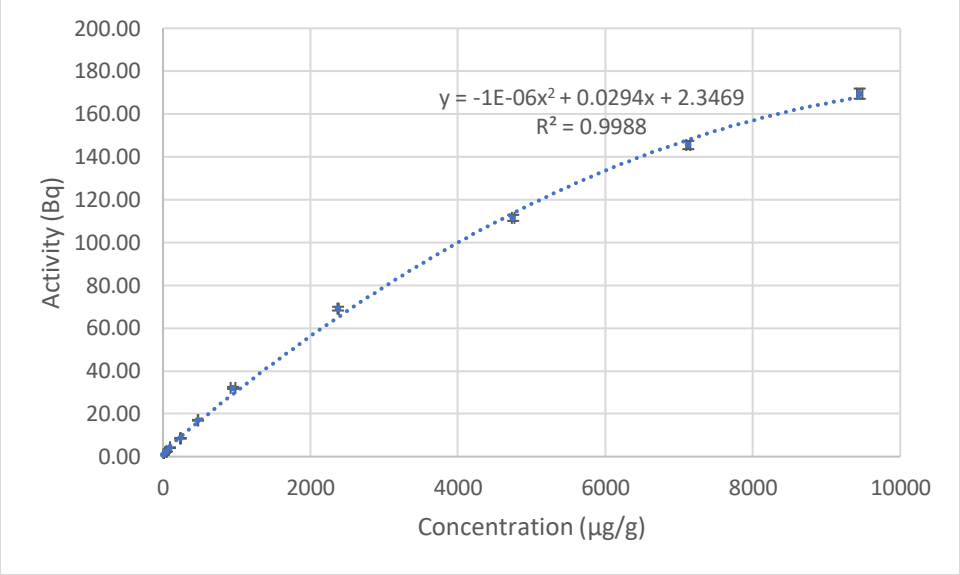

Figure B-7: Gadolinium Counting Data Plot

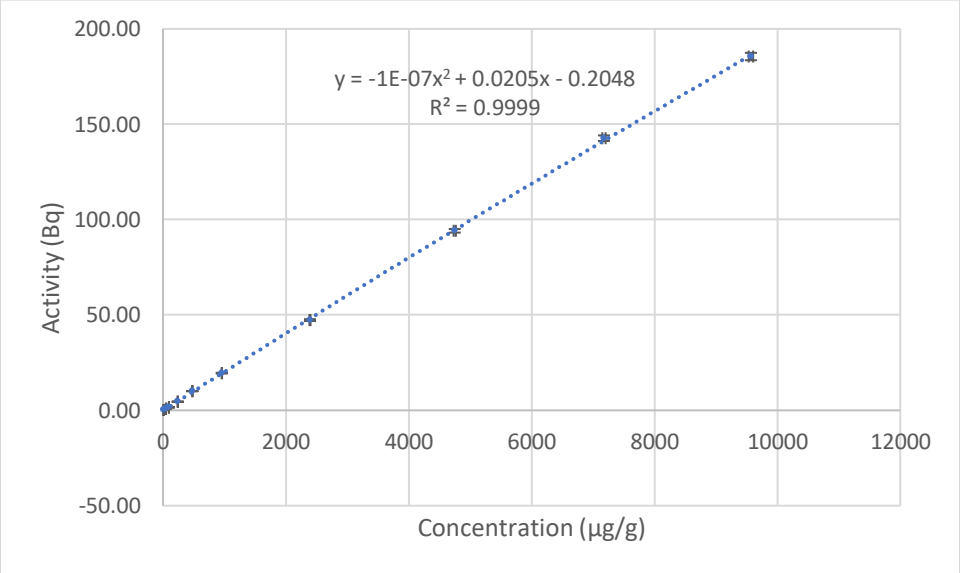

Figure B-8: Terbium Counting Data Plot

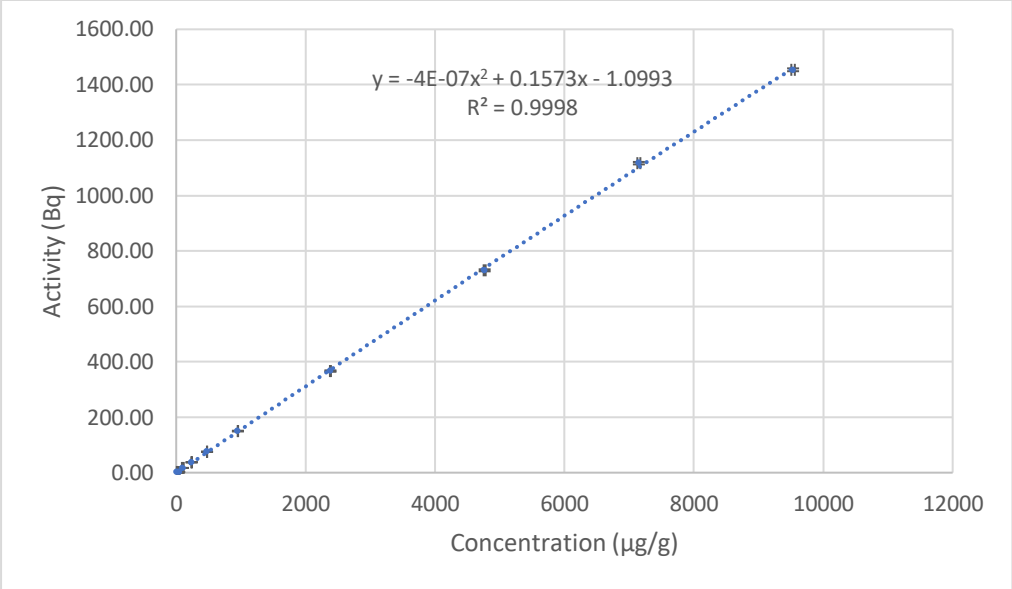

Figure B-9: Dysprosium Counting Data Plot

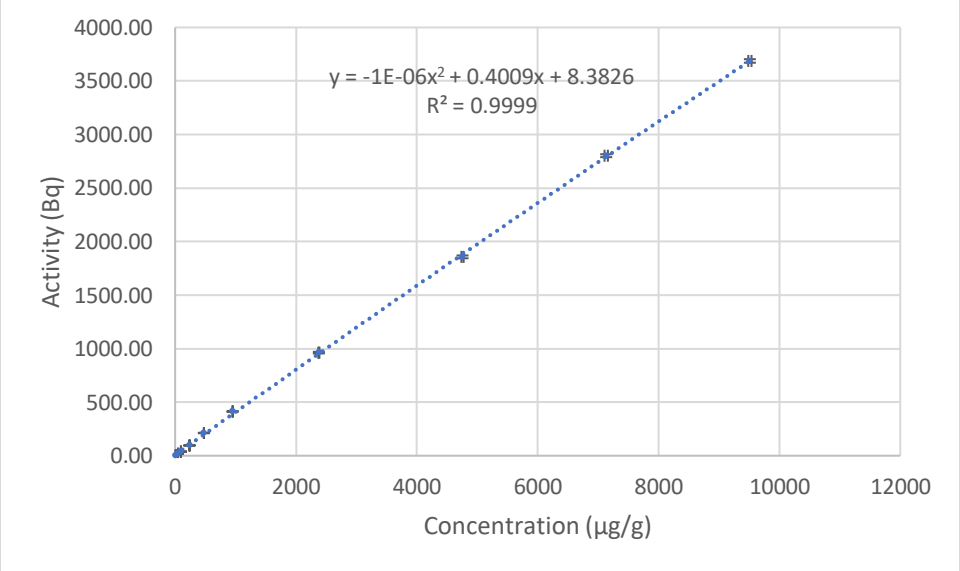

Figure B-10: Holmium Counting Data Plot

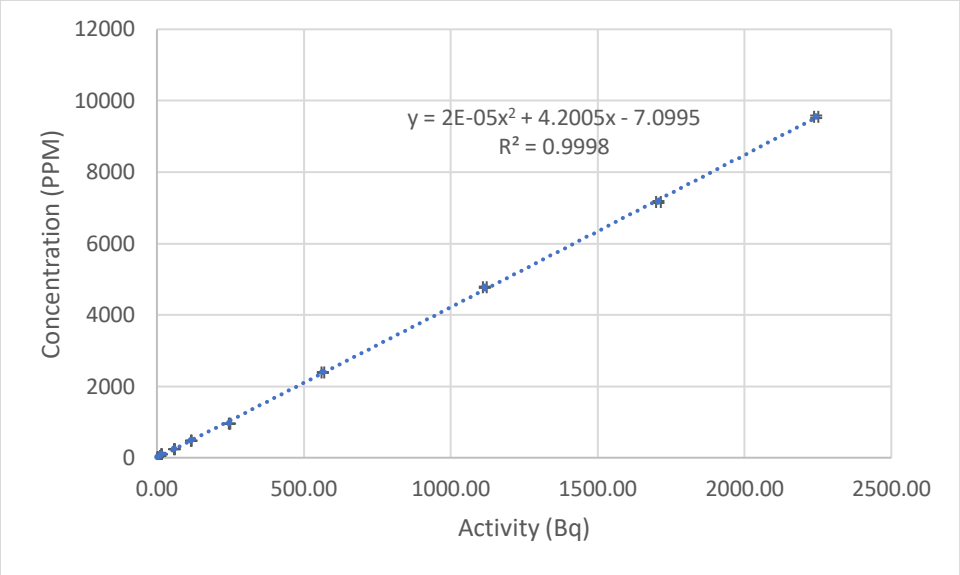

Figure B-11: Erbium Counting Data Plot

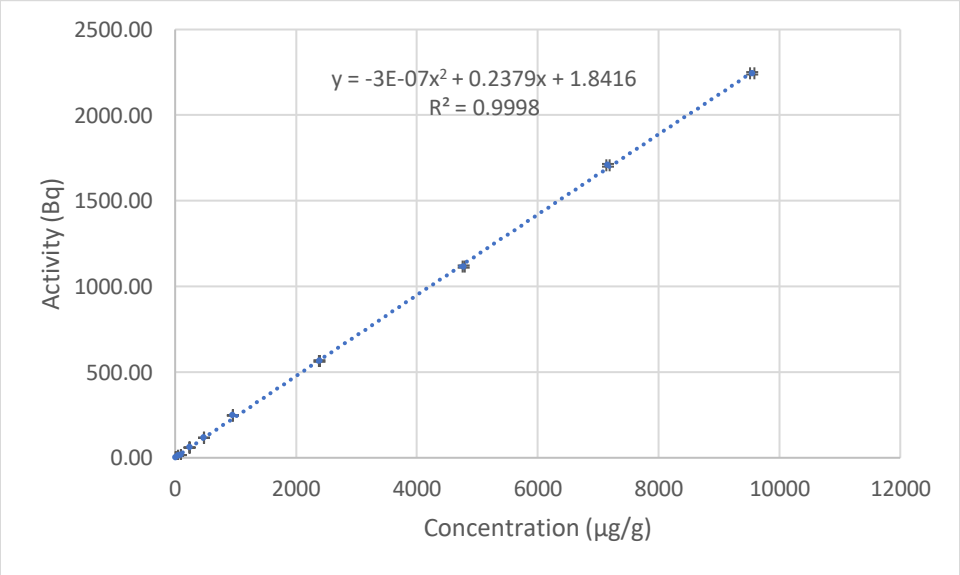

Figure B-12: Thulium Counting Data Plot

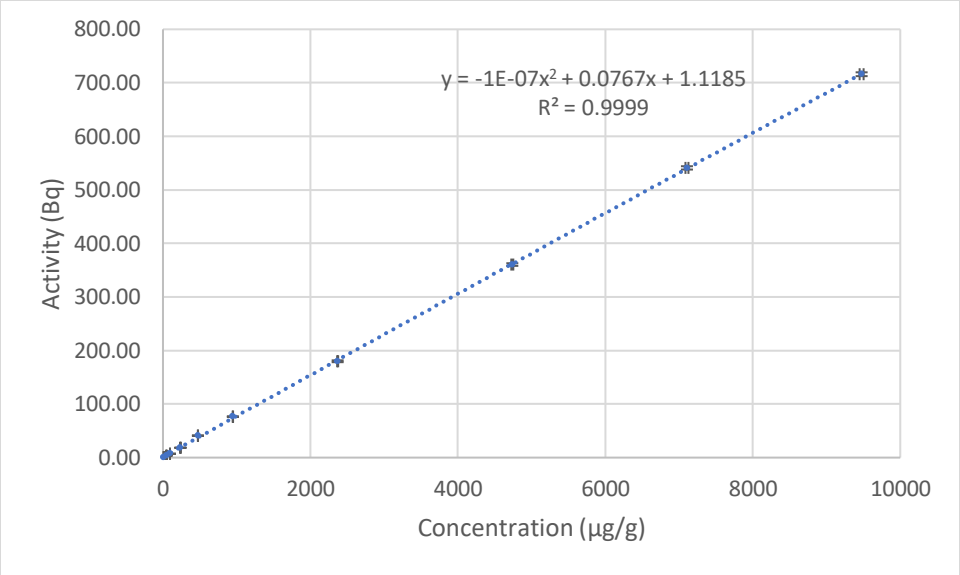

Figure B-13: Ytterbium Counting Data Plot

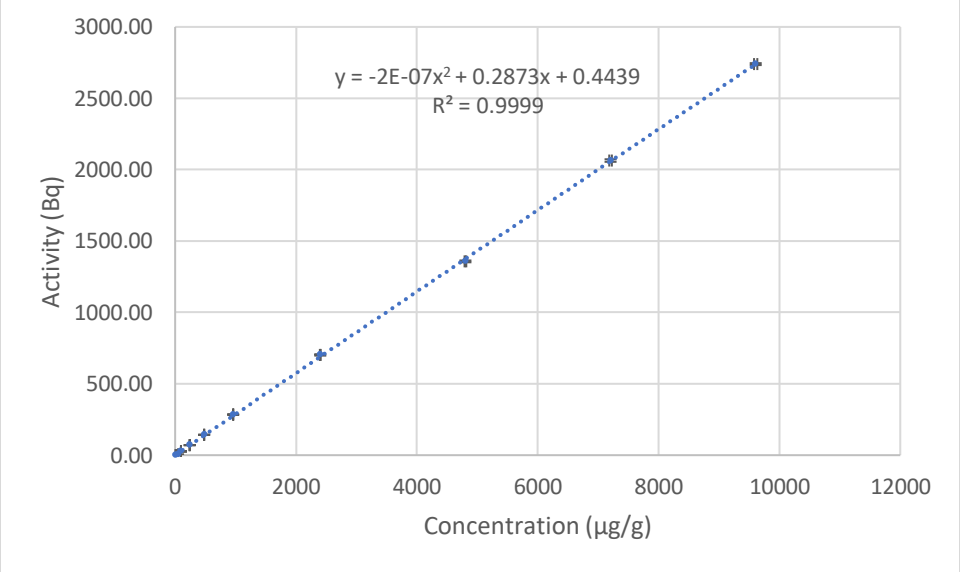

Figure B-14: Lutetium Counting Data Plot

APPENDIX C: EXPERIMENTAL SELF-SHIELDING FACTORS

Table C-1: Lanthanum Self-Shielding Factors

µg/g	±	Activity	±	µg/g Relation	±	Activity Relation	±	SSF	±
9500	21	3205.5	12.51	842.400	2.43	811.989	9.117	0.964	0.011
7125	15.75	2362.9	9.38	631.800	1.83	598.538	6.734	0.947	0.011
4750	10.5	1628.1	5.91	421.200	1.22	412.409	4.592	0.979	0.011
2375	5.25	826.42	4.74	210.600	0.61	209.339	2.510	0.994	0.012
950.0	2.1	364.79	2.66	84.240	0.24	92.405	1.183	1.097	0.014
474.98	1.05	168.47	1.48	42.120	0.12	42.675	0.586	1.013	0.014
237.49	0.525	83.49	0.80	21.060	0.06	21.148	0.300	1.004	0.015
90.21	0.21	31.47	0.30	8.000	0.02	7.971	0.113	0.996	0.014
45.11	0.105	15.80	0.16	4.000	0.01	4.002	0.059	1.000	0.015
11.28	0.021	3.95	0.04	1.000	0.00	1.000	0.015	1.000	0.015

Table C-2: Cerium Self-Shielding Factors

µg/g	±	Activity	±	µg/g Relation	±	Activity Relation	±	SSF	±
8959	23	459.88	3.22	83.334	0.303	75.253	2.131	0.903	0.026
6719	17.25	349.02	2.86	62.500	0.227	57.112	1.635	0.914	0.026
4479	11.5	247.47	2.45	41.667	0.151	40.495	1.181	0.972	0.029
2240	5.75	114.64	1.35	20.833	0.076	18.759	0.560	0.900	0.027
895.9	2.3	51.17	0.71	8.334	0.030	8.374	0.258	1.005	0.031
447.9	1.15	24.90	0.42	4.167	0.015	4.075	0.131	0.978	0.032
250.8	0.644	14.10	0.29	2.333	0.008	2.307	0.079	0.989	0.034
107.51	0.276	6.11	0.17	1.000	0.004	1.000	0.039	1.000	0.039
53.75	0.138	-	-	-	-	-	-	-	-
8.958	0.023	-	-	-	-	-	-	-	-

Table C-3: Praseodymium Self-Shielding Factors

µg/g	±	Activity	±	µg/g Relation	±	Activity Relation	±	SSF	±
9483	27	552.34	4.54	1000.000	4.256	774.950	8.000	0.775	0.009
7112	22.5	439.55	3.09	750.000	3.355	616.695	5.795	0.822	0.009
4741	15	298.92	2.66	500.000	2.237	419.392	4.557	0.839	0.010
2371	7.5	149.07	1.46	250.000	1.118	209.152	2.432	0.837	0.010
948.3	3	63.88	0.64	100.000	0.447	89.624	1.058	0.896	0.011
474.1	1.5	32.07	0.32	50.000	0.224	44.989	0.532	0.900	0.011
237.1	0.75	15.07	0.15	25.000	0.112	21.143	0.251	0.846	0.011
94.83	0.3	5.86	0.06	10.000	0.045	8.216	0.100	0.822	0.011
47.41	0.15	3.06	0.03	5.000	0.022	4.297	0.049	0.859	0.010
9.483	0.03	0.71	0.00	1.000	0.004	1.000	0.009	1.000	0.010

Table C-4: Neodymium Self-Shielding Factors

µg/g	±	Activity	±	µg/g Relation	±	Activity Relation	±	SSF	±
9560	31	430.54	3.27	99.583	0.456	96.073	1.707	0.965	0.018
7200	23	335.05	3.02	75.000	0.341	74.765	1.377	0.997	0.019
4800	16	227.02	2.45	50.000	0.232	50.659	0.981	1.013	0.020
2400	7.8	114.11	1.27	24.999	0.115	25.462	0.498	1.019	0.020
960.0	3.1	46.68	0.54	10.000	0.046	10.417	0.206	1.042	0.021
240.0	0.78	11.09	0.16	2.500	0.011	2.475	0.053	0.990	0.022
480.0	1.6	22.13	0.19	5.000	0.023	4.938	0.090	0.988	0.019
96.00	0.31	4.48	0.07	1.000	0.005	1.000	0.023	1.000	0.023
48.00	0.16	-	-	-	-	-	-	-	-
9.600	0.031	-	-	-	-	-	-	-	-

Table C-5: Samarium Self-Shielding Factors

µg/g	±	Activity	±	µg/g Relation	±	Activity Relation	±	SSF	±
9529	26	8909.35	10.74	842.400	2.780	578.052	2.868	0.686	0.004
7147	19.5	7107.10	7.37	631.800	2.085	461.119	2.270	0.730	0.004
4764	13	5041.72	5.02	421.200	1.390	327.115	1.607	0.777	0.005
2382	6.5	2810.71	3.67	210.600	0.695	182.363	0.909	0.866	0.005
952.9	2.6	1112.36	7.04	84.240	0.278	72.171	0.574	0.857	0.007
476.4	1.3	555.65	3.14	42.120	0.139	36.051	0.268	0.856	0.007
238.2	0.68	294.69	2.48	21.060	0.072	19.120	0.185	0.908	0.009
90.49	0.21	112.86	1.30	8.000	0.024	7.322	0.091	0.915	0.012
45.25	0.13	59.68	0.27	4.000	0.014	3.872	0.026	0.968	0.007
11.312	0.021	15.41	0.07	1.000	0.003	1.000	0.007	1.000	0.007

Table C-6: Europium Self-Shielding Factors

µg/g	±	Activity	±	µg/g Relation	±	Activity Relation	±	SSF	±
9979	37	1435.00	8.67	1046.017	5.485	775.547	10.056	0.741	0.010
7484	27.75	1115.30	7.60	784.486	4.114	602.765	8.044	0.768	0.011
4990	18.5	783.47	6.30	523.061	2.743	423.425	5.933	0.810	0.012
2495	9.251	347.57	2.95	261.530	1.371	187.843	2.681	0.718	0.011
947.0	3.511	172.84	1.72	99.266	0.521	93.414	1.420	0.941	0.015
473.0	1.754	87.55	0.66	49.581	0.260	47.318	0.651	0.954	0.014
238.0	0.882	42.91	0.33	24.948	0.131	23.190	0.320	0.930	0.014
95.00	0.352	16.71	0.12	9.958	0.052	9.029	0.122	0.907	0.013
47.90	0.178	8.71	0.10	5.021	0.026	4.705	0.078	0.937	0.016
9.540	0.035	1.85	0.02	1.000	0.005	1.000	0.016	1.000	0.017

Table C-7: Gadolinium Self-Shielding Factors

µg/g	±	Activity	±	µg/g Relation	±	Activity Relation	±	SSF	±
9450	36	169.48	2.39	994.787	5.345	171.950	2.831	0.173	0.003
7125	27	145.50	1.91	750.000	4.020	147.623	2.315	0.197	0.003
4750	18	111.48	1.40	500.000	2.680	113.105	1.717	0.226	0.004
2375	9	69.09	0.89	250.000	1.340	70.094	1.081	0.280	0.005
949.9	32.4	32.08	0.48	99.994	3.432	32.551	0.558	0.326	0.012
475.0	2.7	16.95	0.18	50.000	0.342	17.196	0.234	0.344	0.005
237.5	0.9	8.51	0.09	25.000	0.134	8.635	0.116	0.345	0.005
95.00	0.36	4.17	0.04	10.000	0.054	4.227	0.055	0.423	0.006
47.50	0.18	2.34	0.02	5.000	0.027	2.372	0.030	0.474	0.007
9.500	0.036	0.99	0.01	1.000	0.005	1.000	0.012	1.000	0.013

Table C-8: Terbium Self-Shielding Factors

µg/g	±	Activity	±	µg/g Relation	±	Activity Relation	±	SSF	±
9570	36	185.52	1.93	997.862	4.882	966.752	13.157	0.969	0.014
7177	27	142.69	1.46	748.394	3.662	743.568	10.008	0.994	0.014
4749	18	94.14	0.96	495.182	2.434	490.597	6.581	0.991	0.014
2392	9	47.32	0.48	249.468	1.221	246.574	3.301	0.988	0.014
957.0	3.6	19.50	0.20	99.791	0.488	101.625	1.375	1.018	0.015
478.5	1.8	10.05	0.08	49.896	0.244	52.374	0.634	1.050	0.014
239.8	0.75	4.56	0.03	25.002	0.111	23.741	0.261	0.950	0.011
95.91	0.3	1.53	0.02	10.001	0.044	7.991	0.120	0.799	0.012
47.95	0.15	0.86	0.00	5.000	0.022	4.498	0.043	0.900	0.010
9.590	0.03	0.19	0.00	1.000	0.004	1.000	0.012	1.000	0.013

Table C-9: Dysprosium Self-Shielding Factors

µg/g	±	Activity	±	µg/g Relation	±	Activity Relation	±	SSF	±
9371	36	26023.75	7.68	1000.000	4.802	870.611	10.025	0.871	0.011
7029	27	20083.97	5.04	750.000	4.075	671.899	7.736	0.896	0.011
4686	18	13368.04	7.32	500.000	2.716	447.221	5.154	0.894	0.011
2343	9	6887.74	7.24	250.000	1.358	230.426	2.663	0.922	0.012
937.1	3.6	2582.56	9.92	100.000	0.543	86.398	1.048	0.864	0.011
468.6	1.8	1423.90	7.27	50.000	0.272	47.636	0.600	0.953	0.013
234.3	0.9	701.20	4.83	25.000	0.136	23.458	0.315	0.938	0.014
93.71	0.36	702.35	4.92	10.000	0.054	23.497	0.317	2.350	0.034
46.86	0.18	142.37	1.55	5.000	0.027	4.763	0.076	0.953	0.016
9.371	0.036	29.89	0.34	1.000	0.005	1.000	0.016	1.000	0.017

Table C-10: Holmium Self-Shielding Factors

µg/g	±	Activity	±	µg/g Relation	±	Activity Relation	±	SSF	±
9511	27	3687.12	16.34	1000.000	4.816	835.122	9.835	0.835	0.011
7134	27.75	2802.04	13.65	750.000	4.126	634.654	7.584	0.846	0.011
4756	18.5	1857.14	13.12	500.000	2.751	420.636	5.468	0.841	0.012
2378	9.25	962.54	7.49	250.000	1.375	218.012	2.922	0.872	0.013
951.1	3.7	413.10	2.99	100.000	0.550	93.565	1.225	0.936	0.013
475.6	1.85	212.06	2.18	50.000	0.275	48.031	0.721	0.961	0.015
237.8	0.925	95.77	0.96	25.000	0.138	21.692	0.321	0.868	0.014
95.11	0.37	38.53	0.39	10.000	0.055	8.728	0.130	0.873	0.014
47.56	0.185	18.49	0.22	5.000	0.028	4.189	0.067	0.838	0.014
9.511	0.037	4.42	0.05	1.000	0.006	1.000	0.015	1.000	0.016

Table C-11: Erbium Self-Shielding Factors

µg/g	±	Activity	±	µg/g Relation	±	Activity Relation	±	SSF	±
9534	27	1453.93	5.16	842.400	115.398	579.817	2.108	0.688	0.094
7150	23.25	1116.94	4.45	631.800	86.555	445.428	1.812	0.705	0.097
4767	15.5	730.25	3.62	421.200	57.703	291.219	1.464	0.691	0.095
2383	7.75	366.68	2.51	210.600	28.852	146.228	1.008	0.694	0.095
953.4	3.1	150.02	1.33	84.240	11.541	59.826	0.534	0.710	0.097
476.7	1.55	75.46	0.66	42.120	5.770	30.092	0.264	0.714	0.098
238.3	0.775	37.35	0.34	21.060	2.885	14.893	0.135	0.707	0.097
101.86	13.95	17.05	0.17	9.000	1.743	6.800	0.068	0.756	0.147
45.27	6.2	2.26	0.00	4.000	0.775	0.901	0.001	0.225	0.044
11.317	1.55	2.51	0.00	1.000	0.194	1.000	0.001	1.000	0.194

Table C-12: Thulium Self-Shielding Factors

µg/g	±	Activity	±	µg/g Relation	±	Activity Relation	±	SSF	±
9550	36	2244.37	7.18	1000.000	5.331	963.019	15.732	0.963	0.017
7163	27	1707.38	8.06	750.052	3.998	732.609	12.235	0.977	0.017
4775	18	1116.21	6.50	500.000	2.666	478.945	8.163	0.958	0.017
2388	9	564.89	4.65	250.052	1.333	242.386	4.365	0.969	0.018
955.0	0.36	247.18	2.45	100.000	0.379	106.062	1.998	1.061	0.020
477.5	1.8	117.04	1.26	50.000	0.267	50.218	0.970	1.004	0.020
238.8	0.9	59.69	0.16	25.001	0.133	25.612	0.416	1.024	0.018
95.50	0.36	15.70	0.19	10.000	0.053	6.735	0.135	0.673	0.014
47.75	0.18	11.17	0.14	5.000	0.027	4.791	0.098	0.958	0.020
9.550	0.036	2.33	0.04	1.000	0.005	1.000	0.023	1.000	0.023

Table C-13: Ytterbium Self-Shielding Factors

µg/g	±	Activity	±	µg/g Relation	±	Activity Relation	±	SSF	±
9476	27	716.11	3.56	1000.000	4.030	901.837	5.892	0.902	0.007
7107	20.25	541.18	3.08	750.000	3.022	681.529	4.834	0.909	0.007
4738	13.5	360.60	2.47	500.000	2.015	454.124	3.662	0.908	0.008
2369	6.75	179.93	1.73	250.000	1.007	226.591	2.382	0.906	0.010
947.6	2.7	76.52	0.72	100.000	0.403	96.360	0.994	0.964	0.011
473.8	1.35	40.99	0.37	50.000	0.201	51.623	0.516	1.032	0.011
236.9	0.675	18.42	0.18	25.000	0.101	23.198	0.249	0.928	0.011
94.76	0.27	7.18	0.08	10.000	0.040	9.046	0.106	0.905	0.011
47.38	0.135	3.60	0.04	5.000	0.020	4.530	0.055	0.906	0.012
9.476	0.027	0.79	0.00	1.000	0.004	1.000	0.006	1.000	0.007

Table C-14: Lutetium Self-Shielding Factors

µg/g	±	Activity	±	µg/g Relation	±	Activity Relation	±	SSF	±
9607	27	2739.50	6.87	1000.000	4.124	3294.823	76.703	3.295	0.078
7206	21.75	2063.87	9.02	750.000	3.202	2482.239	58.466	3.310	0.079
4804	14.5	1357.55	6.49	500.000	2.134	1632.731	38.586	3.265	0.078
2402	7.25	702.39	5.01	250.000	1.067	844.768	20.460	3.379	0.083
960.7	2.9	284.55	2.82	100.000	0.427	342.232	8.614	3.422	0.087
480.4	1.45	143.01	1.23	50.000	0.213	171.997	4.247	3.440	0.086
240.2	0.725	69.93	0.69	25.000	0.107	84.108	2.114	3.364	0.086
96.07	0.29	26.00	0.18	10.000	0.043	31.272	0.754	3.127	0.077
48.04	0.145	3.77	0.05	5.000	0.021	4.533	0.123	0.907	0.025
9.607	0.029	0.83	0.02	1.000	0.004	1.000	0.033	1.000	0.033

APPENDIX D: MCNP Results

Table D-1: MCNP Results for Lanthanum

µg/g	MCNP Tally T	±	Relative Activity
10	4.58E-09	0.0033	1.00E+00
50	2.29E-08	0.0033	5.00E+00
100	4.58E-08	0.0033	9.99E+00
250	1.14E-07	0.0033	2.50E+01
500	2.28E-07	0.0033	4.99E+01
1000	4.55E-07	0.0033	9.94E+01
2500	1.13E-06	0.0032	2.46E+02
5000	2.22E-06	0.0032	4.85E+02
7500	3.29E-06	0.0032	7.19E+02
10000	4.32E-06	0.0031	9.43E+02

Table D-2: MCNP Results for Cerium

µg/g	MCNP Tally 1	±	MCNP Tally 2	±	MCNP Tally 3	±
10	4.97E-09	0.0107	7.01E-10	0.0095	2.85E-10	0.0024
50	2.48E-08	0.0107	3.51E-09	0.0095	1.42E-09	0.0024
100	4.97E-08	0.0107	7.01E-09	0.0095	2.85E-09	0.0024
250	1.24E-07	0.0107	1.75E-08	0.0095	7.11E-09	0.0024
500	2.48E-07	0.0107	3.50E-08	0.0095	1.42E-08	0.0024
1000	4.96E-07	0.0107	7.00E-08	0.0095	2.84E-08	0.0024
2500	1.23E-06	0.0107	1.74E-07	0.0095	7.07E-08	0.0024
5000	2.45E-06	0.0107	3.46E-07	0.0095	1.40E-07	0.0024
7500	3.66E-06	0.0107	5.16E-07	0.0095	2.09E-07	0.0024
10000	4.86E-06	0.0107	6.86E-07	0.0095	2.78E-07	0.0024

Table D-3: MCNP Results for Cerium Continued

MCNP Tally 4	±	MCNP Tally T	±	Relative Activity
4.83E-10	0.0024	6.44E-09	0.0034	1.00E+00
2.41E-09	0.0024	3.22E-08	0.0034	5.00E+00
4.83E-09	0.0024	6.44E-08	0.0034	1.00E+01
1.21E-08	0.0024	1.61E-07	0.0034	2.50E+01
2.41E-08	0.0024	3.21E-07	0.0034	4.99E+01
4.82E-08	0.0024	6.42E-07	0.0034	9.98E+01
1.20E-07	0.0024	1.60E-06	0.0034	2.48E+02
2.38E-07	0.0024	3.18E-06	0.0034	4.94E+02
3.55E-07	0.0024	4.74E-06	0.0034	7.36E+02
4.72E-07	0.0024	6.29E-06	0.0034	9.78E+02

Table D-4: MCNP Results for Praseodymium

µg/g	MCNP Tally T	±	Relative Activity
10	5.89E-09	0.0025	1.00E+00
50	2.94E-08	0.0025	5.00E+00
100	5.88E-08	0.0025	1.00E+01
250	1.47E-07	0.0025	2.50E+01
500	2.94E-07	0.0025	4.99E+01
1000	5.87E-07	0.0025	9.97E+01
2500	1.46E-06	0.0025	2.48E+02
5000	2.89E-06	0.0025	4.91E+02
7500	4.30E-06	0.0025	7.31E+02
10000	5.69E-06	0.0025	9.67E+02

Table D-5: MCNP Results for Neodymium

µg/g	MCNP Tally 1	±	MCNP Tally 2	±	MCNP Tally 3	±	MCNP Tally 4	±
10	9.13E-09	0.0024	1.59E-07	0.0024	1.82E-09	0.0024	2.42E-08	0.004
50	4.56E-08	0.0024	7.94E-07	0.0024	9.11E-09	0.0024	1.21E-07	0.004
100	9.13E-08	0.0024	1.59E-06	0.0024	1.82E-08	0.0024	2.42E-07	0.004
250	2.28E-07	0.0024	3.97E-06	0.0024	4.55E-08	0.0024	6.05E-07	0.004
500	4.56E-07	0.0024	7.93E-06	0.0024	9.09E-08	0.0024	1.21E-06	0.004
1000	9.10E-07	0.0024	1.58E-05	0.0024	1.82E-07	0.0024	2.41E-06	0.004
2500	2.26E-06	0.0024	3.93E-05	0.0024	4.51E-07	0.0024	5.99E-06	0.0039
5000	4.48E-06	0.0024	7.80E-05	0.0024	8.94E-07	0.0024	1.19E-05	0.0039
7500	6.48E-06	0.0024	1.13E-04	0.0024	1.29E-06	0.0024	1.71E-05	0.0039
10000	8.80E-06	0.0024	1.53E-04	0.0024	1.76E-06	0.0024	2.33E-05	0.0039

Table D-6: MCNP Results for Neodymium Continued

MCNP Tally 5	±	MCNP Tally 6	±	MCNP Tally 7	±	MCNP Tally T	±	Relative Activity
7.76E-10	0.0031	1.55E-09	0.0053	8.08E-10	0.0185	1.97E-07	0.0203	1.00E+00
3.88E-09	0.0031	7.76E-09	0.0053	4.04E-09	0.0185	9.86E-07	0.0203	5.00E+00
7.76E-09	0.0031	1.55E-08	0.0053	8.07E-09	0.0185	1.97E-06	0.0203	1.00E+01
1.94E-08	0.0031	3.88E-08	0.0053	2.02E-08	0.0185	4.92E-06	0.0203	2.50E+01
3.87E-08	0.0031	7.75E-08	0.0053	4.03E-08	0.0185	9.84E-06	0.0203	4.99E+01
7.73E-08	0.0031	1.55E-07	0.0053	8.05E-08	0.0185	1.96E-05	0.0203	9.96E+01
1.92E-07	0.0031	3.85E-07	0.0053	2.01E-07	0.0188	4.88E-05	0.0206	2.48E+02
3.81E-07	0.0031	7.63E-07	0.0052	3.98E-07	0.0189	9.68E-05	0.0206	4.91E+02
5.51E-07	0.0032	1.10E-06	0.0053	5.74E-07	0.0189	1.40E-04	0.0207	7.09E+02
7.50E-07	0.0032	1.50E-06	0.0052	7.79E-07	0.0188	1.90E-04	0.0206	9.64E+02

Table D-7: MCNP Results for Samarium

µg/g	MCNP Tally 1	±	MCNP Tally 2	±	MCNP Tally 3	±
10	8.26E-10	0.0025	4.16E-08	0.0061	1.89E-09	0.013
50	4.10E-09	0.0025	2.07E-07	0.0061	9.40E-09	0.0131
100	8.10E-09	0.0025	4.10E-07	0.0061	1.87E-08	0.0132
250	1.96E-08	0.0025	1.00E-06	0.0062	4.57E-08	0.0134
500	3.73E-08	0.0026	1.94E-06	0.0064	8.85E-08	0.0138
1000	6.82E-08	0.0026	3.63E-06	0.0067	1.67E-07	0.0144
2500	1.36E-07	0.0028	7.81E-06	0.0075	3.64E-07	0.0164
5000	2.06E-07	0.0031	1.31E-05	0.0084	6.24E-07	0.0184
7500	2.51E-07	0.0034	1.74E-05	0.009	8.44E-07	0.0199
10000	2.86E-07	0.0037	2.12E-05	0.0094	1.04E-06	0.0208

Table D-8: MCNP Results for Samarium Continued (1)

MCNP Tally 4	±	MCNP Tally 5	±	MCNP Tally 6	±
2.89E-05	0.0024	5.43E-08	0.005	1.52E-07	0.0094
1.43E-04	0.0024	2.69E-07	0.005	7.53E-07	0.0094
2.82E-04	0.0024	5.33E-07	0.0051	1.49E-06	0.0094
6.79E-04	0.0024	1.29E-06	0.0052	3.63E-06	0.0094
1.28E-03	0.0024	2.47E-06	0.0054	6.94E-06	0.0093
2.28E-03	0.0025	4.54E-06	0.0058	1.28E-05	0.0091
4.31E-03	0.0025	9.19E-06	0.0068	2.59E-05	0.0087
6.10E-03	0.0025	1.43E-05	0.0082	4.04E-05	0.0086
7.06E-03	0.0025	1.78E-05	0.0094	5.04E-05	0.0084
7.68E-03	0.0025	2.06E-05	0.0105	5.80E-05	0.0082

Table D-9: MCNP Results for Samarium Continued (2)

MCNP Tally 7	±	MCNP Tally T	±	Relative Activity
4.69E-09	0.0073	2.91E-05	0.0196	1.00E+00
2.33E-08	0.0073	1.44E-04	0.0197	4.95E+00
4.61E-08	0.0074	2.85E-04	0.0198	9.77E+00
1.12E-07	0.0076	6.85E-04	0.0201	2.35E+01
2.14E-07	0.0078	1.29E-03	0.0205	4.42E+01
3.95E-07	0.0084	2.31E-03	0.0213	7.91E+01
8.07E-07	0.0099	4.35E-03	0.0236	1.49E+02
1.27E-06	0.012	6.17E-03	0.0266	2.12E+02
1.61E-06	0.0136	7.15E-03	0.0290	2.45E+02
1.89E-06	0.0149	7.79E-03	0.0307	2.67E+02

Table D-10: MCNP Results for Europium

µg/g	MCNP Tally 1	±	MCNP Tally 2	±	MCNP Tally T	±	Relative Activity
10	4.56E-06	0.0025	1.97E-07	0.0024	4.76E-06	0.0035	1.00E+00
50	2.26E-05	0.0025	9.76E-07	0.0024	2.36E-05	0.0035	4.96E+00
100	4.49E-05	0.0025	1.94E-06	0.0024	4.68E-05	0.0035	9.84E+00
250	1.10E-04	0.0025	4.75E-06	0.0024	1.14E-04	0.0035	2.40E+01
500	2.11E-04	0.0025	9.18E-06	0.0024	2.20E-04	0.0035	4.62E+01
1000	3.91E-04	0.0025	1.72E-05	0.0025	4.08E-04	0.0035	8.58E+01
2500	8.02E-04	0.0025	3.64E-05	0.0025	8.39E-04	0.0035	1.76E+02
5000	1.25E-03	0.0025	5.90E-05	0.0026	1.31E-03	0.0036	2.74E+02
7500	1.53E-03	0.0025	7.49E-05	0.0027	1.60E-03	0.0037	3.36E+02
10000	1.72E-03	0.0025	8.70E-05	0.0028	1.80E-03	0.0038	3.79E+02

Table D-11: MCNP Results for Gadolinium

µg/g	MCNP Tally 1	±	MCNP Tally 2	±	MCNP Tally 3	±	MCNP Tally 4	±
10	4.43E-08	0.0032	2.46E-05	0.0025	2.85E-09	0.0216	1.03E-04	0.0025
50	2.11E-07	0.0032	1.16E-04	0.0025	1.41E-08	0.0219	4.86E-04	0.0025
100	4.00E-07	0.0033	2.19E-04	0.0025	2.76E-08	0.0223	9.12E-04	0.0025
250	8.65E-07	0.0036	4.61E-04	0.0025	6.61E-08	0.0233	1.93E-03	0.0025
500	1.42E-06	0.0041	7.31E-04	0.0025	1.26E-07	0.0244	3.05E-03	0.0025
1000	2.16E-06	0.005	1.03E-03	0.0025	2.36E-07	0.0259	4.32E-03	0.0025
2500	3.44E-06	0.0074	1.37E-03	0.0025	5.43E-07	0.0277	5.74E-03	0.0025
5000	4.88E-06	0.01	1.55E-03	0.0025	1.02E-06	0.0289	6.47E-03	0.0025
7500	6.07E-06	0.0117	1.62E-03	0.0025	1.49E-06	0.0293	6.75E-03	0.0025
10000	7.17E-06	0.013	1.66E-03	0.0025	1.93E-06	0.0294	6.90E-03	0.0025

Table D-12: MCNP Results for Gadolinium Continued

MCNP Tally 5	±	MCNP Tally 6	±	MCNP Tally T	±	Relative Activity
2.36E-09	0.0225	8.39E-10	0.0091	1.27E-04	0.0328	1.00E+00
1.15E-08	0.023	4.02E-09	0.0094	6.03E-04	0.0335	4.74E+00
2.25E-08	0.0236	7.67E-09	0.0099	1.13E-03	0.0343	8.89E+00
5.27E-08	0.0252	1.70E-08	0.0112	2.39E-03	0.0365	1.88E+01
9.73E-08	0.0272	2.88E-08	0.0131	3.79E-03	0.0392	2.98E+01
1.76E-07	0.0299	4.63E-08	0.0162	5.36E-03	0.0432	4.21E+01
3.86E-07	0.0336	8.29E-08	0.0224	7.12E-03	0.0497	5.60E+01
7.05E-07	0.0358	1.32E-07	0.0278	8.03E-03	0.0548	6.31E+01
1.00E-06	0.0368	1.77E-07	0.0308	8.38E-03	0.0575	6.58E+01
1.29E-06	0.0372	2.21E-07	0.0328	8.57E-03	0.0592	6.74E+01

Table D-13: MCNP Results for Terbium

µg/g	MCNP Tally T	±	Relative Activity
10	1.89E-08	0.0068	1.00E+00
50	9.45E-08	0.0068	5.00E+00
100	1.89E-07	0.0068	9.99E+00
250	4.71E-07	0.0067	2.49E+01
500	9.41E-07	0.0067	4.97E+01
1000	1.87E-06	0.0065	9.89E+01
2500	4.61E-06	0.0061	2.44E+02
5000	9.01E-06	0.0056	4.77E+02
7500	1.33E-05	0.0052	7.01E+02
10000	1.74E-05	0.005	9.19E+02

Table D-14: MCNP Results for Dysprosium

µg/g	MCNP Tally 1	±	MCNP Tally 2	±	MCNP Tally 3	±
10	3.38E-08	0.0065	2.46E-08	0.0045	4.71E-08	0.0093
50	1.69E-07	0.0065	1.23E-07	0.0045	2.36E-07	0.0093
100	3.38E-07	0.0065	2.45E-07	0.0046	4.70E-07	0.0093
250	8.43E-07	0.0065	6.10E-07	0.0046	1.17E-06	0.0094
500	1.68E-06	0.0065	1.21E-06	0.0046	2.33E-06	0.0094
1000	3.33E-06	0.0066	2.39E-06	0.0046	4.62E-06	0.0095
2500	8.13E-06	0.0067	5.75E-06	0.0047	1.12E-05	0.0097
5000	1.57E-05	0.0069	1.08E-05	0.005	2.15E-05	0.01
7500	2.27E-05	0.0071	1.54E-05	0.0052	3.09E-05	0.0104
10000	2.94E-05	0.0073	1.95E-05	0.0054	3.96E-05	0.0106

Table D-15: MCNP Results for Dysprosium Continued (1)

MCNP Tally 4	±	MCNP Tally 5	±	MCNP Tally 6	±
3.06E-07	0.0024	1.43E-07	0.0084	8.69E-08	0.0051
1.53E-06	0.0024	7.11E-07	0.0084	4.34E-07	0.0051
3.05E-06	0.0024	1.42E-06	0.0084	8.66E-07	0.0051
7.60E-06	0.0024	3.53E-06	0.0083	2.16E-06	0.0051
1.51E-05	0.0024	6.98E-06	0.0082	4.28E-06	0.0051
2.97E-05	0.0024	1.37E-05	0.008	8.46E-06	0.0051
7.12E-05	0.0024	3.22E-05	0.0075	2.03E-05	0.0051
1.33E-04	0.0024	5.89E-05	0.0068	3.81E-05	0.0051
1.87E-04	0.0024	8.16E-05	0.0063	5.39E-05	0.0051
2.35E-04	0.0024	1.01E-04	0.006	6.80E-05	0.0051

Table D-16: MCNP Results for Dysprosium Continued (2)

MCNP Tally 7	±	MCNP Tally T	±	Relative Activity
1.27E-06	0.0024	1.91E-06	0.0160	1.00E+00
6.36E-06	0.0024	9.56E-06	0.0160	4.99E+00
1.27E-05	0.0024	1.91E-05	0.0161	9.97E+00
3.16E-05	0.0024	4.75E-05	0.0161	2.48E+01
6.27E-05	0.0024	9.42E-05	0.0160	4.92E+01
1.24E-04	0.0024	1.86E-04	0.0160	9.70E+01
2.95E-04	0.0024	4.44E-04	0.0160	2.32E+02
5.50E-04	0.0024	8.28E-04	0.0160	4.33E+02
7.71E-04	0.0024	1.16E-03	0.0162	6.07E+02
9.66E-04	0.0024	1.46E-03	0.0164	7.62E+02

Table D-17: MCNP Results for Holmium

µg/g	MCNP Tally T	±	Relative Activity
10	4.36E-08	0.0051	1.00E+00
50	2.18E-07	0.0051	5.00E+00
100	4.36E-07	0.005	9.99E+00
250	1.09E-06	0.005	2.49E+01
500	2.17E-06	0.005	4.97E+01
1000	4.31E-06	0.0049	9.88E+01
2500	1.06E-05	0.0046	2.43E+02
5000	2.07E-05	0.0043	4.73E+02
7500	3.03E-05	0.004	6.94E+02
10000	3.95E-05	0.0038	9.06E+02

Table D-18: MCNP Results for Erbium

µg/g	MCNP Tally 1	±	MCNP Tally 2	±	MCNP Tally 3	±	MCNP Tally 4	±
10	1.74E-08	0.0079	9.55E-09	0.0058	1.00E-08	0.0054	4.27E-07	0.0029
50	8.70E-08	0.0079	4.77E-08	0.0058	5.01E-08	0.0054	2.14E-06	0.0029
100	1.74E-07	0.0079	9.55E-08	0.0058	1.00E-07	0.0053	4.27E-06	0.0029
250	4.35E-07	0.0079	2.38E-07	0.0058	2.50E-07	0.0053	1.07E-05	0.0029
500	8.68E-07	0.0079	4.76E-07	0.0058	4.99E-07	0.0053	2.13E-05	0.0029
1000	1.73E-06	0.0079	9.49E-07	0.0058	9.95E-07	0.0053	4.23E-05	0.0028
2500	4.29E-06	0.008	2.35E-06	0.0059	2.46E-06	0.0053	1.04E-04	0.0028
5000	8.47E-06	0.008	4.65E-06	0.0059	4.84E-06	0.0052	2.03E-04	0.0028
7500	1.25E-05	0.0081	6.84E-06	0.0059	7.08E-06	0.0051	2.96E-04	0.0027
10000	1.65E-05	0.0081	9.06E-06	0.006	9.35E-06	0.0051	3.89E-04	0.0027

Table D-19: MCNP Results for Erbium Continued

MCNP Tally 5	±	MCNP Tally 6	±	MCNP Tally T	±	Relative Activity
2.06E-09	0.0157	5.06E-09	0.0055	4.71E-07	0.0203	1.00E+00
1.03E-08	0.0157	2.53E-08	0.0055	2.36E-06	0.0203	5.00E+00
2.06E-08	0.0157	5.05E-08	0.0055	4.71E-06	0.0202	9.99E+00
5.13E-08	0.0157	1.26E-07	0.0054	1.18E-05	0.0202	2.49E+01
1.02E-07	0.0157	2.52E-07	0.0054	2.35E-05	0.0202	4.98E+01
2.04E-07	0.0157	5.02E-07	0.0054	4.67E-05	0.0202	9.90E+01
5.05E-07	0.0157	1.24E-06	0.0054	1.15E-04	0.0203	2.44E+02
9.93E-07	0.0156	2.44E-06	0.0053	2.25E-04	0.0201	4.77E+02
1.45E-06	0.0155	3.56E-06	0.0049	3.28E-04	0.0199	6.95E+02
1.92E-06	0.0153	4.72E-06	0.0051	4.30E-04	0.0199	9.13E+02

Table D-20: MCNP Results for Thulium

µg/g	MCNP Tally T	±	Relative Activity
10	7.96E-08	0.0085	1.00E+00
50	3.97E-07	0.0085	4.99E+00
100	7.92E-07	0.0084	9.95E+00
250	1.96E-06	0.0082	2.47E+01
500	3.88E-06	0.0079	4.87E+01
1000	7.58E-06	0.0074	9.52E+01
2500	1.80E-05	0.0062	2.26E+02
5000	3.41E-05	0.005	4.28E+02
7500	4.92E-05	0.0044	6.18E+02
10000	6.36E-05	0.0039	7.99E+02

Table D-21: MCNP Results for Lutetium

µg/g	MCNP Tally T	±	Relative Activity
10	2.24E-08	0.0065	1.00E+00
50	1.12E-07	0.0065	5.00E+00
100	2.24E-07	0.0065	9.99E+00
250	5.60E-07	0.0065	2.49E+01
500	1.12E-06	0.0064	4.97E+01
1000	2.22E-06	0.0064	9.89E+01
2500	5.46E-06	0.0061	2.43E+02
5000	1.07E-05	0.0058	4.75E+02
7500	1.56E-05	0.0055	6.97E+02
10000	2.04E-05	0.0053	9.10E+02

Table D-22: MCNP Self-Shielding Factors

µg/g	La	Ce	Pr	Nd	Sm	Eu
10000	0.943	0.978	0.967	0.964	0.267	0.379
7500	0.958	0.981	0.975	0.946	0.327	0.449
5000	0.971	0.987	0.983	0.982	0.423	0.549
2500	0.985	0.994	0.991	0.991	0.597	0.705
1000	0.994	0.998	0.997	0.996	0.791	0.858
500	0.997	0.999	0.998	0.998	0.885	0.923
250	0.999	0.999	0.999	0.999	0.940	0.960
100	0.999	1.000	1.000	9.997	0.977	0.984
250	1.000	1.000	1.000	1.000	0.990	0.992
100	1.000	1.000	1.000	1.000	1.000	1.000

Table D-23: MCNP Self-Shielding Factors

Gd	Tb	Dy	Ho	Er	Tm	Yb	Lu
0.067	0.919	0.762	0.906	0.913	0.799	-	0.910
0.088	0.935	0.810	0.925	0.927	0.824	-	0.929
0.126	0.953	0.865	0.946	0.954	0.856	-	0.949
0.224	0.975	0.928	0.971	0.976	0.906	-	0.974
0.421	0.989	0.970	0.988	0.990	0.952	-	0.989
0.595	0.995	0.984	0.994	0.995	0.974	-	0.994
0.751	0.997	0.992	0.997	0.997	0.987	-	0.997
0.889	0.999	0.997	0.999	0.999	0.995	-	0.999
0.948	1.000	0.999	1.000	0.999	0.998	-	1.000
1.000	1.000	1.000	1.000	1.000	1.000	-	1.000

APPENDIX E: CHILIAN SELF-SHIELDING FACTORS

Table E-1: Self-Shielding Factors calculated from Chilian's Computer Code

PPM	La-140	Ce-141	Ce-143	Pr-142	Nd-147	Sm-153	Sm-155	Eu-152	Gd-153
10000	0.998	1.000	1.000	0.998	0.998	0.806	0.877	0.872	0.440
7500	0.998	1.000	1.000	0.998	0.999	0.842	0.903	0.899	0.505
5000	0.999	1.000	1.000	0.999	0.999	0.883	0.932	0.929	0.598
2500	0.999	1.000	1.000	0.999	0.999	0.932	0.963	0.962	0.741
1000	1.000	1.000	1.000	1.000	1.000	0.968	0.984	0.984	0.872
500	1.000	1.000	1.000	1.000	1.000	0.982	0.992	0.992	0.930
250	1.000	1.000	1.000	1.000	1.000	0.990	0.996	0.996	0.963
100	1.000	1.000	1.000	1.000	1.000	0.995	0.998	0.998	0.984
250	1.000	1.000	1.000	1.000	1.000	0.997	0.999	0.999	0.992
100	1.000	1.000	1.000	1.000	1.000	0.999	1.000	1.000	0.998

Table E-2: Self-Shielding Factors calculated from Chilian's Computer Code Continued

Gd-159	Tb-160	Dy-165	Ho-166	Er-171	Tm-170	Yb-169	Yb-175	Lu-177
0.796	0.973	0.970	0.974	0.992	0.939	0.998	0.998	0.997
0.821	0.978	0.977	0.979	0.994	0.950	0.999	0.999	0.998
0.855	0.984	0.985	0.985	0.996	0.963	0.999	0.999	0.998
0.907	0.991	0.992	0.991	0.998	0.978	1.000	0.999	0.999
0.954	0.996	0.997	0.996	0.999	0.989	1.000	1.000	1.000
0.975	0.998	0.998	0.998	0.999	0.994	1.000	1.000	1.000
0.987	0.999	0.999	0.999	1.000	0.997	1.000	1.000	1.000
0.994	0.999	1.000	0.999	1.000	0.998	1.000	1.000	1.000
0.997	1.000	1.000	1.000	1.000	0.999	1.000	1.000	1.000
0.999	1.000	1.000	1.000	1.000	1.000	1.000	1.000	1.000

Appendix F: PERCENT DIFFERENCE COMPARISON GRAPHS

In the cases of both Cerium, and Ytterbium there are no significant differences between the two sets Chilian self-shielding factors, and were grouped into a single comparison set.

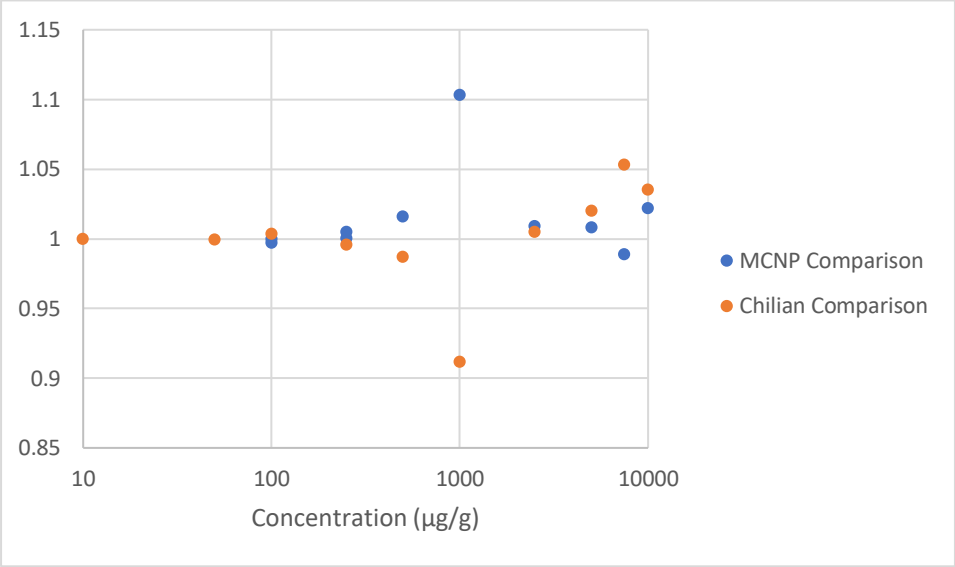

Figure F-1: Models vs Experimental Self-Shielding Factors for Lanthanum

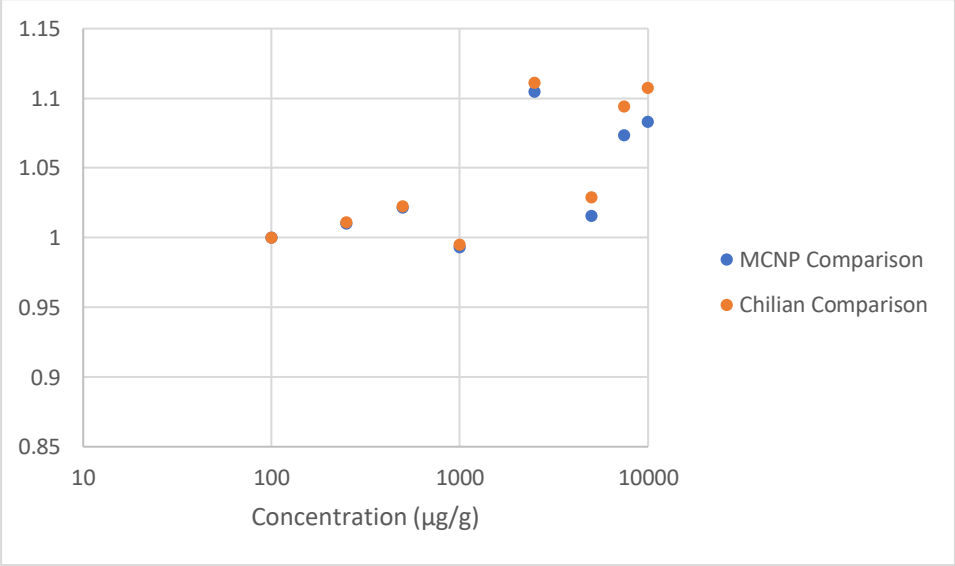

Figure F-2: Models vs Experimental Self-Shielding Factors for Cerium

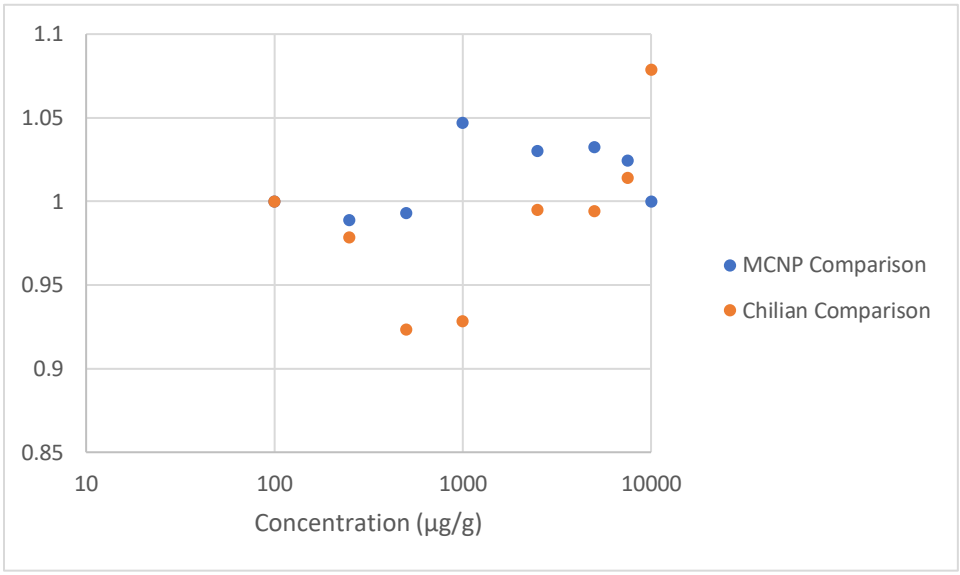

Figure F-3: Models vs Experimental Self-Shielding Factors for Praseodymium

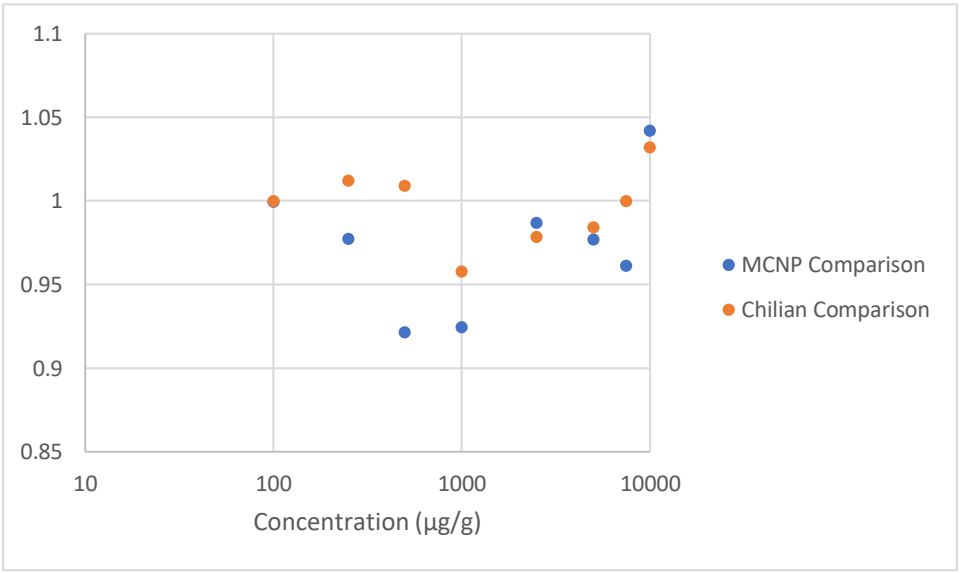

Figure F-4: Models vs Experimental Self-Shielding Factors for Neodymium

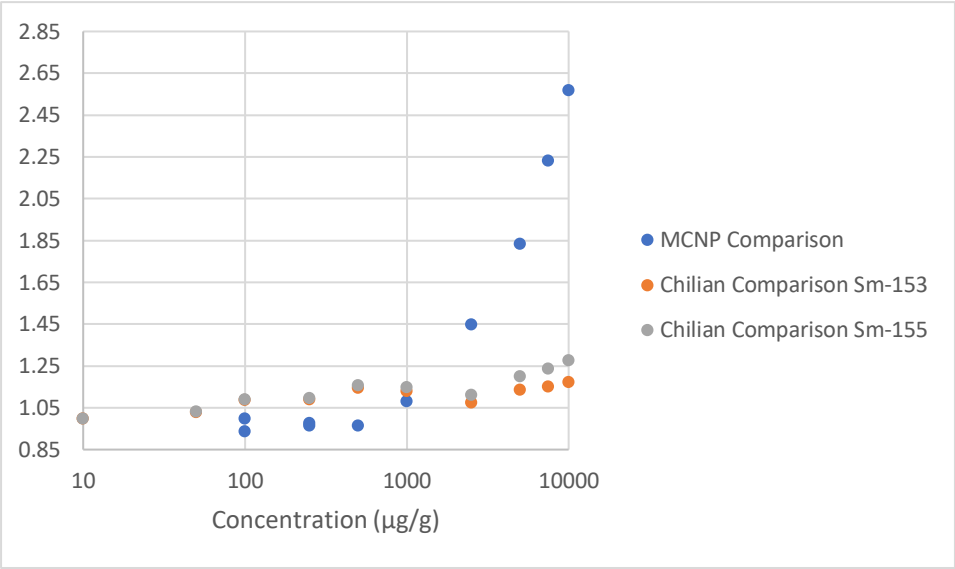

Figure F-5: Models vs Experimental Self-Shielding Factors for Samarium

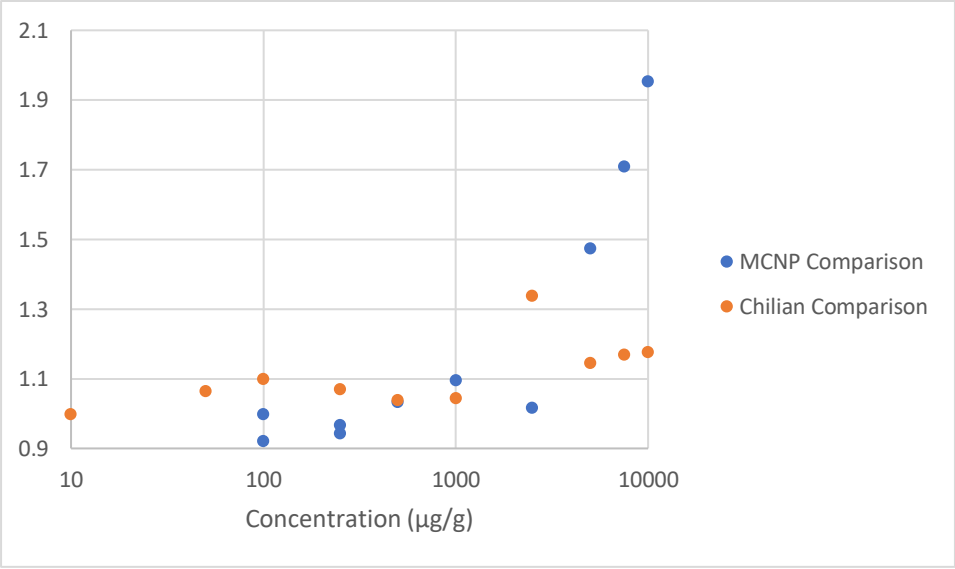

Figure F-6: Models vs Experimental Self-Shielding Factors for Europium

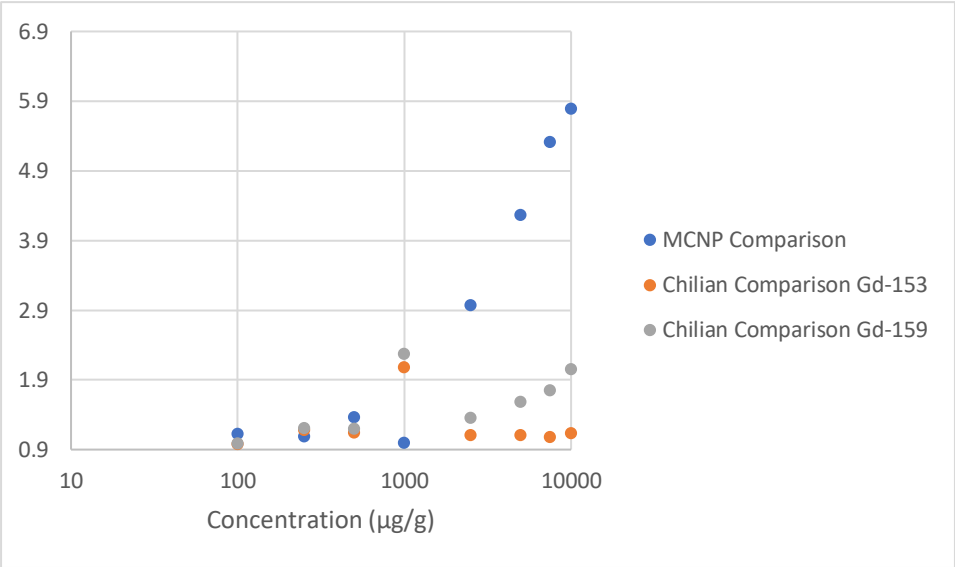

Figure F-7: Models vs Experimental Self-Shielding Factors for Gadolinium

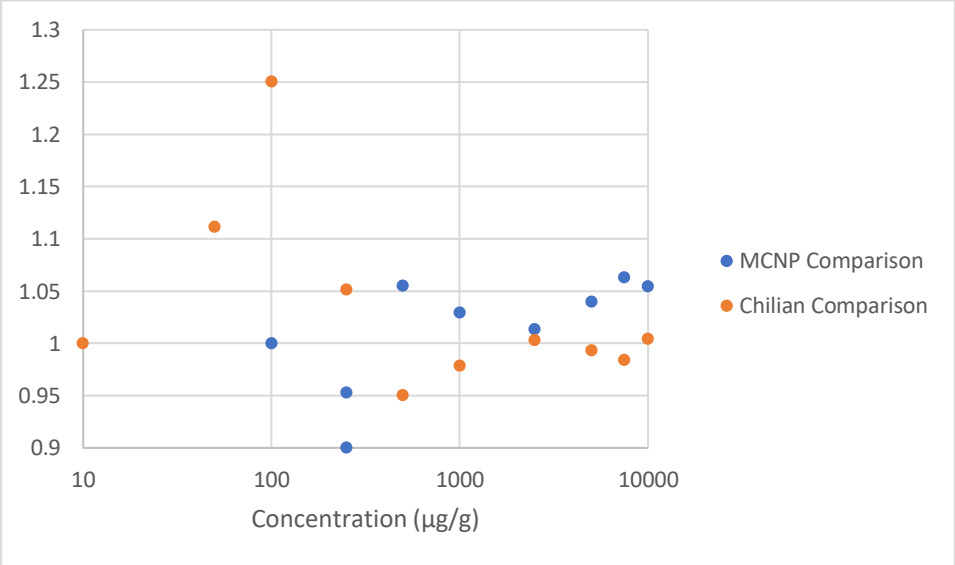

Figure F-8: Models vs Experimental Self-Shielding Factors for Terbium

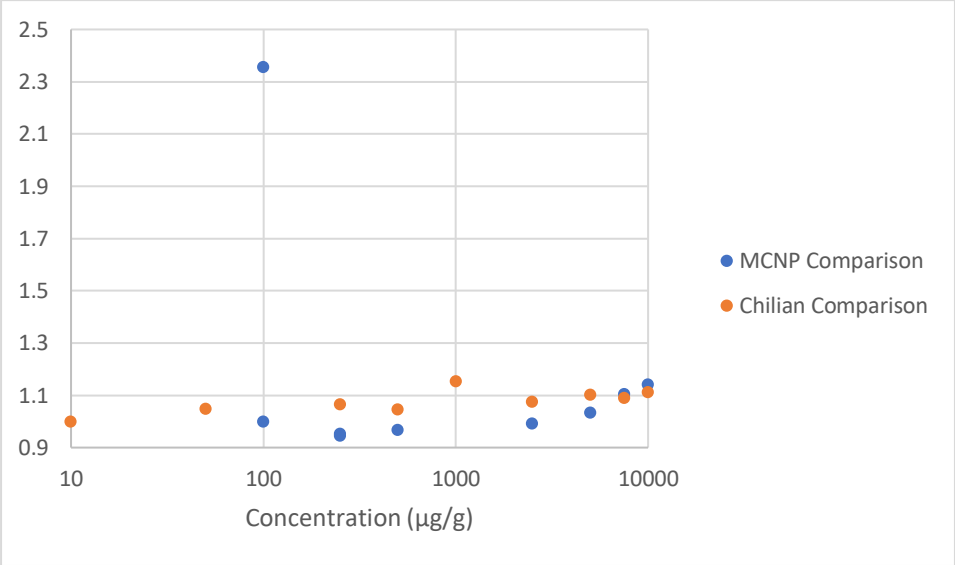

Figure F-9: Models vs Experimental Self-Shielding Factors for Dysprosium

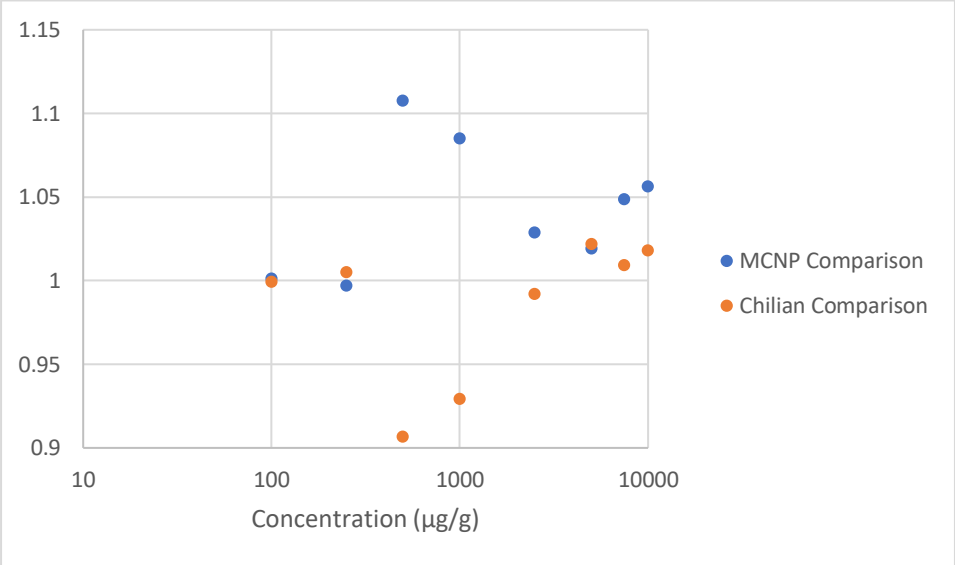

Figure F-10: Models vs Experimental Self-Shielding Factors for Holmium

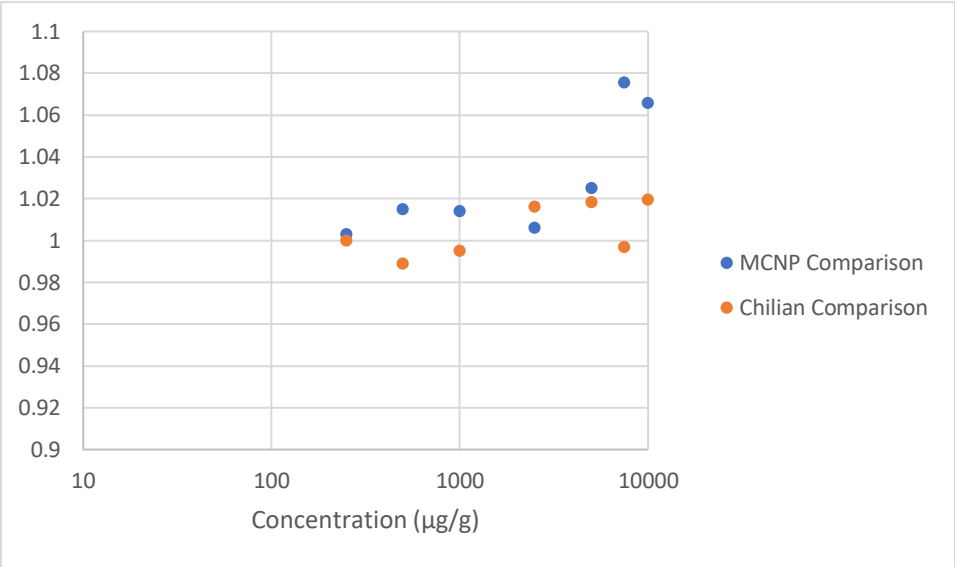

Figure F-11: Models vs Experimental Self-Shielding Factors for Erbium

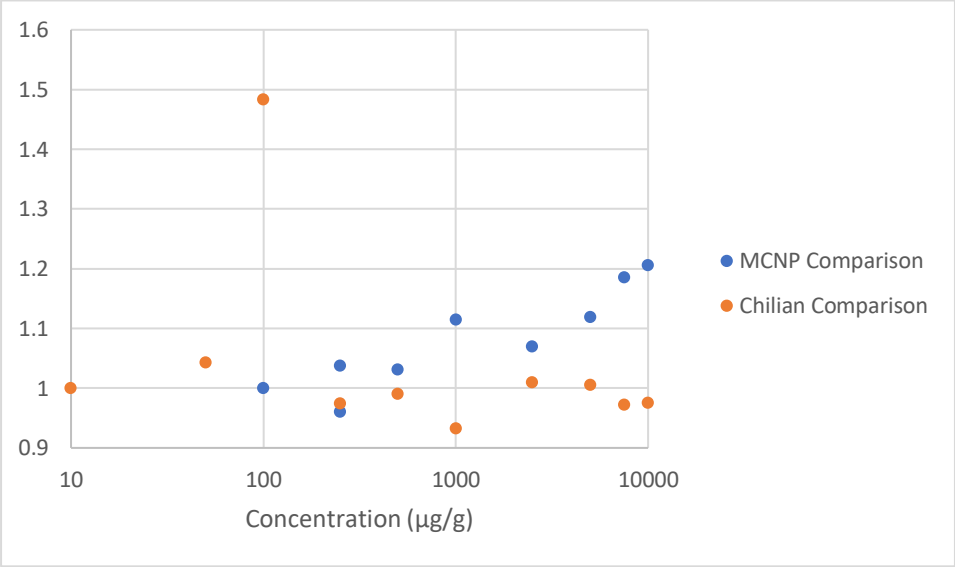

Figure F-12: Models vs Experimental Self-Shielding Factors for Thulium

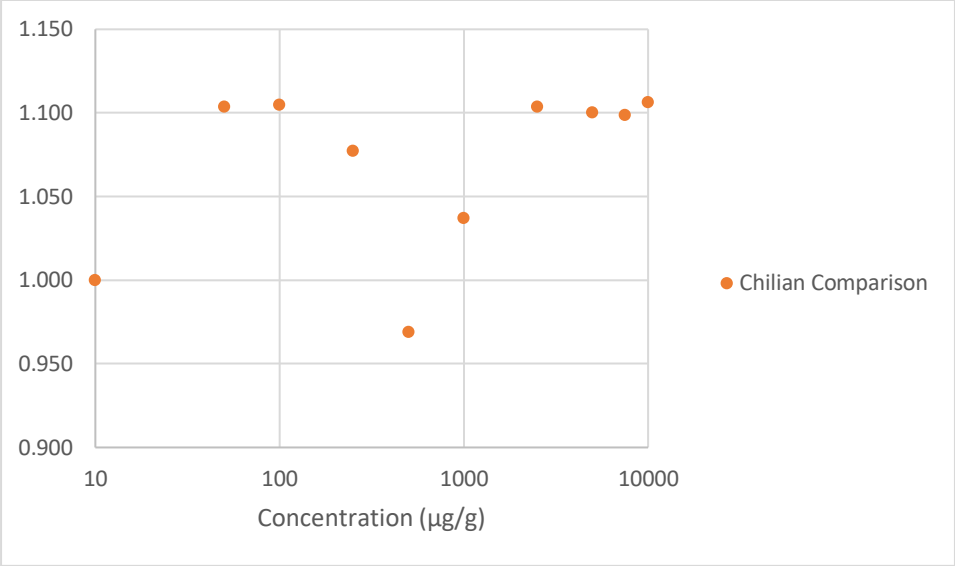

Figure F-13: Models vs Experimental Self-Shielding Factors for Ytterbium

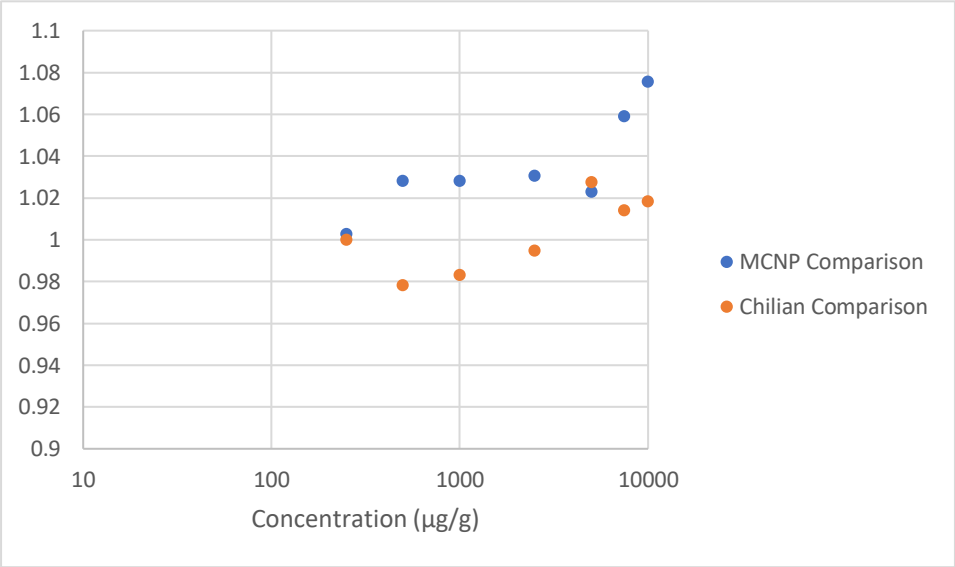

Figure F-14: Models vs Experimental Self-Shielding Factors for Lutetium

APPENDIX G: MCNP CODE 1 – REACTOR CORE CODE

An MCNP deck modeling a TRIGA Mark II Reactor was provided by the NETL staff. This code was utilized in order to create an energy and flux distribution for neutrons moving into the RSR positions. As the code is tens of thousands of lines of code in length, it is superfluous to include it in this appendix. Instead, the source definition and tallying specifications that were tailored for this investigation are included below.

```
F2:N    1301

C2      0     1

E2      1e-10 400log 20

MODE N

KCODE 500000 1.0 25 100

IMP:N 0 1 1359r
```

APPENDIX H: MCNP CODE 2 – NAA SIMULATION

```
c       material    density          surfaces          imp          descriptions
c       --------   ---------    --------------------  -------   ----------------------
1       1          -0.970000    +1 -4 -101 +102        imp:n=1    $ Cell for HDPE casing
2       2          -0.997060    +5 -6 -103 Vol=9.76264 imp:n=1    $ Cell for REE Solution
3       0                  +2 -3 -102 #2          imp:n=1    $ Cell for inside large vial and excluding the
2/5 dram vial
4       0                  -11 +14 -104 #1 #2 #3  imp:n=1    $ Cell for inside RSR Rabbit
5       0                  +12 -13 -104           imp:n=1    $ Cell for RSRRT hole
6       1          -0.970000    -13 +15 -105 #4 #5     imp:n=1    $ Cell for HDPE RSR Rabbit
7       0                  #1 #2 #3 #4 #5 #6 -201 imp:n=1    $ Cell for surrounding environment
c --------------------------------------------------------------------------------
c       OUTSIDE THE SYSTEM
c       material   density     surfaces      imp       descriptions
c       -----------   ----------     -----------      -------      ----------------
101     0                  +201      imp:n=0    $boundary of universe


c       Surface Cards
c       -------------
c       Plane      Z
c       -----   -------
1       Pz      0.3900          $Used for outside bottom of vial
2       Pz      0.5100          $Used for inside bottom of vial
3       Pz      5.8200          $Used for inside top of vial
4       Pz      5.5400          $Used for Outside top of vial
5       Pz      0.5400          $Used for bottom of the 2/5 dram vial
6       Pz      2.7900          $Used for top of the 2/5 dram vial
11      Pz      12.1869           $Bottom of RSRRTop
```

```
12      Pz     13.0759          $Bottom of Hole on RSRRTop
13      Pz     16.4287          $Top of RSRRTop
14      Pz      0.3810          $Inside Bottom of RSR Rabbit
15      Pz      0.0000          $Outside Bottom of RSR Rabbit
c ------------------------------------------------------------------------------
c      Cyln      R
c      -----     -----
101     CZ     0.825            $Used for outer vial wall
102     CZ     0.765            $Used for inner vial wall
103     CZ     0.725            $Used for 2/5 dram wall
104     CZ     1.24968           $RSR Rabbit ID and RSRRT hole
105     CZ     1.42875           $RSR Rabbit OD
c ------------------------------------------------------------------------------
c       Sphere    R        description
c       ----------  -----     ------------------------
201     SO      30.00     $outer universe
c ------------------------------------------------------------------------------

c     Data Cards
c     ----------
MODE     N
NPS      2E6
SDEF     SUR=201 PAR=1 ERG=d1 DIR=1 NRM=-1
SI1      H  0 1e-12 400log 20
SP1      D  0 0.00e+00 0.00e+00 0.00e+00 0.00e+00 0.00e+00 0.00e+00 0.00e+00 0.00e+00
0.00e+00 0.00e+00 0.00e+00 0.00e+00

     0.00e+00 9.12e-11 1.74e-10 1.65e-10 0.00e+00 0.00e+00 0.00e+00 8.56e-11 0.00e+00
0.00e+00 7.64e-11 2.95e-10 0.00e+00
```

5.25e-10 9.92e-10 6.50e-10 7.62e-10 7.71e-10 6.82e-10 1.26e-09 1.72e-09 1.94e-09 9.66e-10 1.14e-09 1.49e-09 3.01e-09

2.45e-09 2.06e-09 3.25e-09 3.46e-09 2.92e-09 4.59e-09 3.74e-09 4.00e-09 6.55e-09 7.41e-09 8.54e-09 1.14e-08 9.33e-09

1.14e-08 1.26e-08 1.76e-08 1.76e-08 2.32e-08 2.69e-08 2.73e-08 2.40e-08 3.70e-08 3.71e-08 4.09e-08 4.48e-08

4.98e-08 6.47e-08 6.26e-08 7.89e-08 8.35e-08 9.46e-08 1.14e-07 1.27e-07 1.33e-07 1.45e-07 1.87e-07 1.90e-07

2.02e-07 2.25e-07 2.64e-07 2.77e-07 2.95e-07 3.19e-07 3.71e-07 3.97e-07 4.43e-07 4.72e-07 5.04e-07 5.63e-07

5.67e-07 6.46e-07 6.59e-07 7.36e-07 6.95e-07 7.76e-07 8.01e-07 8.56e-07 8.28e-07 8.05e-07 8.56e-07 8.15e-07

8.53e-07 8.18e-07 8.18e-07 7.36e-07 7.68e-07 7.19e-07 6.87e-07 5.99e-07 5.33e-07 5.33e-07 4.41e-07 3.80e-07

3.51e-07 3.06e-07 2.71e-07 2.21e-07 1.73e-07 1.60e-07 1.48e-07 1.20e-07 9.94e-08 9.30e-08 8.34e-08 8.86e-08

6.57e-08 8.10e-08 8.56e-08 7.59e-08

8.14e-08 6.17e-08 7.12e-08 6.17e-08 7.07e-08 7.15e-08 5.93e-08 5.69e-08 6.29e-08 4.57e-08 6.19e-08 5.61e-08 5.94e-08

5.34e-08 5.72e-08 5.21e-08 7.23e-08 5.26e-08 4.54e-08 5.64e-08 5.22e-08 5.89e-08 5.33e-08 5.39e-08 4.59e-08 5.73e-08

4.21e-08 5.03e-08 4.49e-08 4.41e-08 4.39e-08 5.76e-08

4.81e-08 5.83e-08 6.08e-08 5.08e-08 4.82e-08 5.76e-08 4.63e-08 5.02e-08 4.13e-08 4.61e-08 5.81e-08 6.99e-08 5.40e-08

5.05e-08 4.63e-08 5.29e-08 5.44e-08 5.19e-08 4.85e-08 4.86e-08 5.96e-08 4.85e-08 4.49e-08 4.72e-08 4.93e-08 5.33e-08

5.11e-08 5.29e-08 4.42e-08 4.99e-08 4.54e-08 5.07e-08 5.72e-08 6.00e-08 6.08e-08 5.72e-08 5.20e-08 5.22e-08 4.90e-08

4.79e-08 4.96e-08 5.20e-08 4.69e-08 5.24e-08 5.31e-08 4.50e-08 4.93e-08 6.01e-08

5.02e-08 5.17e-08 4.90e-08 5.43e-08 5.74e-08 5.06e-08 5.26e-08 5.93e-08 4.82e-08 4.86e-08 4.87e-08 6.05e-08 5.60e-08

4.84e-08 5.20e-08

4.94e-08 5.06e-08 4.92e-08 4.83e-08 5.69e-08 5.50e-08 4.87e-08 6.52e-08 6.10e-08 5.31e-08 5.64e-08 5.45e-08 6.25e-08

5.07e-08 4.98e-08 5.38e-08

5.01e-08 6.22e-08 5.31e-08 6.51e-08 6.12e-08 5.08e-08 4.62e-08 5.16e-08 5.08e-08 4.84e-08 4.53e-08 5.31e-08 5.92e-08

5.84e-08 6.02e-08 5.73e-08

5.37e-08 5.19e-08 5.39e-08 5.40e-08 6.01e-08 5.60e-08 5.02e-08 5.53e-08 5.20e-08 5.22e-08 5.38e-08 5.30e-08 5.74e-08

6.76e-08 4.84e-08 6.72e-08 5.87e-08

6.23e-08 5.69e-08 5.24e-08 6.43e-08 7.42e-08 5.62e-08 5.04e-08 6.04e-08 5.24e-08 5.89e-08 5.11e-08 5.86e-08 7.12e-08

5.57e-08 5.35e-08 6.41e-08 5.72e-08 6.69e-08

5.31e-08 6.02e-08 6.42e-08 5.81e-08 6.88e-08 5.87e-08 5.90e-08 5.87e-08 6.19e-08 6.38e-08 7.07e-08 7.04e-08 8.36e-08

8.67e-08 6.22e-08 4.26e-08

5.54e-08 6.39e-08 6.99e-08 8.67e-08 7.27e-08 6.95e-08 8.15e-08 8.62e-08 7.83e-08 8.10e-08 9.45e-08 1.08e-07 6.72e-08

6.63e-08 7.07e-08 8.91e-08

9.51e-08 8.70e-08 9.30e-08 1.04e-07 9.43e-08 8.72e-08 8.35e-08 9.97e-08 1.11e-07 1.26e-07 1.06e-07 9.33e-08 1.17e-07

1.14e-07 1.27e-07 1.12e-07

1.31e-07 1.29e-07 1.24e-07 1.31e-07 1.35e-07 1.20e-07 1.39e-07 1.46e-07 1.51e-07 1.83e-07 1.49e-07 1.87e-07 1.71e-07

1.85e-07 1.90e-07 1.71e-07

1.74e-07 1.72e-07 1.73e-07 1.77e-07 1.96e-07 1.96e-07 1.71e-07 1.93e-07 1.75e-07 1.92e-07 1.81e-07 1.92e-07 1.82e-07

1.94e-07 1.88e-07 1.89e-07 1.78e-07 1.45e-07 1.63e-07

1.32e-07 1.12e-07 9.29e-08 8.87e-08 8.73e-08 7.29e-08 7.11e-08 6.48e-08 5.55e-08 5.03e-08 3.96e-08 2.61e-08 2.86e-08

2.53e-08 1.56e-08 1.05e-08

9.89e-09 7.84e-09 4.98e-09 2.90e-09 5.31e-10 6.76e-10 3.36e-10 2.01e-10 0.00e+00 0.00e+00 0.00e+00 0.00e+00 0.00e+00 0.00e+00

```
    0.00e+00
F4:N     2
FM4      (-3.33543E-07 3 102) (-3.33543E-07 4 102)
         (-3.33543E-07 5 102) (-3.33543E-07 6 102)
         (-3.33543E-07 7 102) (-3.33543E-07 8 102)
         (-3.33543E-07 9 102)
c
c      Materials
c      Material id   Atomfraction   Element     Material
c      ------------   -----------------   -----------     ----------
M1     6000.60c      1           $C
       1001.60c      2           $H        HDPE
c
M2     70168.80c     0.0123      $Yb
       70170.80c     0.2982
       70171.80c     1.409
       70172.80c     2.168
       70173.80c     1.6103
       70174.80c     3.2026
       70176.80c     1.2996
       1001.60c      1999980       $H
       8016.60c      999990        $O
c
M3     70168.80c     0.0123
M4     70170.80c     0.2982
M5     70171.80c     1.409
M6     70172.80c     2.168
M7     70173.80c     1.6103
```

M8 70174.80c 3.2026

M9 70176.80c 1.2996

VITA

Isaac Nathan Kravitz was born in Austin, Texas to Larry and Laura Kravitz. After graduating from L.C. Anderson High school in Austin, Texas he attended the University of Texas at Austin. There he studied Mechanical Engineering in the Cockrell School of Engineering, and ultimately received his Bachelor of Science in Mechanical Engineering in May 2018. In the fall of 2018, he continued his education by attending Graduate School at the University of Texas at Austin, where he received his Master's in Nuclear and Radiation Engineering.

Address: isaacnkravitz@gmail.com

This manuscript was typed by the author.